Universität Ulm
Sektion Kernresonanzspektroskopie

Molecular dynamics in porous media studied by Nuclear Magnetic Resonance Techniques

DISSERTATION

zur Erlangung des Doktorgrades Dr. rer. nat.
der Fakultät Naturwissenschaften
der Universität Ulm

vorgelegt von

Carlos Mattea
aus Villa Maria, Argentinien



Ulm, 2006

Amtierender Dekan: Prof. Dr. Klaus-Dieter Spindler

Erstgutachter: Prof. Dr. Rainer Kimmich
Zweitgutachter: Prof. Dr. Peter Reineker

Tag der Promotion: 20. März 2006

Molecular dynamics in porous media studied by Nuclear Magnetic Resonance Techniques

Abstract

Nuclear magnetic resonance (NMR) techniques cover a broad range of length and time scales on which dynamic properties of fluids in porous media can be investigated. Field-cycling NMR relaxometry was used to study dynamics of fluids under the influence of confinement and surface interactions in different scenarios. These are: (*i*) fluids flowing through porous media, (*ii*) fluids partially filling porous media and (*iii*) polymer melts in nanoscopic pores. Diffusion in partially filled porous media was also studied with the aid of an NMR diffusometry technique.

It is shown that hydrodynamic flow influences the spin-lattice relaxation rate of water confined in mesoscopic porous media under certain conditions. When hydrodynamic flow and diffusion in porous media are superimposed, the orientational dynamic process of adsorbed molecules taking place at the adsorbate/matrix interface will be accelerated by a sort of rotational analogue to translational hydrodynamic (or Taylor-Aris) dispersion. The effect is predicted by an analytical theory and Monte Carlo simulations, and confirmed experimentally by field-cycling NMR relaxometry. Actually, the first NMR relaxation experiment of this sort is presented here.

In liquids partially filling porous media, three different mobility states of the fluid molecules are distinguished: The adsorbed state at the pore walls, the bulklike liquid phase, and the vapor phase. Field-cycling NMR relaxometry has been applied to polar and non polar adsorbates in partially filled silica porous glasses. The dependence of the spin-lattice relaxation rate on the filling degree shows that limits for slow and fast exchange between the adsorbed and the bulklike phases, can be distinguished and identified under certain conditions. These conditions depend on the pore size and polarity of the solvents. Porous media with mean pore sizes of nano- ($\sim$ 4 nm) and micrometers ($\sim$ 1 and $\sim$ 10 μm) were chosen.

Diffusion in the same unsaturated systems was studied with the aid of NMR diffusometry technique. The results show that the effective diffusion coefficient of solvents with different polarities displays opposite tendencies as a function of the liquid content. A two-phase fast-exchange model theory is presented accounting for these phenomena. In the vapor phase, both Knudsen and ordinary diffusion are considered. The different dependencies on the filling factor for polar and nonpolar adsorbate species are attributed to different effective tortuosities.

In the case of polymers melts confined in narrow artificial tubes of a porous solid matrix with variable diameter (9 to 57 nm), the characteristics of reptation were experimentally verified using proton field cycling NMR relaxometry technique. This observation is independent of the molecular mass and pore size and essentially reproduces the behavior found in a previous deuteron study. In bulk, the same polymer melts show either Rouse or renormalized Rouse dynamics, depending on the molecular mass. Remarkable, polymers under confinement show features specific for reptation even with a pore diameter 15 times larger

that the Flory radius while bulk melts of the same polymers do not. An estimation of the diameter of the effective tubes in which reptation occurs is discussed.

Contents

Title Page i
Abstract v
Table of Contents vi
Acknowledgments ix
Dedication x

1 Cumulative Thesis **1**
1 Introduction 2
2 Theoretical background 3
2.1 NMR spin-lattice relaxation 3
2.2 Diffusion 4
2.3 Reorientation Mediated by Translational Displacement: RMTD . . . 5
3 Experimental methods 6
3.1 Field-cycling NMR relaxometry method 6
3.2 NMR Diffusometry 8
4 Experimental and theoretical results 9
4.1 NMR relaxation due to rotational hydrodynamic dispersion in porous media 9
Introduction to hydrodynamic dispersion 9
Experiments 10
Flow-Relaxation effect 11
Monte Carlo Simulations 11
4.2 Molecular exchange dynamics in unsaturated porous media 12
4.3 Low frequency NMR relaxation mechanism 17
4.4 Confined polymer melts 17
5 Discussion and Conclusions 20

2 Zusammenfassung **21**

Bibliography **24**

3 Publication List **31**

4 Curriculum Vitae **33**

5 Original papers **37**

Acknowledgments

I would like to thank especially my supervisor Prof. Rainer Kimmich, who gave me the opportunity to work in his laboratory, the prestigious "Sektion Kernresonanzspektroskopie" of the University of Ulm. I will be indebted with him for ever. His help and useful feedback during all the work we have shared together was invaluable.

I would like to thank Prof. Esteban Anoardo, for his friendship, his support in my work, but also because he had trusted in me, together with Federico Casanova, four long years ago.

I would like particularly to thank Hans Wiringer, Brigitte Kast and Birgit Körner for their every day help.

I am grateful for suggestions, discussions, comments and contributions from my friends and colleagues in our Sektion Kernresonanzspektroskopie, German Farrher, Ravinath Kausik, Markus Kehr, Bogdan Buhai, Elke Kossel, Elmar Fischer, Prof. Ioan Ardelean, Prof. Nail Fatkulin and Karl-Heinz Spohn.

Thanks to my friends in the life, Omar, Bogdan, Rodi, Dario, Favio, Ramiro, Marcelo, Dani, Fede, Gri, Karina, Willy. With them, I was tears and gladness. Thanks to Elmar, Belen, Juan, Chavez, Sergio, Maquina, Chaco, Ale, Bula, Otito, Gallego, Tucu, Vincent.

I would like to thank Prof. Aldo Brunetti and the people that was forming part of his group and today are in the NMR group in Córdoba, Argentina: Alberto, Clide and specially Clemar and Elizabeth.

Thanks Nico, Vero, Brenda and Javi, with whom I have a friendship and it is just a gift from them.

Thanks to Ravi and Markus, who helped me a lot during writing my thesis.

My thanks also go for my family, who although far in Argentina, are dreaming together with me this moments... I love them. Thanks to tio Meco. Also to Matias, Antonella, Denisse, Desiree, Claudia, Juanita, my ants Odilia and Miñu.

Finally, I would like to thank the University of Ulm and the Deutsche Forschungsgemeinschaft (DFG) for its financial support of my doctoral research.

Dedicated to my father Jose Carlos,
my mother Liliana,
my brothers Sergio and Rubén, my sister Gabriela,
and to miamor Violeta.

...

Temprano levantó la muerte el vuelo,
temprano madrugó la madrugada,
temprano estás rodando por el suelo.

No perdono a la muerte enamorada,
no perdono a la vida desatenta,
no perdono a la tierra ni a la nada.

...

Miguel Hernandez

1

Cumulative Thesis

The present thesis summarizes the results of my work at the University of Ulm. The thesis consists of an introductory part followed by the articles listed below, which are referred to in the text by Roman numbers.

I. C. Mattea, H. Tiraboschi and R. Kimmich, **Effect of hydrodynamic flow on low-field spin-lattice relaxation in liquids in the nanoscopic vicinity of solid surfaces: Theory and Monte Carlo simulations of model pore spaces**, Phys. Rev. E. **72**, 021602 (2005).

II. C. Mattea and R. Kimmich, **Flow-Enhanced Molecular Reorientations and Interfacial Slip Probed by Field-Cycling NMR Relaxometry in Microscopic Pores**, Phys. Rev. Lett. **94**, 024502 (2005).

III. C. Mattea, R. Kimmich, I. Ardelean, S.Wonorahardjo and G. Farrher, **Molecular exchange dynamics in partially filled microscale and nanoscale pores of silica glasses studied by field-cycling nuclear magnetic resonance relaxometry**, J. Chem. Phys. **121**, 10648 (2004).

IV. C. Mattea, N. Fatkullin, E. Fischer, U. Beginn, E. Anoardo, M. Kroutieva and R. Kimmich, **The "corset effect" of spin-lattice relaxation in polymer melts confined in nanoporous media**, Appl. Magn. Reson. **27**, 371 (2004).

V. I. Ardelean, C. Mattea, G. Farrher, S. Wonorahardjo and R. Kimmich, **Nuclear magnetic resonance study of the vapor phase contribution to diffusion in nanoporous glasses partially filled with water and cyclohexane**, J. Chem. Phys. **119**, 10358 (2003).

1 Introduction

Since its discovery in 1946 independently by Felix Bloch and Edward M. Purcell, up to the current days, Nuclear Magnetic Resonance (NMR) has shown to be a valuable tool in fields as diverse as medicine, biology, chemistry and physics [nob03]. NMR is widely spread in its applications such as magnetic resonance imaging for medical diagnosis as well as in chemical studies. The NMR techniques known as relaxometry and diffusometry [kim97] are extensively used to get insight into the physicochemical properties of an object. In particular an active research field related with the topics in this thesis is the characterization of the properties of fluids within porous structures. Flow and mass transport in porous media are complex problems with many applications in systems such as oil recovery from geological formations, groundwater flow in aquifers, fuel cells and chemical reactors [sah95, vaf00].

Molecular dynamics of liquids under confinement in porous media differ substantially from that of the same liquids in bulk. This was demonstrated in numerous self-diffusion[1] and spin-lattice relaxation[2] studies in systems like water and organic solvents confined in porous glasses, or linear chains of polymer melts under confinement in a solid methacrylate matrix [fis99, kim99, sta96]. One of the main conclusions from these studies is that deviations from bulk properties can be explained by the restrictions imposed by the pore space or adsorption at pore surfaces.

Unlike NMR diffusometry where adsorption at pore walls plays a minor role [kim96] and can be neglected, the dominant NMR relaxation mechanism occurs at the pore walls, due to the so-called reorientation mediated by translational displacements (RMTD) process [kim97]. All cases reported in the literature until now refer to confinements of liquids in porous materials with polar surfaces. The question is how non-polar pore surfaces affect the T_1 dispersion of polar and non-polar liquids, and whether the RMTD mechanism still applies.

The research problem of this thesis was primarily to find under what conditions the two different scenarios, (*i*) fluids flowing through porous media and (*ii*) fluids in coexistence with their vapor phase in porous media, affect molecular rotational dynamics at the interfaces between fluid and pore walls. The second question was how geometrical constraints influence chain dynamics in polymers melts.

Hydrodynamic dispersion is a well known transport mechanism of actual interest[3] consisting in the combined action of incoherent Brownian motion and coherent laminar flow. Superimposed hydrodynamic flow and surface diffusion are expected to modify the RMTD process and affect the relaxation process in this way. The question is how translational and rotational diffusion are correlated when intermittent adsorption-desorption process at pore walls occur, and whether it is possible that rotational diffusion can be influenced by flow.

In the vicinity of surfaces the question arises whether interfacial slip exists. Since one is dealing with a surface relaxation process, a detailed examination of the boundary condition is expected to be possible. Field-cycling NMR relaxometry probes molecular mechanisms

[1] See bibliography: [aks99, V, ard04, ban87, dor89, dor90a, dor90b, kim94, kim96, kor97]
[2] See bibliography: [aks99, ban87, kor97, lev03, sei00, sta95, zav98, zav99]
[3] See bibliography: [gho04, com97, gau04, kan02, low96, sch01]

on a time scale up to 10^{-4} s. The corresponding molecular root mean square displacements by Brownian motions are much less than 100 nm in water at room temperature. Flow can therefore influence surface relaxation only in a surface layer thinner than 100 nm. In a sense, nanofluidics can be examined on this basis.

Other systems of interest here are porous media partially filled with liquids. Most investigations published so far refer to saturated samples where one merely needs to distinguish between adsorbed and bulklike mobility states of the adsorbate molecules. The adsorbed state corresponds to molecules in the interface liquid/pore wall which are subject to the RMTD mechanism. The bulklike phase refers to molecules with reorientation times scales typical for bulk liquids. In partially filled porous samples. The question arises: is there any perceptible influence of molecular exchange between the liquid and the vapor phases and does the fast exchange limit relative to T_1 apply?

Previous field-cycling NMR relaxometry and field-gradient NMR diffusometry [fis99, kim99, sta96] studies of polymer melts confined in porous media showed that the dynamical limits predicted by the tube/reptation model [gen71, doi86] could be well reproduced. The results suggest the intriguing question whether a crossover from "bulk" to "confined" dynamics could be reached by varying the pore diameter.

The main techniques employed in this study are field-cycling NMR relaxometry and field-gradient NMR diffusometry. We therefore begin with a description of the methodological background.

2 Theoretical background

2.1 NMR spin-lattice relaxation

The evolution of the bulk magnetization ($\vec{M}$) in an external magnetic field with a flux density $\vec{B}_0$ can be described by a set of phenomenological differential equations known as the Bloch equations [kim97], in the laboratory frame read in vectorial form

$$\frac{d\vec{M}}{dt} = \gamma\ \vec{M} \times \vec{B}_0 - \frac{M_x}{T_2}\ \vec{u}_x - \frac{M_y}{T_2}\ \vec{u}_y - \frac{M_z - M_0}{T_1}\ \vec{u}_z, \tag{1}$$

where γ is the gyromagnetic ratio and T_1 is the spin-lattice relaxation time. M_0 is the equilibrium value of the magnetization $\vec{M}$. The magnetization components in the transverse plane relax with the time constant T_2 towards their equilibrium value 0.

A general treatment of NMR relaxation is obtained considering the time-evolution of the density operator. This formalism (see chapters 11-13 of ref. [kim97]), developed by Redfield following ideas introduced by Wangsness and Bloch, generalizes the theories based on the standard time-dependent perturbation theory [blo48].

Spin relaxation is assumed to be due to intramolecular spin interactions, i.e., dipolar or quadrupolar couplings. Molecular motions in the sense of reorientations of molecules or chemical groups lead to fluctuating polar coordinates r, θ and φ of the internuclear vector relative to the external magnetic field. As a consequence, the dipolar or quadrupolar Hamiltonians [abr61, kim97] become time dependent, and hence, induce spin transitions

as predicted by time dependent perturbation theory. Homonuclear dipolar interaction is the dominantly relaxation mechanism in our systems. The standard expression for the spin-lattice relaxation rate $1/T_1$ is the given by

$$\frac{1}{T_1} = \left(\frac{\mu_0}{4\pi}\right)^2 \frac{1}{5\ r^6}\ \gamma^4\hbar^2 I(I+1)\ [\mathcal{I}(\omega) + 4\mathcal{I}(2\omega)] \tag{2}$$

where μ_0 is the permeability of vacuum and r is the fixed internuclear distance. $\omega = 2\pi\nu = \gamma|\vec{B}_0|$ is the circular Larmor frequency in the external flux density $\vec{B}_0$. The intensity function $\mathcal{I}(\omega)$ is defined as the cosine Fourier transform of the reduced dipolar correlation function $G(t)$

$$\mathcal{I}(\omega) = 2\int_0^\infty G(t)\ cos(\omega t)\ dt, \tag{3}$$

where the reduced dipolar correlation function is given by

$$G(t) = \frac{\langle F_i(0)F_i^*(t)\rangle}{\langle|F_i|^2\rangle} \approx \frac{\langle F_2(0)F_2^*(t)\rangle}{\langle|F_2|^2\rangle}. \tag{4}$$

The quantities F_i (with its complex conjugate F_i^*) are functions of the polar coordinates r, θ and φ, of the internuclear vectors of nearest neighbors with respect to the external magnetic field. They are proportional to second order spherical harmonics [abr61, kim97]. For intramolecular interactions, the correlation function exclusively reflects molecular reorientations.

2.2 Diffusion

Self-diffusion refers to equilibrium systems and is a consequence of Brownian motion. All information about displacements by translational diffusion is contained in the diffusion propagator $\Psi(\vec{r},t)$ defined as the probability density that a molecule is displaced a distance $\vec{r}$ after a time t. $\Psi(\vec{r},t)$ obeys the diffusion equation

$$\frac{\partial\Psi(\vec{r},t)}{\partial t} = D\nabla^2\Psi(\vec{r},t), \tag{5}$$

where D is the diffusion coefficient. In the case of isotropic and unrestricted diffusion it is a scalar constant. The solution of Eq. (5) with a Dirac delta-function as initial condition $\Psi(\vec{r},0) = \delta(\vec{r})$, and the boundary condition $\Psi(\vec{r}\to\infty,t)\to 0$, is the normalized Gaussian function

$$\Psi(\vec{r},t) = \frac{1}{(4\pi Dt)^{\zeta/2}}\ \exp\left[-\frac{\vec{r}^{\,2}}{4Dt}\right], \tag{6}$$

where ζ is the spatial dimensionality.

The second moment of the distribution (6), the mean square displacement defined as

$$\langle r^2\rangle = \int \vec{r}^{\,2}\ \Psi(\vec{r},t)\ d^\zeta\vec{r}\ =\ 2\zeta Dt, \tag{7}$$

is used to characterize the diffusion process and is accessible in field gradient NMR difussometry experiments as well as in numerical simulations where diffusion is modelled as

a Random Walk (RW). Free or unrestricted diffusion implies that there are no geometrical limitations to the molecular displacements on the time-scale considered, and Eq. (7) holds with constant diffusion coefficient D.

Restrictions in translational displacements by geometrical constrains or if the space in which diffusion takes place is not of an Euclidean nature [bro03, kla96, vis96], lead to some deviations from the ordinary diffusion behavior and the linear time dependence in Eq. (7). This is often referred to as "anomalous diffusion". The time dependence of the mean-squared displacement often obeys a power law of the form

$$\langle r^2 \rangle = B\ t^{\kappa}. \tag{8}$$

Normal diffusion leads to $\kappa = 1$ and $B = 2\zeta D$. An exponent in the interval $0 < \kappa < 1$ corresponds to "subdiffusive behavior". An example is diffusion in random-percolation clusters, which are known to be fractal [bun96] within the correlation length[4] ξ [orb82, orb86, kim02]. The case $\kappa > 1$ is referred to as "superdiffusive behavior". It is present, for example, in confined liquids having strong interactions with the container walls. In this case, the adsorbate displacements along the pore surfaces can be subject to strong diffusion anomalies on a certain time scale leading to Lévy walk diffusion mechanisms [kla96, byc95, zav98].

2.3 Reorientation Mediated by Translational Displacement: RMTD

When a liquid is confined, adsorbate molecules diffusing in the vicinity of the pore surfaces can perform adsorption, desorption, and readsorption cycles. Repeated many times, the adsorption/desorption events separated by bulk-mediated excursions will result in an effective motion of a given molecule along the surface (termed "bulk mediated surface diffusion" or BMSD) [byc94, byc95, cop04, lev97, lev05]. Since the surface determines the orientation of the adsorbed molecule relative to the external flux density $\vec{B}_0$, desorption at one site and readsorption at another site of a nonplanar surface will cause molecular reorientation as illustrated in Fig.1. In the so-called "strong-adsorption limit," [byc95, kim02] which typically applies to polar liquids confined by polar surfaces, reorientation correlation times up to eight orders of magnitude longer than in the bulk have been observed [sta95] using field-cycling NMR relaxometry [kim97, kim04a]. This is the basis of the "reorientation mediated by translational displacements" (RMTD) relaxation mechanism in NMR [sta95, kim02].

Following the BMSD formalism, different adsorption and desorption probabilities per time unit, Q_{ads} and Q_{des}, respectively, can be distinguished. The adsorption on surfaces can be characterized by a number of characteristic parameters. The retention time t_h reflects how long it takes until the initial adsorbate population on a surface is finally replaced by molecules initially in the bulklike phase. The retention time is related to the so-called adsorption depth h according to $t_h = h^2/D_m$, where D_m is the molecular diffusion constant in the bulk.

[4] The correlation length gives an estimation of the distance from a point beyond which there is no further correlation of a physical property associated with that point. Values for a given property at distances beyond the correlation length can be considered to be uncorrelated.

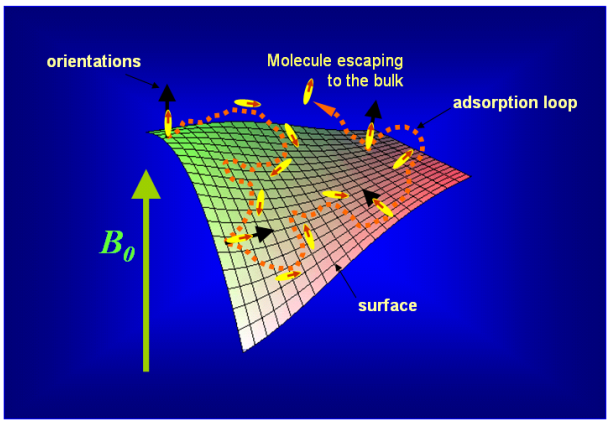

Figure 1: Molecules diffusing in the vicinity of pore surfaces can perform adsorption, desorption, and readsorption cycles before escaping to the bulk. RMTD means that molecules probe the surface topology via translational diffusion and molecular exchange.

On the other hand, the adsorption length can be expressed by $h = \lambda Q_{ads}/Q_{des}$, where λ is the capture range within which a molecule can directly be adsorbed on the surface. This equation is based on a dynamic equilibrium of the one-dimensional "reaction-diffusion" process as which adsorption and translational diffusion to and from the surface can be interpreted. The time scale of desorption-diffusion-readsorption cycles is given by $Q_{des}^{-1} < t < t_h$, and was shown to be of the same order of magnitude as the time scale probed by field-cycling NMR relaxometry [kim04a, zav98].

Depending the adsorption properties, two limits can be distinguished. The weak-adsorption limit is characterized by

$$t_h \; Q_{des} << 1. \tag{9}$$

That is, the adsorbate molecules are most likely exchanged to the bulklike phase immediately after desorption. This is in contrast to the strong-adsorption limit

$$t_h \; Q_{des} >> 1, \tag{10}$$

in which numerous desorption-readsorption cycles occur before an adsorbate molecule finally disappears in the bulklike phase.

3 Experimental methods

3.1 Field-cycling NMR relaxometry method

The field-cycling NMR relaxometry method, also referred to as nuclear magnetic relaxation dispersion (NMRD), is a technique for measuring relaxation times in a very large range of Larmor frequencies (10^3 Hz $< \nu <$ 10^8 Hz for protons). This feature makes it a powerful tool for the identification and characterization of molecular dynamics in complex systems [kim04a, noa86].

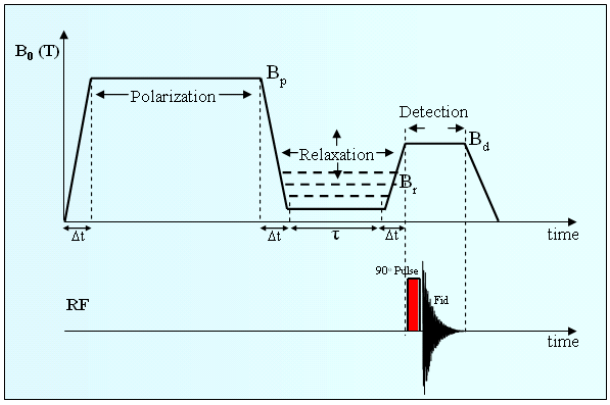

Figure 2: Schematic representation of a typical field cycle of the main magnetic field B_0 employed with field-cycling NMR relaxometry. The sample is first polarized in a magnetic field with a flux density B_p during a time that is typically chosen to be five times the spin-lattice relaxation time in that field. The magnetization after the relaxation interval τ in the flux density B_r, is recorded in the detection interval with a flux density B_d, in the form of a free induction decay (FID) after a 90^0 radio frequency (RF) pulse.

The principle of a typical field-cycling NMR relaxometry experiment is illustrated in Fig.2. The sample is polarized in a magnetic field with a flux density B_p. The relaxation process takes place in a low-field interval varied with respect to length τ and flux density B_r. The signal remaining after this relaxation interval is detected in a field of fixed flux density B_d as high and homogeneous as possible. Then an extended recycle delay for the restoration of thermal equilibrium and polarization follows until the next cycle begins.

One of the crucial limitations of field-cycling applications is the signal-to-noise ratio. It can be expressed as [hou76]:

$$S/N = B_p \varsigma \sqrt{\frac{\eta Q V_s \nu_d}{k_B T \Delta\nu}} , \tag{11}$$

where η is the filling factor of the RF coil, Q is the quality factor of that coil, V_s is the sample volume, k_B is the Boltzmann constant, T is the absolute temperature, ν_d is the Larmor frequency of the detection field, $\Delta\nu$ is the bandwidth of the receiver filtering and amplification system, and $\varsigma < 1$ represents the reciprocal noise level of the receiver electronics. High polarization and detection flux densities are then crucial for a good sensitivity.

The finite interval Δt between polarization, relaxation and detection fields (see Fig.2) will not introduce any systematic experimental error in the determination of T_1 for a given relaxation field. This is demonstrated in ref. [kim97], where the switching interval is taken into account explicitly in the derivation of the relaxation curve formula

$$M_z(\tau) = M_z^{\infty} + \Delta M_z^{eff} \; e^{-\tau/T_1(B_r)} \tag{12}$$

to be fitted to the acquired experimental data. M_z^{∞} is an "effective" equilibrium magnetization in the relaxation field and ΔM_z^{eff} is the "effective" variation range of the magnetization [kim97, kim04a].

The field-variation rates at the switching time interval Δt has to be fast enough to avoid equilibration during the time Δt [noa86]. This condition may be expressed

$$\Delta t << T_1(B_r). \tag{13}$$

In practice, the restriction is less strict mainly due to the fact that relaxation times in general decrease with $\vec{B}_0$ [kim80]. One can have [kim04a]

$$\Delta t \leq T_1(B_r) \ , \tag{14}$$

with the only consequence of the reduction in the signal variation range ΔM_z^{eff} and, hence, the experimental accuracy of relaxation time measurements.

The complementary condition to Eq. (13) is that the field-variation rates at the switching time intervals must be as high as technically possible as long as the adiabatic condition [abr61, pak73] is fulfilled,

$$\frac{1}{B^2}\left|\vec{B} \times \frac{d\vec{B}}{dt}\right| << \gamma B, \tag{15}$$

where $B = |\vec{B}_0 + \vec{B}_{loc}|$ is the total flux density "seen" by the nuclei. $\vec{B}_{loc}$ is the local field caused by (residual) secular spin interactions. In the cases where the direction of $\vec{B}$ remains stationary, the condition (15) becomes trivial. At low frequencies the "local fields", with no definite direction, may exceed the external flux density in the relaxation interval of the field cycle. Then the local fields tend to govern the quantization field and the condition (15) may be violated.

Another factor that may restrict the applicability of the field-cycling technique is the presence of the earth field (or other magnetic stray fields in the lab) at the sample position. For this reason, the field-cycling relaxometer used in the experiments is equipped with homemade auxiliary coils for compensation. Finally the case may arise that the low-field spin-lattice relaxation time is shorter than the longest time constant of the correlation function so that a validity condition of the Bloch/Wangsness/Redfield theory [abr61, kim97] is not fulfilled.

In order to avoid experimental artifacts by imperfections of the field cycle it is very important in this technique to check and calibrate the field cycle with the aid of a fast field probe placed at the sample position [kim04a]. The crucial problem is the time resolution of the field measurement. That is, the field control and calibration must be performed with a time resolution better than the shortest relaxation time to be expected for the samples under consideration. A sensitive digital teslameter (Projekt Elektronik FM210, with a measuring principle based on the Hall effect) with a bandwidth of 35 kHz and a resolution of 0.01 mT was used for the calibration of our field cycles in the field-cycling relaxometer.

3.2 NMR Diffusometry

The Pulsed Field Gradient Stimulated Echo (PFG-STE) sequence [ard03, kim97] used in the experiments is shown in Fig.3. It consists of a preparation interval where a first gradient pulse labels the spins with a position dependent phase shift and a read interval where a second gradient pulse reverses the phase shifts. Diffusion between the preparation

and read intervals, in the interval Δ, results in incomplete phase reversal and attenuation of the echo.

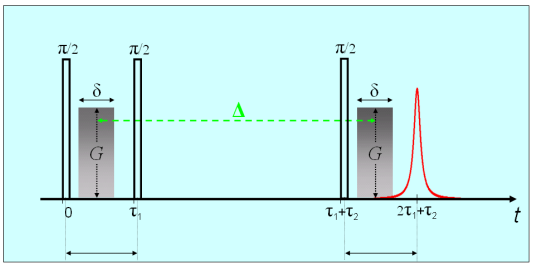

Figure 3: Pulse sequence for the generation of a stimulated echo. G represents the field gradient applied in pulses of width δ, separated by the "diffusion time" Δ. The RF pulses are applied in the times 0, τ_1 and $\tau_1 + \tau_2$, whereas the stimulated echo is formed at the time τ_1 after the third $\pi/2$ pulse.

The echo attenuation A_{diff} due to translational diffusion is given by [kim97]

$$A_{diff} = e^{-(\gamma G\delta)^2 D(\Delta - \delta/3)} \tag{16}$$

where γ is the gyromagnetic ratio, G is the gradient strength, and δ is the gradient pulse length.

4 Experimental and theoretical results

This section reviews the main findings of the study. The original communications I-V are referred to for further details.

4.1 NMR relaxation due to rotational hydrodynamic dispersion in porous media

Introduction to hydrodynamic dispersion

Hydrodynamic dispersion is a phenomenon involving transport of a neutral tracer in a flowing carrier fluid. It has been widely investigated in the fields of oil recovery and chemical engineering (see for instance ref. [sah95] and references therein). Hydrodynamic dispersion properties are usually characterized by the Péclet number, defined as $\mathrm{Pe} = v\,\xi/D_m = t_D/t_v$, which is the ratio between the diffusion time $t_D = \xi^2/D_m$ and the convection time $t_v = \xi/v$. v is the average velocity of the flow, ξ is a characteristic length (compare footnote 4) of the system and D_m is the diffusion coefficient of the particle or molecule of interest. The basic theory of dispersion in the case of laminar flow in a straight capillary was established by Taylor and Aris [tay53, ari56]. Koch and Brady [koc85, koc87] developed a theoretical analysis of dispersion in random media composed of randomly distributed fixed particles. An approach to model dispersion in porous media is to consider microscopically disordered and macroscopic isotropic and homogeneous porous materials. Under these conditions,

dispersion is said to be Gaussian and the phenomenon can be represented by the convection-diffusion equation [sah95]

$$\frac{\partial \Psi}{\partial t} + \vec{V} \cdot \nabla \Psi = D_{\perp} \, \nabla_{\perp}^2 \Psi + D_{\parallel} \, \frac{\partial^2 \Psi}{\partial x^2}, \tag{17}$$

where $D_{\perp}$ and $D_{\parallel}$ are the orthogonal and parallel components of the dispersion coefficient D with respect to the average flow velocity $\vec{V}$. $\nabla_{\perp}^2$ is the Laplace operator in the transverse direction applied to the propagator Ψ. In the limit of vanishing flow velocities, $D_{\parallel}$ becomes equal to the molecular diffusion coefficient (D_m) diminished by the tortuosity factor[5].

The solution for the longitudinal part of this equation, that is, its projection on the x direction is

$$\Psi(x,t) \; = \; \frac{c_0}{2\pi} \int_{-\infty}^{+\infty} e^{-(Dtk^2 \, + \, ikvt)} \; e^{ixk} dk, \tag{18}$$

with the initial condition $\Psi(x,0) = c_0 \, \delta(x)$. $D \equiv D_{\parallel}$. The "wave number" k is the reciprocal space variable conjugate to the real-space variable x and v is the velocity component in longitudinal direction.

Experiments

Field-cycling NMR relaxometry experiments were performed to measure T_1 dispersion in water confined in a porous sample[6] in two different situations: (i) stationary and (ii) flowing through the sample [II]. The flux was induced by a pressure gradient produced by a chromatographic pump ensuring continuum flow under pressure up to 25 bar.

Several attempts were undertaken to find the right sample and experimental conditions for the measurement. Porous glasses with a pore size in the order of nanometers were used in the first experiments because large surface/volume ratios are more favorable for the expected effect. However, it is difficult to embed the sample in the sample tube in such a way that bypassing of water is avoided. The pressure needed to force water through the pores turned out to be immense. Other porous glasses with micrometer pores were not stable enough to withstand the required pressure gradient. With a monolithic chromatographic column, all these problems did not arise. The main difficulty one is still facing is that hydrodynamic flow tends to occur along certain percolation pathways as demonstrated in the computational fluid dynamics simulation shown in Fig.6b. Most of the sample volume then is not subject to flow of sufficient velocity. The effect of flow can consequently be expected only little above the experimental error intrinsic to the field-cycling technique.

The results of the measurements are shown in Fig.4. In the presence of flow, the T_1 values are shifted to higher values in the main-dispersion regime while the data around 10 MHz coincide with the measurements in the static state.

[5]Tortuosity is defined as the ratio of the actual path length of the diffusing molecules through a porous material to the corresponding trajectory lengths in the bulk liquid phase, free of obstacles, for the same mean square displacements [dul92].

[6] The sample is a commercial high-pressure liquid chromatography column consisting of a bimodal silica skeleton with meso- (13 nm pore size) and macroporous (2 μm pore size) structure, and overall porosity of about 85% [II]. In the inset in Fig.4 are shown two micrographies corresponding to the meso- and macro-structure

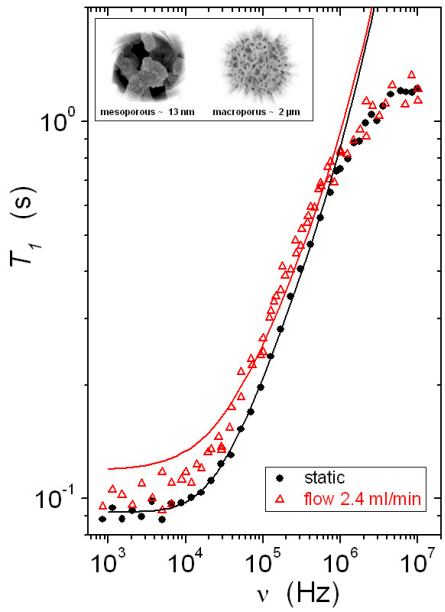

Figure 4: Comparison of the proton spin-lattice relaxation dispersion in water in Chromolith under static and flow conditions. The solid lines are obtained with the combination of Eqs. (2) and (20) for $v_{max} = 0$ (lower line) and $v_{max} = 0.04$ m/s (upper line). The inset shows micrographs of the bimodal porous structure (see footnote 6).

Flow-Relaxation effect

The flow-relaxation effect was described in the frame of the RMTD formalism. Following the calculation in refs. [II, I], the correlation function becomes

$$G(t) = \int_{-\infty}^{+\infty} S(k)\ e^{-(Dtk^2+ikvt)}\ dk. \tag{19}$$

After Fourier transformation and assuming a distribution of flow velocities $P(v)$, one arrives at the spectral density

$$\mathcal{I}(\omega) \ = \ \int_{v_{min}}^{v_{max}} P(v) \int_{-\infty}^{+\infty} S(k) \frac{2Dk^2}{(Dk^2)^2 + (kv+\omega)^2}\ dk\ dv, \tag{20}$$

where v_{min} and v_{max} indicate the velocity range. $S(k)$ is the orientational structure factor, which represents information of the surface orientation in terms of surface modes with wave numbers k [zav98]. Combining this expression for the spectral density with Eq. (2) provides a *velocity dependent spin-lattice relaxation rate*. The influence of flow velocity on spin-lattice relaxation was termed *the flow-relaxation effect*.

Monte Carlo Simulations

The flow-relaxation effect was also examined with the aid of Monte Carlo simulations [I] for a number of simple model structures (Fig.6 shows an example). The displacement of

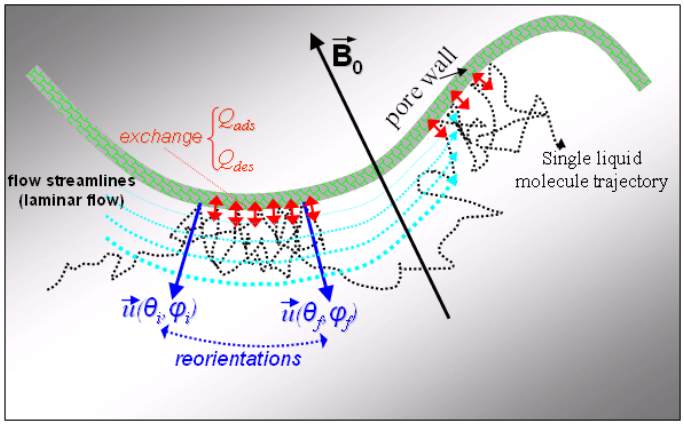

Figure 5: Illustration of the adsorbate reorientation by hydrodynamic dispersion. The liquid flows along the pore surfaces. The dotted line represents a trajectory of a molecule by Brownian motion in the presence of laminar flow along the interface. Flow streamlines are drawn as broken lines. The adsorption and exchange with the solid matrix is indicated by the double arrows. The long arrows refer to the local preferential orientations of molecules at the initial $\vec{u}(\theta_i, \varphi_i)$ and final $\vec{u}(\theta_f, \varphi_f)$ pore surface sites. The interface in which the flow enhanced RMTD process is expected to take place ranges from molecular diameters up to about 100 nm [II]. The probabilities Q_{ads} and Q_{des} refer to the exchange process taking place at the surface (see section 2.3).

particles are mimicked by Monte Carlo generated random walks and superimposed displacements by laminar flow (see Fig.5). The Monte Carlo simulations provide the correlation function $G_T(t)$ of the molecular orientations. Details can be found in reference [I]. Numerical Fourier transformation of the function $G_T(t)$ leads to the spectral density which in combination with Eq. (2), permits predictions for the spin-lattice relaxation dispersion. Fig.7 shows correlation functions obtained from Monte Carlo simulations. The corresponding T_1 dispersion curves are shown as well. The spectral densities, proportional to the relaxation rates $(1/T_1)$, are affected only at low frequencies perceptibly, as observed in the experiments.

4.2 Molecular exchange dynamics in unsaturated porous media

Molecular dynamics of liquids with different wettabilities partially filling porous glasses were studied with NMR diffusometry and field-cycling NMR relaxometry. The pore size ranges from 4 nm up to 10 μm (See Fig.8).

Diffusion in porous glass Vycor (4 nm pore size) was studied with the NMR Pulsed Field Gradient Stimulated Echo technique, described in section 3.2. The solvents, water and cyclohexane, were chosen as examples for polar and nonpolar species. The results are shown in the Fig.9. The different dependences on the filling degree can be well explained on the basis of a two-phase fast-exchange model between liquid and vapor phases [V]. The solid lines in Fig.9, correspond to Eq. (9) of reference [V]. The effective diffusion coefficient D is reduced by the tortuosity factor with respect to the bulk value D_0. It can be expressed by Archie's law $D = \Phi^m D_0$ [dor89, sah95], where Φ is the porosity of the sample and m is an

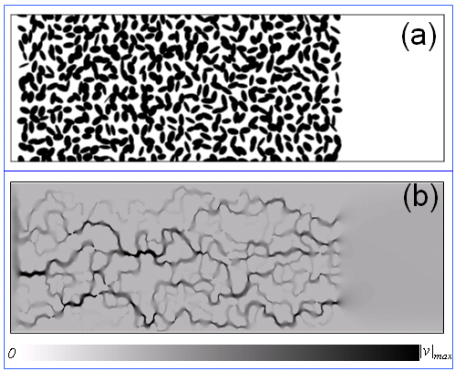

Figure 6: (a) Ellipsoidal-grain pack geometry used for Monte Carlo simulations. The pores are represented in white. (b) A map of the magnitudes of the flow velocity simulated with the finite volume method.

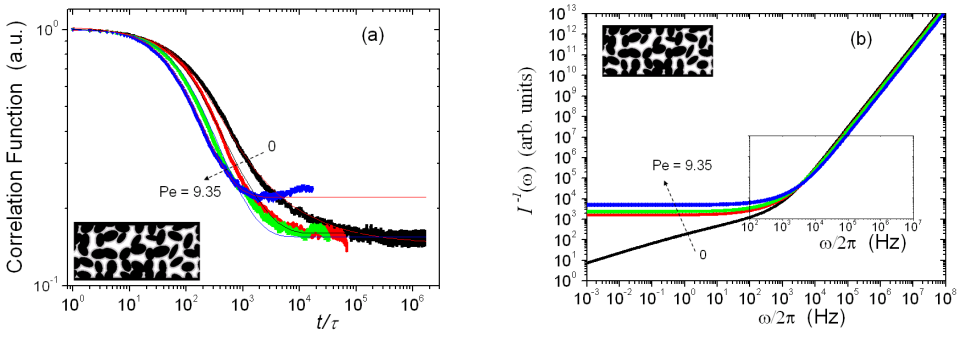

Figure 7: (a) Correlation functions from the MC simulations and (b) the corresponding T_1 dispersion for the ellipsoidal-grain pack model in Fig.6.

empirical exponent. In the two-phase fast-exchange model Archie's law is used to describe diffusion in both the liquid and vapor phases. Knudsen[7], together with ordinary (Einstein) diffusion in the vapor phase is taken also into account [V]. What is remarkable here is that the different tendencies observed for different species are predicted by the model by merely varying the empirical parameters m in Archie's law [V]. When the pore diameters are in the micrometer range or above, the validity of the fast exchange regime appears to be no longer valid [ard04].

In comparison with the typical diffusion times in NMR diffusometry [ard03] (10^{-3} to 10^{0} s), field-cycling NMR relaxometry can probe dynamics on much shorter time-scales, typically in the interval 10^{-10}-10^{-4} s.

With field-cycling NMR relaxometry we are preferentially probing the long-time limit $t >> \tau_{rot}$, where τ_{rot} is the correlation time for rotational diffusion in bulk or, in restricted form, in the adsorbed phase. Contributions by rotational diffusion therefore do not affect the low-frequency relaxation dispersion monitored with this technique. Field-cycling NMR

[7]The Knudsen regime occurs when the gas-wall collisions dominate over the gas-gas collisions.

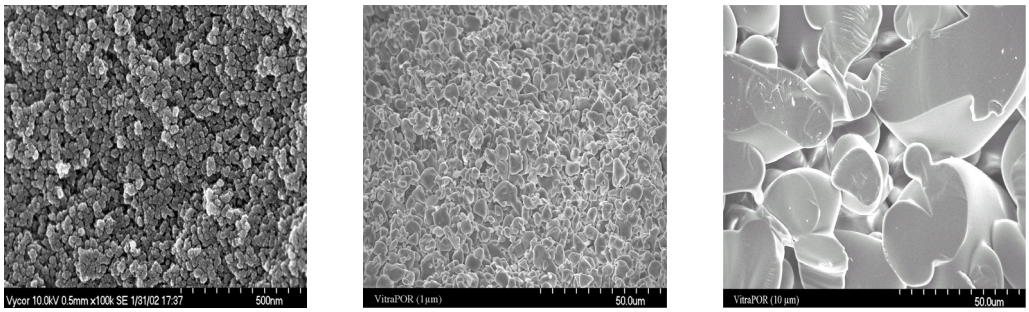

Figure 8: Electron micrographs of (from left to right) Vycor porous glass with a nominal mean pore size of 4 nm ($\pm$ 0.6 nm), VitraPOR#5 with a pore size specified between 1.0 μm and 1.6 μm and VitraPOR#4 with a pore size specified between 10.0 μm and 16.0 μm.

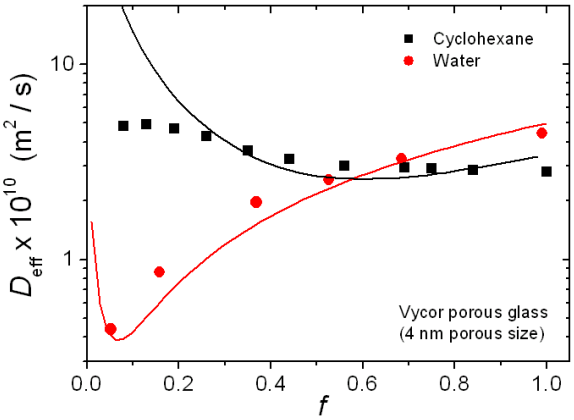

Figure 9: Effective water and cyclohexane diffusion coefficients in Vycor as a function of the filling factor f. The lines have been calculated with the two-phase fast-exchange model (see ref. [V]).

relaxometry measurements were performed in water and cyclohexane partially filling Vycor and VitraPOR porous glasses [III]. An illustration of the situation under consideration is represented in Fig.10, where a two-step exchange scheme of molecules in the adsorbed, liquid, and gaseous states is assumed.

A formalism involving molecular exchange was developed to explain the experimental spin-lattice relaxation times (Fig.11) obtained as a function of the filling degree. To simplify the analysis, exchange with the vapor phase is neglected. Its influence is considered later separately to explain some deviation of the model in the limit of very low filling degrees. Two limits are distinguished [III] with respect to the characteristic times $\tau_{a,b}$, corresponding to molecular exchange between the adsorption layer and the bulk-like phase, and τ_{rot}, the correlation time of rotational diffusion:

i) Fast correlation exchange limit, defined by $t >> \tau_{a,b} >> \tau_{rot}$. The relaxation rate is then

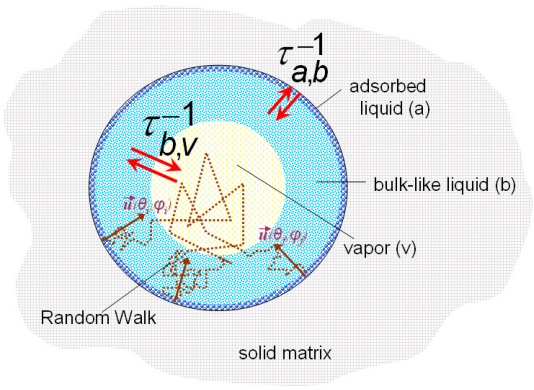

Figure 10: Schematic representation of a pore partially filled with an adsorbate liquid. Three phases, "adsorbed", "bulklike", and "vapor" are distinguished. NMR signals are dominated by the two liquid phases. The exchange rate between the adsorption layer and the bulklike liquid, $\tau^{-1}_{a,b}$, directly affects spin-lattice relaxation to be examined in this study. $\tau^{-1}_{b,v}$ is the exchange rate between the bulklike and the vapor phases. The orientation vectors on the surface $\vec{u}(\theta,\varphi)$ are represented together with a random walk of a molecule that exchange within the three phases.

$$\frac{1}{T_1} = \frac{1}{T_{1,b}} + \left(\frac{\lambda A}{V_0}\right)^2 \left(\frac{1}{T_{1,a}} - \frac{1}{T_{1,b}}\right) \frac{1}{f^2} \tag{21}$$

ii) Slow correlation exchange limit, defined by $\tau_{rot} << t << \tau_{a,b}$. In this case, the relaxation rate is

$$\frac{1}{T_1} = \frac{1}{T_{1,b}} + \frac{\lambda A}{V_0} \left(\frac{1}{T_{1,a}} - \frac{1}{T_{1,b}}\right) \frac{1}{f}, \tag{22}$$

where $T_{1,a}$ and $T_{1,b}$ are the spin-lattice relaxation times selectively expected for the RMTD mechanism in the adsorbed layer and the rotational diffusion process in the bulklike phase, respectively. A is the total area of the liquid-solid interface, and λ is the average width of the adsorbed layer. V_0 represents the total pore volume.

The deviation of the experimental data in Fig.11d at low filling degree f is remarkable and arises because of the influence of the vapor phase on spin-lattice relaxation in the adsorption layer. The exchange rate between the bulklike and the vapor phases, $\tau^{-1}_{b,v}$, is shown to affect spin-lattice relaxation only indirectly via the enhanced diffusivity in the vapor phase. At very low filling degrees when the contribution of the bulklike phase almost vanishes, a direct impact on the relaxation values can be seen. In all other cases, the effect is an indirect one due to the different populations of the adsorbed and bulklike phases [III]. No effect on the surface reorientation process is then observed, i.e., the relaxation time $T_{1,a}$ remains constant. In the case of fast correlation exchange and at very low filling factor, the indirect exchange between the three phases affects the reorientation mechanism. To account for these changes in an analytical way, one can refer to expression (20) of the spectral density for the static case ($v = 0$)

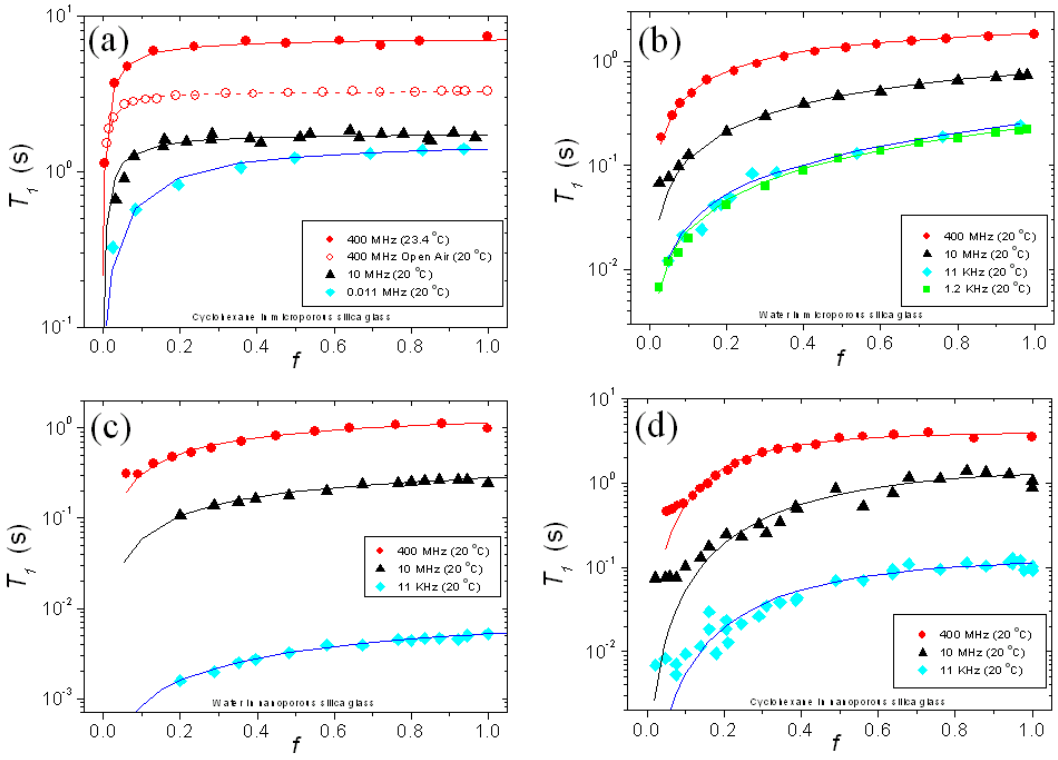

Figure 11: Spin-lattice relaxation rates as a function of the filling factor f. (a) Cyclohexane and (b) water in microporous glass (VitraPOR #5). (c) Water and (d) cyclohexane in nanoporous glass (Vycor). The solid lines in (a), (b) and (c) represent fits of the slow correlation exchange limit according to Eq. (22). The solid line in (d) represents the fast correlation exchange limit, according to Eq. (21).

$$\mathcal{I}(\omega) \;=\; \int_{-\infty}^{+\infty} S(k)\frac{2D_{eff}k^2}{(D_{eff}k^2)^2+\omega^2}\;dk. \tag{23}$$

D_{eff} is the effective diffusion coefficient, which is enhanced due to the exchange with the vapor phase, only relevant in the limit (*i*). $T_{1,a}$ is obtained by combining Eqs. (2) and (23).

A conspicuous observation here is that slow hydrodynamic flow and diffusion in the vapor phase in the fast correlation exchange limit affect the reorientation process at the liquid/solid interface in a similar way.

T_1 relaxation data of water and acetone in VitraPOR #4 porous glass (nominal pore size 10 μm) are shown in Fig.12a (these results are not published). The slow correlation exchange limit (*ii*) is observed in this case. Fig.12b shows high-frequency T_1 data of water and acetone as a function of the filling factor f. The slightly stronger dispersion of the water data indicates its stronger polar character, relative to acetone.

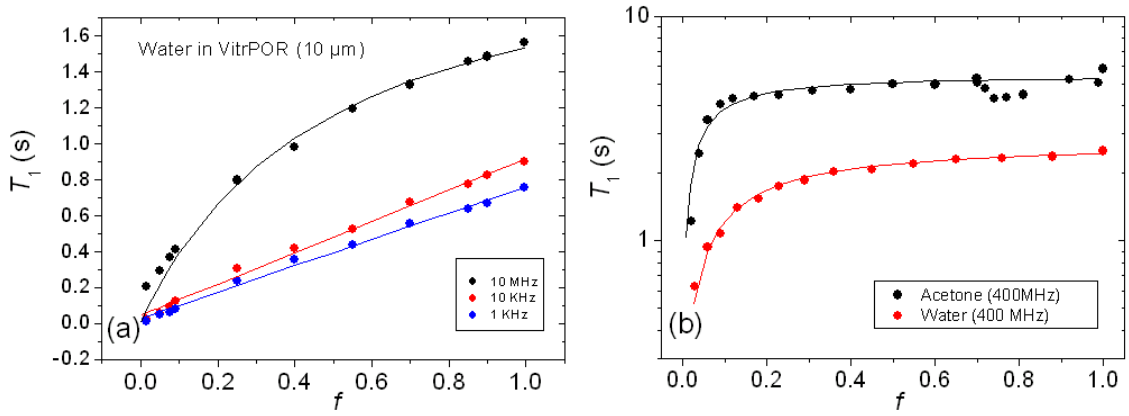

Figure 12: T_1 relaxation for unsaturated VitraPOR#4 with a pore size specified between 10.0 μm and 16.0 μm. These results are not published

4.3 Low frequency NMR relaxation mechanism

The RMTD relaxation mechanism was demonstrated by field-cycling NMR relaxometry in polar liquids confined in porous glasses [sta95, zav98]. A field-cycling experiment was performed with organic solvents of different polarities, acetone and cyclohexane in pore spaces of the same geometry but with polar and non-polar walls. The porous matrix[8] consists of a monolithic bimodal structure with pore sizes in the order of several nanometers and hundreds of nanometers. The experimental data are shown in Fig.13. The low frequency T_1 dispersion observed for both adsorbates can be completely analyzed in terms of the RMTD model assuming equipartition of wave numbers [kim97]. The data can be fitted with the combination of the Eq.(2) and the spectral density

$$\mathcal{I}(\omega) \;=\; \frac{2}{k_u - k_l} \int_{k_l}^{k_u} \frac{Dk^2}{(Dk^2)^2 + \omega^2}\, dk, \tag{24}$$

where k_u and k_l are the upper and lower cut-off magnitude values of the wave number describing the surface orientation [kim97, zav98] of the polar matrix (the fitted parameters are given in the caption of Fig.13). D is the diffusion coefficient of the confined liquid. These results confirm that the RMTD mechanism shows up also in the complementary limit of non-polar liquids confined in porous media with non-polar walls.

4.4 Confined polymer melts

NMR proton spin-lattice relaxation in PEO melts with molecular weights both above and below the critical molecular mass ($M_c \approx 5000$) was measured [IV] with the aid of the field-cycling technique, both in bulk and confined to nanoscopic strands embedded in a quasi-solid and impenetrable methacrylate matrix [fis04]. The frequency dependence of T_1 in bulk PEO for a molecular mass below the critical value is characteristic for Rouse

[8]The sample was synthesized in the department of Inorganic Chemistry I of the University of Ulm.

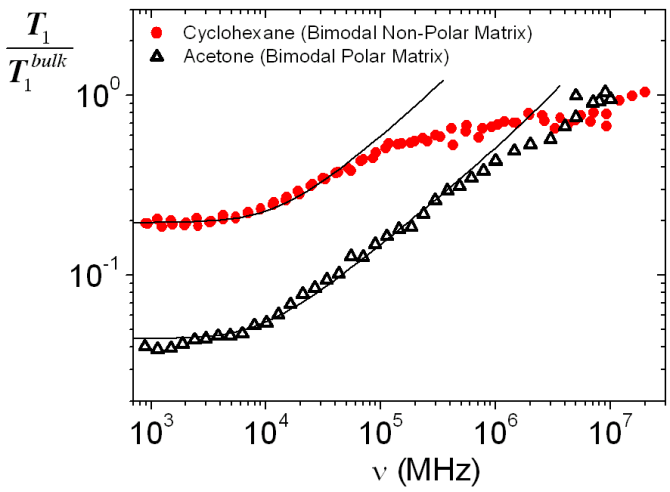

Figure 13: Organic liquids confined in monolithic bimodal porous matrices with different surface properties. The data are plotted relative to the values measured in bulk. The polarity of the solvent and the matrix is the same in each case: polar(non-polar) solvent in polar(non-polar) matrix. The solid lines represent Eq.(2) in combination with the spectral density (24). The diffusion coefficient was assumed to be the same as in bulk for each adsorbate at 20 ^{0}C. The fitted parameters were the wave vectors $k_u^{cyclohexane} = 10^8$ m^{-1}, $k_l^{cyclohexane} = 3.5{\times}10^6$ m^{-1}, $k_u^{acetone} = 1.35 \times 10^8$ m^{-1} and $k_l^{acetone} = 1.7 \times 10^6$ m^{-1}. The inverse of these values represent in a good approximation the two different porous sizes of the sample (see the text).

dynamics [kim04b]. For molecular masses above the critical value, T_1 has a power law dependence, as predicted by the renormalized Rouse theory [kim04b, fat94]. The situation changes dramatically when the PEO chains are confined in pores (see Fig.14) irrespective of whether their molecular mass is below or above M_c [IV]. T_1 dispersion above 300 kHz follows a power law characteristic for the tube/reptation model ($T_1 \propto \nu^{3/4}$) [doi86, kim04b]. PEO melts with molecular weights very close to M_c were also measured [kim05] under the same conditions. T_1 in bulk shows a behavior intermediate between Rouse and renormalized Rouse dynamics whereas under confinement, T_1 above 300 kHz follows a power law predicted by the tube/reptation model.

A "tube" diameter of only 0.5 nm was concluded [IV] to be effective on this time scale even when the diameter of the strands was larger than the radius of gyration of the PEO random coils. This confinement effect was called "corset effect" [IV, fat04] and results from the impenetrability of the pore walls, the low compressibility and the uncrossability of the polymer chains. The confinement dimension, expressed as a pore diameter, at which the cross-over from confined to bulk chain dynamics is expected was estimated [IV]:

$$d_{pore} >> \frac{b}{(k_B T \kappa_T)^{1/3}} R_F, \tag{25}$$

where b is the Kuhn segment length, R_F is the Flory radius, k_BT is the Boltzmann factor multiplied by the absolute temperature and κ_T is the isothermal compressibility. For PEO at 85^{0}C, Eq. (25) suggests $d_{pore} >> 10R_F$ as a condition for bulk behavior. This condition

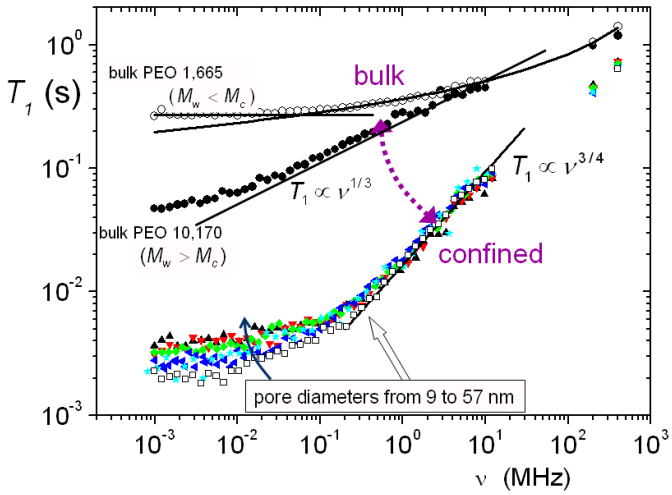

Figure 14: Frequency dependence of the proton spin-lattice relaxation times of linear PEO in bulk and confined in porous methacrylate samples at 85°C. The molecular masses of PEO were M_w = 1665 and 10 170. The data for PEO 1665 and PEO 10 170 are represented by open and filled symbols, respectively. The respective pore diameters of the different methacrylate samples were evaluated from NMR diffusometry data [fis04] to be 8, 13, 21, 33 and 58 nm. The PEO 1665 data refer to a pore diameter of 8 nm. The data at 200 and 400 MHz have been recorded with conventional high-field NMR spectrometers. The low-frequency T_1 values slightly increase with increasing pore diameter consistently. The upper solid curves were fitted to the experimental data of bulk PEO 1665 using equations predicted for the Rouse model with some influence of local segment dynamics. The straight lines refer to predictions by the renormalized Rouse theory and the tube/reptation concept.

was not fulfilled in the experiments reported here.

5 Discussion and Conclusions

The present work concerns the study of molecular dynamics in liquids confined in porous glasses and polymer melts confined in polymethacrylate matrices with field-cycling NMR relaxometry and field gradient NMR diffusometry experiments, combined with analytical model formalisms and numerical simulations. The main findings of this thesis can be summarized as follows:

- The effect of hydrodynamic flow on spin-lattice relaxation has been experimentally established and the effect explained by an analytical model and confirmed by Monte Carlo simulations.

- In porous silica glasses partially filled with liquids, a formalism for the description of the experimental effective spin-lattice relaxation times as a function of the filling degree was developed. Fast and slow correlation exchange limits are distinguished between the adsorption and bulklike phase. The slow correlation exchange limit characterized by a linear dependence of the spin-lattice relaxation rate on the filling degree was verified for all samples except for cyclohexane in nanoscopic pores. In the latter case, the quadratic dependence characteristic for the fast correlation exchange limit fits much better to the experimental data. This finding correlates well with the direct influence of the vapor phase for filling factors less than 0.2 observed for cyclohexane in Vycor.

- Diffusion in fluids confined in mesoporous glasses as a function of the liquid content is described in the limit of fast exchange relative to the diffusion time irrespective of the polarity of the solvents. Knudsen diffusion in the vapor phase turned out to be more effective in the case of the polar solvent (water in Vycor porous glass).

- Dynamics of polymers melts under confinement was found to differ strongly from the bulk behavior. Linear polyethylene oxide (PEO) was studied in a quasi-solid, cross-linked polymethacrylate matrix. That is, instead of the fictitious tubes assumed by Doi and Edwards to represent entanglements by neighboring chains, now real tubes formed by the nanoporous matrix are considered. The most relevant result is that neither the Doi/Edwards fictitious tube diameter nor the real pore diameter limit fluctuations by chain modes. It is rather an effective tube diameter essentially coinciding with the nearest neighbour distance characteristic for the tight chain packing in polymer melts. The pore diameter at which the crossover from confined to bulk behaviour occurs have been estimated to be d_{pore} much bigger that 10 times the Flory radius, as a condition for bulk behaviour.

2

Zusammenfassung

Seit die Wissenschaftler Felix Bloch und Edward M. Purcell im Jahre 1946 unabhängig voneinander die Kernmagnetische Resonanz (NMR) entdeckten, hat sich diese bis zum heutigen Tage in den Naturwissenschaften Medizin, Biologie, Chemie und der Physik als überaus nützliche Forschungstechnik erwiesen [nob03]. Die Kernmagnetische Resonanz bietet ein breites Feld von Anwendungen, wie beispielsweise bildgebende Verfahren "Magnetic Resonance Imaging" (MRI), welche in der Nuklearmedizin zu diagnostisdchen Zwecken oder auch für Studien in Bereichen der Chemie herangezogen werden. Die NMR-Techniken Relaxometrie und Diffusometrie [kim97] finden verstärkt Anwendung bei der Erforschung physikalisch-chemischer Eigenschaften von Objekten. Ein zentrales Forschungsgebiet, welches mit den Themen dieser Doktorarbeit in engem Zusammenhang steht, ist die Charakterisierung der Eigenschaften von Flüssigkeiten in porösen Materialien. Fluss und Massentransport in porösem Material stellen komplizierte Aufgabenstellungen dar und sind zum Beispiel in Bereichen wie Ölförderung, Grundwasserleitung, Brennstoffzellen und Kernreaktoren von besonderem Interesse [sah95, vaf00] .

Die Moleküldynamik einer Flüssigkeit in eingeschränkten Geometrien eines porösen Materials unterscheidet sich wesentlich von der derselben Flüssigkeit ohne Einschränkung durch Porenräume. Dies wurde durch zahlreiche Selbstdiffusions- [aks99, V, ard04, ban87, dor89, dor90a, dor90b, kim94, kim96, kor97] und Relaxationsuntersuchungen [aks99, ban87, kor97, lev03, sei00, sta95, zav98, zav99] an Systemen wie Wasser und organischen Lösungsmitteln in porösen Glassubstanzen und auch an Polymerschmelzen linearer Polymere unter Einschränkung in einer festen Methacrylat Matrix [fis99, kim99, sta96] unterstrichen. Eine der wichtigsten Folgerungen aus diesen Untersuchungen ist die Tatsache, dass die Abweichungen in den Versuchsergebnissen auf die Einschränkung der Moleküle durch den Porenraum oder auf deren Adsorption an der Porenoberfläche zurückgeführt werden können.

Im Unterschied zur NMR-Diffusometrie, wo Adsorption an den Porenwänden eine untergeordnete Rolle spielt [kim96] und vernachlässigt werden kann, können NMR-Relaxationsprozesse zur Erklärung der physikalischen Vorgänge an den Porenwänden aufgrund von "Reorientation mediated by translational displacements" (RMTD) Prozessen [kim97, sta95] als dominant angesehen werden. In solch einer Situation spiegelt die Spin-Gitter-Relaxations-Dispersionskurve bei niedrigen Frequenzen, also jenseits des Bereichs,

wo lokale Reorientierungen dominieren, die molekularen Bewegungen und auch die Oberflächentopologie wider. Hintergrund sind häufige Adsorptions-Desorptions-Wiederadsorptions Zyklen an den Porenwänden [byc95], die effektiv zu einer Diffusion der Moleküle entlang der Oberfläche führen. Im sogenannten "Strong-adsorption-limit" [kim02, zav98], beobachtbar bei polaren Flüssigkeiten, welche auf poröse Materialien mit polaren Oberflächen beschränkt sind, wurden mittels Field-cycling NMR relaxometry Korrelationszeiten acht Zehnerpotenzen höher als im "Bulk" beobachtet [sta95]. Während sich alle in der Literatur befindlichen Untersuchungen bis heute auf Flüssigkeiten in porösen Materialien mit polaren Oberflächen beziehen, soll in dieser Doktorarbeit auch auf nicht-polare Flüssigkeiten in porösen Materialien mit nicht-polaren Oberflächen eingegangen werden. Auch die Ergebnisse diese Untersuchungen können im Rahmen des RMTD Modells erklärt werden.

Das Forschungsproblem dieser Arbeit bestand hauptsächlich darin herauszufinden, unter welchen Bedingungen die beiden Szenarien, *(i)* Flüssigkeitsfluss durch das poröse Material und *(ii)* Flüssigkeiten in Koexistenz mit ihrer Gasphase im porösen Medium, die Dynamik der molekularen rotatorischen Bewegungen in der Grenzschicht zwischen Flüssigkeit und Porenwänden beeinflusst. Eine weitere Fragestellung bestand darin, wie geometrische Einschränkungen die Kettendynamik der Polymerschmelzen beeinträchtigen.

Hydrodynamische Dispersion ist ein Transportprozess von aktuellem Interesse [gho04, com97, gau04, kan02, low96, sch01]. Sie kann als eine überlagerung aus inkohärenter Brownscher Bewegung und kohärentem laminaren Fluss angesehen werden. In diesem Zusammenhang wird erwartet, dass ein gleichzeitiges Auftreten von hydrodynamischem Fluss und Oberflächendiffusion den RMTD Prozess ändert und so den Relaxationsvorgang beeinflusst. Das Field-cycling NMR Relaxometer wurde herangezogen, um die Auswirkung langsamer Fließgeschwindigkeiten, d.h. Geschwindigkeiten einiger Millimeter pro Sekunde, auf die Spin-Gitter-Relaxationsrate von Flüssigkeiten in porösen Materialien zu untersuchen [II]. Dies ist das erste NMR Relaxationsexperiment dieser Art. Die Auswirkung eines Flussexperiments auf die Spin-Gitter-Relaxationsrate wurde durch eine analytische Theorie, einer Kombination von hydrodynamischer Dispersion und dem RMTD-Modell, erklärt und zudem durch Monte Carlo (MC) Simulationen an Porenraum-Modellen gestützt [I].

In diesem Zusammenhang sind teilgefüllte poröse Materialien, ebenfalls von Interesse. In solchen Systemen werden für die Flüssigkeitsmoleküle drei Mobilitätszustände unterschieden: Adsorption an den Porenwänden, "bulkähnliche" flüssige Phase und die Gasphase. Älteren Veröffentlichungen [dor89, dor90a, dor90b, kim94] kann man entnehmen, dass der Selbstdiffusionskoeffizient von Wasser, in Silika-Gel-Glassubstanzen durch den Austausch mit der Gasphase beträchtlich ansteigt. In der vorliegenden Arbeit wurden Relaxation und Diffusion von Lösungsmitteln mit unterschiedlichen Benetzungseigenschaften in porösem Glas mit NMR Methoden untersucht. Die Ergebnisse zeigen, dass der effektive Diffusionskoeffizient von polaren und nicht-polaren Lösungsmitteln unterschiedliche Tendenzen aufweist, abhängig von der Art der Flüssigkeit [V]. Der effektive Diffusionskoeffizient von nicht-polaren Flüssigkeiten wird durch Anwesenheit der Gasphase im Porenraum erhöht, wohingegen das Diffusionsvermögen von Wasser mit abnehmendem Füllfaktor sinkt. Ein Zwei-Phasen-Austausch-Modell erklärt diese Erscheinungen. In der Gasphase werden beide, die Knudsen und die gewöhliche Diffusion, betrachtet. Die unterschiedlichen

Abhängigkeiten vom Füllfaktor für polare und nicht-polare Stoffe werden unterschiedlichen effektiven Tortuositäten zugeschrieben.

Spin-Gitter-Relaxationsexperimente mit teilweise gefülltem porösen Material zeigen ebenso starke Abhängigkeiten vom Füllfaktor, der Porengröße, sowie der Polarität [III]. Die Abhängigkeit der Spin-Gitter-Relaxationsrate vom Füllfaktor zeigt, dass Grenzen zwischen schnellem und langsamen Austausch zwischen adsorbierter und "bulkähnlicher" Phase ausgemacht und unterschieden werden können.

Im Fall von Polymerschmelzen, die in künstliche und dünnen Röhren einer porösen, festen Matrix mit einem variablen Durchmesser (9-57nm) eingebettet wurden, konnten Eigenschaften des Reptationsmodells [gen71, doi86] experimentell mit dem Field-cycling NMR Relaxometer (Protonenresonanz) nachgewiesen werden. Diese Beobachtungen sind unabhängig vom Molekulargewicht und von der Porengröße und reproduzieren im Wesentlichen die Inhalte einer früheren Deuteronen-Studie [kim99]. Ohne "Confinement" zeigt das gleiche Polymer Rouse- oder Renormalized Rouse Verhalten, jeweils abhängig vom Molekulargewicht. Bemerkenswert ist, dass die eingesperrten Polymere Reptation zeigen, selbst wenn der Porendurchmesser 15 mal größer als der Flory-Radius ist, wohingegen im "Bulk" keine Reptation bei gleichartigen Polymeren zu beobachten ist [IV]. Dieses Verhalten wurde "Korsett-Effekt" genannt und rührt von der Undurchdringbarkeit der festen Porenwände, der Undurchkreuzbarkeit der Polymerketten untereinander ("Excluded volume") und vom geringen Wert der Kompressibilität der Polymerschmelzen her. Der "Korsett-Effekt" schränkt seitliche Bewegungen der Polymerketten bis auf eine Längenskala von wenigen Zehntel Nanometer ein.

Bibliography

[abr61] A. Abragam, The Principles of Nuclear Magnetism (Clarendon Press, Oxford, 1961).

[aks99] D. W. Aksnes and L. Gjerdaker, NMR line width, relaxation and diffusion studies of cyclohexane confined in porous silica, J. Mol. Struct. **475**, 27 (1999).

[orb82] S.Alexander and R.Orbach, Density of states on fractals: "fractons.", J. Phys. Lett. (Paris) **43**, L-625 (1982).

[orb86] R. Orbach, Dynamics of Fractal Networks, Science **231**, 814 (1986).

[gho04] M. Al-Ghoul and B. C. Eu, Generalized hydrodynamics and microflows, Phys. Rev. E **70**, 016301 (2004).

[ano03] E. Anoardo and G. M. Ferrante, Magnetic Field Compensation for Field-Cycling NMR Relaxometry in the ULF Band, Appl. Magn. Reson. **24**, 85 (2003).

[ard03] I. Ardelean and R. Kimmich, Principles and Unconventional Aspects of NMR Diffusometry, Ann. Rep. NMR Spectrosc. **49**, 43 (2003).

[V] I. Ardelean, C. Mattea, G. Farrher, S. Wonorahardjo and R. Kimmich, Nuclear magnetic resonance study of the vapor phase contribution to diffusion in nanoporous glasses partially filled with water and cyclohexane, J. Chem. Phys. **119**, 10358 (2003).

[ard04] I. Ardelean, G. Farrher, C. Mattea and R. Kimmich, Nuclear magnetic resonance study of the vapor contribution to diffusion in silica glasses with micrometer pores partially filled with liquid cyclohexane or water, J. Chem. Phys. **120**, 9809 (2004).

[ari56] R. Aris, On the dispersion of a solute in a fluid flowing trough a tube, Proc. Roy. Soc. (London) A **235**, 67 (1956).

[ban87] J. R. Banavar and L. M. Schwartz, Magnetic resonance as a probe of permeability in porous media, Phys. Rev. Lett. **58**, 1411 (1987).

[blo48] N. Bloembergen, E. M. Purcell and R. V. Pound, Relaxation Effects in Nuclear Magnetic Resonance Absorption, Phys. Rev. **73**, 679 (1948).

[bro03] D. Brockmann and T. Geisel, Lévy Flights in Inhomogeneous Media, Phys. Rev. Lett. **90**, 170601 (2003);

[bun96] A. Bunde and S. Havlin (Eds.), Fractals and Disordered Systems (Springer, Berlin, 1996).

[byc94] O. V. Bychuk and B. O'Shaughnessy, Anomalous surface diffusion: A numerical study, J. Chem. Phys. **101**, 772 (1994).

[byc95] O. V. Bychuk and B. OShaughnessy, Anomalous diffusion at liquid surfaces, Phys. Rev. Lett. **74**, 1795 (1995).

[com97] A. Compte and J. Camacho, Lévy statistics in Taylor dispersion, Phys. Rev. E **56**, 5445 (1997).

[cop04] M. Coppey, O. Bénichou, J. Klafter, M. Moreau and G. Oshanin, Catalytic reactions with bulk-mediated excursions: Mixing fails to restore chemical equilibrium, Phys. Rev. E **69**, 036115 (2004).

[doi86] M. Doi and S. F. Edwards, The Theory of Polymer Dynamics (Oxford: Clarendon, 1986).

[dor89] F. D'Orazio, S. Bhattacharja, W. P. Halperin, and R. Gerhardt, Enhanced self-diffusion of water in restricted geometry, Phys. Rev. Lett. **63**, 43 (1989).

[dor90a] F. D'Orazio, S. Bhattacharja, W. P. Halperin, and R. Gerhardt, Fluid transport in partially filled porous sol-gel silica glass, Phys. Rev. B **42**, 6503 (1990).

[dor90b] F. D'Orazio, S. Bhattacharja, W. P. Halperin, K. Eguchi and T. Mizusaki, Molecular diffusion and nuclear-magnetic-resonance relaxation of water in unsaturated porous silica glass, Phys. Rev. B **42**, 9810 (1990).

[dul92] F. A. L. Dullien, Porous Media: Fluid Transport and Pore Structure (Academic Press, San Diego, 1992).

[fat94] N. Fatkullin and R. Kimmich, Nuclear spin-lattice relaxation dispersion and segment diffusion in entangled polymers. Renormalized Rouse formalism, J. Chem. Phys. **101**, 822 (1994).

[fat04] N. Fatkullin, R. Kimmich, E. Fischer, C. Mattea, U. Beginn and he confined-to-bulk dynamics transition of polymer melts in nanoscopic pores of solid matrices with varying pore diameter, New J. Phys. **6**, 46 (2004).

[fis99] E. Fischer, R. Kimmich, U. Beginn, M. Möller and N. Fatkullin, Segment diffusion in polymers confined in nanopores: A fringe-field NMR diffusometry study, Phys. Rev. E **59**, 4079 (1999).

[fis04] E. Fischer, U. Beginn, N. Fatkullin and R. Kimmich, Nanoscopic Poly(ethylene oxide) Strands Embedded in Semi-Interpenetrating Methacrylate Networks. Preparation Method and Quantitative Characterization by Field-Gradient NMR Diffusometry, Macromolecules **37**, 3277 (2004).

[gau04] M. G. Gauthier, G. W. Slater and K. D. Dorfman, Exact lattice calculations of dispersion coefficients in the presence of external fields and obstacles, Eur. Phys. J. E **15**, 71 (2004).

[gen71] P. G. de Gennes, Reptation of a polymer chain in the presence of fixed obstacles, J. Chem. Phys. **55**, 572 (1971).

[hou76] D.I. Hoult and R.E. Richards, The signal-to-noise ratio of the nuclear magnetic resonance experiment, J. Magn. Reson. **24**, 71 (1976).

[kan02] D. Kandhai, D. Hlushkou, A. G. Hoekstra, P. M. A. Sloot, H. Van As and U. Tallarek, Influence of Stagnant Zones on Transient and Asymptotic Dispersion in Macroscopically Homogeneous Porous Media, Phys. Rev. Lett. **88**, 234501 (2002).

[kim80] R. Kimmich, Field cycling in NMR relaxation spectroscopy: applications in biological, chemical and polymer physics, Bull. Magn. Reson. **1**, 195 (1980).

[kim94] R. Kimmich, S. Stapf, P. Callaghan and A. Coy, Microstructure of porous media probed by NMR techniques in sub-micrometer length scales, Magn. Reson. Imaging **12**, 339 (1994).

[kim96] R. Kimmich, S. Stapf, A. I. Maklalov, V. D. Skirda and E. V. Khozina, Self-Diffusion in fluids in porous glass: Confinement by pores and liquid adsorption layers, Magn. Reson. Imaging **14**, 793 (1996).

[kim97] R. Kimmich, NMR Tomography, Diffusometry, Relaxometry (Springer, Berlin, 1997).

[kim99] R. Kimmich, R-O. Seitter, U. Beginn, M. Möller and N. Fatkullin, Field-cycling NMR relaxometry of polymers confined to artificial tubes: verification of the exponent 3/4 in the spinlattice relaxation dispersion predicted by the reptation model, Chem. Phys. Lett. **307** 147 (1999).

[kim02] R. Kimmich, Strange kinetics, porous media, and NMR, Chem. Phys. **284**, 253 (2002).

[kim04a] R. Kimmich and E. Anoardo, Field-cycling NMR relaxometry, Progr. Nucl. Magn. Reson. Spectr. **44**, 257 (2004).

[kim04b] R. Kimmich and N. Fatkullin, Polymer Chain Dynamics and NMR, Adv. Polym. Sci. **170**, 1 (2004).

[kim05] R. Kimmich, N. Fatkullin, C. Mattea and E. Fischer, Polymer chain dynamics under nanoscopic confinements, Magn. Reson. Imaging. **23**, 191 (2005).

[kla96] J. Klafter, M. F. Shlesinger, G. Zumofen, Beyond Brownian Motion, Physics Today **49**, 33 (1996).

[koc85] D. L. Koch and J. F. Brady, Dispersion in fixed beds, J. Fluid Mech. **154**, 399 (1985).

[koc87] D. L. Koch and J. F. Brady, A non-local description of advection-diffusion with application to dispersion in porous media, J. Fluid Mech. **180**, 387 (1987).

[kor97] J. P. Korb, M. Whaley-Hodges and R. G. Bryant, Translational diffusion of liquids at surfaces of microporous materials: Theoretical analysis of field-cycling magnetic relaxation measurements, Phys. Rev. E **56**, 1934 (1997).

[kru04] M. Krucker, A. Lienau, K. Putzbach, M. D. Grynbaum, P. Schuler, K. Albert, Hyphenation of Capillary HPLC to Microcoil ^{1}H NMR Spectroscopy for the Determination of Tocopherol Homologues, Anal. Chem. **76**, 2623 (2004).

[lac04] A. M. Lacasta, J. M. Sancho, A. H. Romero, I. M. Sokolov and K. Lindenberg, From subdiffusion to superdiffusion of particles on solid surfaces, Phys. Rev. E **70**, 051104 (2004).

[leg03] L. Léger, Friction mechanisms and interfacial slip at fluidsolid interfaces, J. Phys.: Condens. Matter **15**, S19 (2003).

[len05] Y. Leng, P. T. Cummings, Fluidity of Hydration Layers Nanoconfined between Mica Surfaces, Phys. Rev. Letters **94**, 026101-1 (2005).

[lev97] P. Levitz, From Knudsen diffusion to Levy walks, Europhys. Lett. **39**, 593 (1997).

[lev03] P. Levitz, J. P. Korb and D. Petit, Slow dynamics of embedded fluid in mesoscopic confining systems as probed by NMR relaxometry, Eur. Phys. J. E **12**, 29 (2003).

[lev05] P. Levitz, Confined dynamics, forms and transitions in colloidal systems: from clay to DNA, Magn. Reson. Imaging **23**, 147 (2005).

[low96] C. P. Lowe and D. Frenkel, Do Hydrodynamic Dispersion Coefficients Exist?, Phys. Rev. Lett. **77**, 4552 (1996).

[man96] P. Mansfield and B. Issa, Fluid Transport in Porous Rocks. I. EPI Studies and a Stochastic Model of Flow, J. Magn. Reson. A **122**, 137 (1996).

[III] C. Mattea, R. Kimmich, I. Ardelean, S.Wonorahardjo, and G. Farrher, Molecular exchange dynamics in partially filled microscale and nanoscale pores of silica glasses studied by field-cycling nuclear magnetic resonance relaxometry, J. Chem. Phys. **121**, 10648 (2004).

[IV] C. Mattea, N. Fatkullin, E. Fischer, U. Beginn, E. Anoardo, M. Kroutieva and R. Kimmich, The "corset effect" of spin-lattice relaxation in polymer melts confined in nanoporous media, Appl. Magn. Reson. **27**, 371 (2004).

[II] C. Mattea and R. Kimmich, Flow-Enhanced Molecular Reorientations and Interfacial Slip Probed by Field-Cycling NMR Relaxometry in Microscopic Pores, Phys. Rev. Lett. **94**, 024502 (2005).

[I] C. Mattea, H. Tiraboschi and R. Kimmich, Effect of hydrodynamic flow on low-field spin-lattice relaxation in liquids in the nanoscopic vicinity of solid surfaces: Theory and Monte Carlo simulations of model pore spaces, Phys. Rev. E. **72**, 021602 (2005).

[noa86] F. Noack, NMR Field-Cycling Spectrocopy: Principles and applications, Prog. Nucl. Magn. Reson. Spectrosc. **18**, 171 (1986).

[nob03] It is worthy to mention that several Nobel Prizes were awarded in the field of NMR, establishing its importance in various fields: F. Bloch and E. M. Purcell (physics, 1952); R. R. Ernst (chemistry, 1991); K. Wüthrich (chemistry, 2002); P. Mansfield and P. C. Lauterbur (medicine, 2003).

[pak73] G.E. Pake and T.L. Estle, The Physical Principles of Electron Paramagnetic Resonance, Benjamin, Reading, 1973.

[sah95] M. Sahimi, Flow and Transport in Porous Media and Fractured Rock (VCH, Weinheim, 1995) and Rev. Mod. Phys. **65**, 1393 (1993).

[sch01] H. Schwarze, U. Jaekel and H. Vereecken, Estimation of Macrodispersion by Different Approximation Methods for Flow and Transport in Randomly Heterogeneous Media, Transp. Porous Media **43**, 265 (2001).

[sei00] R.-O. Seitter, T. Link (Zavada), R. Kimmich, A. Kobelkov, P. Wolfangel, K. Müller, Deuteron spectroscopy and deuteron field-cycling nuclear magnetic resonance relaxometry of the hydration water of lipid bilayers: The corrugated-sheet model for interface molecular dynamics in the ripple phase, J. Chem. Phys. **112**, 8715 (2000).

[sta95] S. Stapf, R. Kimmich and R.-O. Seitter, Proton and Deuteron Field-Cycling NMR Relaxometry of Liquids in Porous Glasses: Evidence for Lévy-Walk Statistics, Phys. Rev. Lett. **75**, 2855 (1995).

[sta96] S. Stapf and R. Kimmich, Field-cycling NMR relaxometry and field-gradient NMR diffusometry of polymers confined in porous glasses: Evidence for restricted-geometry effect, Macromolecules **29**, 1638 (1996).

[tay53] G. I. Taylor, Dispersion of soluble matter in solvent flowing slowly through a tube, Proc. Roy. Soc. (London) A **219**, 186 (1953).

[tra00] K. P. Travis and K. E. Gubbins, Poiseuille flow of Lennard-Jones fluids in narrow slit pores, J. Chem. Phys. **112**, 1984 (2000).

[vaf00] Handbook of Porous Media, K. Vafai (ed.) (Marcel Dekker, Inc., New York, 2000).

[vis96] G. M. Viswanathan, V. Afanasyev, S. V. Buldyrev, E. J. Murphy, P. A. Prince, and H. E. Stanley, Levy Flight Search Patterns of Wandering Albatrosses Nature (London) **381**, 413 (1996).

[zav98] T. Zavada, R. Kimmich, The anomalous adsorbate dynamics at surfaces in porous media studied by nuclear magnetic resonance methods. The orientational structure factor and Lévy walks, J. Chem. Phys. **109**, 6929 (1998).

[zav99] T. Zavada, R. Kimmich, J. Grandjean and A. Kobelkov, Field-cycling NMR relaxometry of water in synthetic saponites: Lévy walks on finite planar surfaces, J. Chem. Phys. **110**, 6977 (1999).

3

Publication List

1. R. Kausik, C. Mattea, N. Fatkullin and R. Kimmich, *Confinement effect of chain dynamics in micrometer thick layers of a polymer melt below the critical molecular weight*. Submitted.
2. I. Ardelean, G. Farrher, C. Mattea and R. Kimmich, *Fluid diffusion in partially filled nanoscopic and microscopic porous materials*, Modern Magnetic Resonance, 1-9, Graham A. Webb (ed.) Springer, 2006.
3. C. Mattea, H. Tiraboschi and R. Kimmich, *Effect of hydrodynamic flow on low-field spin-lattice relaxation in liquids in the nanoscopic vicinity of solid surfaces: Theory and Monte Carlo simulations of model pore spaces*, Phys. Rev. E. **72**, 021602 (2005). **(Included in the thesis)**
4. C. Mattea and R. Kimmich, *Flow-Enhanced Molecular Reorientations and Interfacial Slip Probed by Field-Cycling NMR Relaxometry in Microscopic Pores*, Phys. Rev. Lett. **94**, 024502 (2005). **(Included in the thesis)**
5. R. Kimmich, N. Fatkullin, C. Mattea and E. Fischer, *Polymer chain dynamics under nanoscopic confinement*, Magn. Res. Imag. **23**, 191 (2005).
6. I. Ardelean, G. Farrher, C. Mattea and R. Kimmich, *NMR study of the vapor phase contribution to diffusion in partially filed silica glasses with nanometer and micrometer pores*, Magn. Res. Imag. **23**, 285 (2005).
7. C. Mattea, R. Kimmich, I. Ardelean, S.Wonorahardjo, and G. Farrher, *Molecular exchange dynamics in partially filled microscale and nanoscale pores of silica glasses studied by field-cycling nuclear magnetic resonance relaxometry*, J. Chem. Phys. **121**, 10648 (2004). **(Included in the thesis)**
8. C. Mattea, N. Fatkullin, E. Fischer, U. Beginn, E. Anoardo, M. Kroutieva and R. Kimmich, *The "corset effect" of spin-lattice relaxation in polymer melts confined in nanoporous media*, Appl. Magn. Reson. **27**, 371 (2004). **(Included in the thesis)**
9. N. Fatkullin, E. Fischer, C. Mattea, U. Beginn and R. Kimmich, *Polymer dynamics under nanoscopic constraints: The "corset effect" as revealed by NMR relaxometry and diffusometry*, Chem. Phys. Chem. **5**, 884 (2004).

10. N. Fatkullin, R. Kimmich, E. Fischer, C. Mattea, U. Beginn and M. Kroutieva, *The confined-to-bulk dynamics transition of polymer melts in nanoscopic pores of solid matrices with varying pore diameter*, New Journal of Physics **6**, 46 (2004).
11. I. Ardelean, G. Farrher, C. Mattea and R. Kimmich, *Nuclear magnetic resonance study of the vapor contribution to diffusion in silica glasses with micrometer pores partially filled with liquid cyclohexane or water*, J. Chem. Phys. **120**, 9809 (2004).
12. R. Kimmich, N. Fatkullin, E. Fischer, C. Mattea and U. Beginn, *Reptation in Artificial Tubes and the Corset Effect of Confined Polymer Dynamics*, Mat. Res. Soc. Symp. Proc. **790** P9.1.1 (2004).
13. I. Ardelean, C. Mattea, G. Farrher, S. Wonorahardjo and R. Kimmich, *Nuclear magnetic resonance study of the vapor phase contribution to diffusion in nanoporous glasses partially filled with water and cyclohexane*, J. Chem. Phys. **119**, 10358 (2003). **(Included in the thesis)**
14. C. Mattea and A. Brunetti, *Nuclear quadrupole resonance in 2,4-dinitrochlorobenzene*, Journal of Molecular Structure (Theochem) **594**, 215 (2002).

4

Curriculum Vitae

Personal Data



- **Name: Mattea Carlos**
- **Nationality:** Argentine
- **Place of Birth:** Villa María, Córdoba, Argentina
- **Date of Birth:** January 27th, 1966
- **e-mail:** carlos.mattea@uni-ulm.de

Academic Degree

- Position as a Ph. D. student in Sektion Kernresonanzspektroskopie (Division for Nuclear Magnetic Resonance) Ulm University, Germany, in the period of November 22nd, 2001 - December 31st, 2005.
- Licentiate in Physics, Facultad de Matemática, Astronomía y Física (Fa.M.A.F.), National University of Córdoba (U.N.C.), Córdoba, Argentine, December 1999.

Fellowships

1. Travel grant offered by GlaxoSmithKline Stiftung (Germany) for the participation to the Gordon Research Conference on Magnetic Resonance. June 2005. New London, Connecticut, USA.
2. Guest in Sektion Kernresonanzspektroskopie (Division for Nuclear Magnetic Resonance) Ulm University, Germany, in the period of May 10th - August 10th, 2001.
3. *NMR study of hydration and solubility of powder-milk.* Fellowship from the National University of Córdoba, Argentine, for university extension activities. From January to December, 2000.
4. *Feasibility study of NMR techniques for quality control in food and/or seeds.* Fellowship from the National University of Córdoba, Argentine, for university extension activities. From January to December, 1992.

Oral Presentations in Congress

1. *Hydrodynamic dispersion in the nanoscopic vicinity of surfaces in porous materials investigated by field-cycling NMR relaxometry and Monte Carlo simulations*, C. Mattea and R. Kimmich. 4th Conference on Field-Cycling NMR Relaxometry, 26th-28th May 2005, Turin, Italy.

Congress Presentations

1. *From "Fast" to "Slow" Liquid-vapor Exchange in Partially Filled Porous Media. A Field-gradient NMR Diffusometry Study*, I. Ardelean, G. Farrher, C. Mattea and R. Kimmich, Diffusion Fundamentals I, 21st-24th September 2005, Leipzig, Germany.
2. *NMR investigation of the vapor contribution to diffusion in porous media partially filled with liquids*, I. Ardelean, G. Farrher, C. Mattea and R. Kimmich, EUROMAR-EENC 2005, Veldhoven, The Netherlands, 3rd-8th July 2005.
3. *Polymer chain dynamics under nanoscopic constrains*, C. Mattea, N. Fatkullin and R. Kimmich. 5th International Discussion Meeting on Relaxations in Complex Systems 2005. July 7th-13th, 2005. Lille, France.
4. *Nano- and micropore confinement effects detected by field-cycling NMR relaxometry*, R. Kimmich, C. Mattea and N. Fatkullin. XXI International Meeting on Radio and Microwave Spectroscopy RAMIS 2005: Application to Modern Materials. Poznan-Bedlewo, Poland, April 24th-28th, 2005.
5. *The flow-relaxation effect: Hydrodynamic dispersion in the nanoscopic vicinity of surfaces in porous materials investigated by field-cycling NMR relaxometry and Monte Carlo simulations*, C. Mattea and R. Kimmich. Gordon Research Conference on Magnetic Resonance. June 5th-10th, 2005. Connecticut College, New London, Connecticut, USA.
6. *Field-cycling and rotating frame relaxometry of mesoscopic polymer melt layers*, R. Kausik, C. Mattea and R. Kimmich, 4th Conference on Field Cycling NMR Relaxometry, 26th-28th May 2005, Turin, Italy.
7. *Molecular exchange dynamics in partially filled micro and nanoscale pores of silica glasses studied by field-cycling NMR relaxometry*, C. Mattea, G. Farrher, I. Ardelean, E. Anoardo and R. Kimmich. 26th Annual Anglo-German Discussion Meeting, University of Aachen RWTH, Germany, September 28th-30th, 2004.
8. *Two Phase Fast Exchange Dynamics in Partially Filled Porous Glasses Studied by Field-Cycling NMR Relaxometry*, C. Mattea, I. Ardelean, E. Anoardo, S. Wonorahardjo and R. Kimmich. 7th International Conference on Magnetic Resonance in Porous Media, July 4th-8th, 2004. Palaiseau, France.
9. *Proposal of a flow induced relaxation mechanism in porous media*, H. Tiraboschi, C. Mattea and R. Kimmich. 7th International Conference on Magnetic Resonance in Porous Media, July 4th-8th, 2004. Ecole Polytechnique, Palaiseau, France.

10. *NMR study of the vapor phase contribution to diffusion in partially filled silica glasses with nanometer and micrometer pores*, I. Ardelean, G. Farrher, C. Mattea and R. Kimmich. 7th International Conference on Magnetic Resonance in Porous Media, July 4th-8th, 2004. Ecole Polytechnique, Palaiseau, France.

11. *Contribution of the Vapor Phase in Molecular Diffusion in Partially Filled Porous glasses*, G. Farrher, I. Ardelean, C. Mattea, R. Kimmich, October 12th-14th 2003, Heinrich-Fabri-Institut, Blaubeuren, Germany.

12. *Molecular Dynamics in Partially Saturated Porous Glasses*, C. Mattea, S. Wonorahardjo, I. Ardelean, E. Anoardo, R. Kimmich; 88th Meeting of the Argentinean Physics Association (AFA), Bariloche, Rio Negro, Argentine, September 2003.

13. *Molecular Diffusion in Partially Filled Porous Media: NMR investigations*, I. Ardelean, C. Mattea, G. Farrher and R. Kimmich; AMPERE XI NMR SCHOOL, June 1st-6th, 2003, Zakopane, Poland.

14. *Molecular Dynamics in Partially Saturated Porous Glasses Studied by NMR Relaxometry*, C. Mattea, S. Wonorahardjo, I. Ardelean, E. Anoardo and R. Kimmich; 3rd Conference on Field Cycling NMR Relaxometry, 23rd-25th May 2003, Turin, Italy.

15. *NMR Diffusion-Relaxation in Three-Phase Fast Exchange System*, S. Wonorahardjo, I. Ardelean, C. Mattea and R. Kimmich. 6th International Conference on Magnetic Resonance in Porous Media, September 8th-12th 2002, Ulm, Germany.

16. *Nuclear quadrupole resonance in 2,4-dinitrochlorobenzene*, C. Mattea and A. Brunetti; 30th Congress Ampere on Magnetic Resonance and Related Phenomena, Lisbon - Portugal, July 2000.

17. *Study of 2,4-dinitroclorobenceno by means of nuclear quadrupolar resonance*, C. Mattea and A. Brunetti, 85th Meeting of the Argentinean Physics Association (AFA), Buenos Aires, Argentine, September 2000.

18. *Study of grain boundary of low energy in polycrystalline of pure ice*, P. Derosa, C. Meriles, C. Mattea, J. Neirotti and C. Di Prinzio, 75th Meeting of the Argentinean Physics Association (AFA), La Plata, Buenos Aires, Argentine, 1990.

Meeting attendance

1. *2nd Stelar Fast Field-Cycling User Meeting*, 23rd May 2003, Turin, Italy.
2. *3rd Stelar Fast Field-Cycling User Meeting*, 25th May 2005, Turin, Italy.

Seminars

1. *"Molecular Surface Reorientation in the frame of Hydrodynamic Dispersion"*, Alpine Group Seminar, March 21st-25th 2005. Hirschegg, Kleines Walsertal, Austria.

2. *"Spin-Lattice NMR Relaxation in Non-Saturated Nano and Microporous Media"*, Transylvanian Workshop in Paltinis: "Frontiers of Magnetic Resonance. Applications to Nano and Microscopically Structured Systems" Alexander-von-Humboldt Institute Partnership. Paltinis, Rumania, February 25th - March 1st, 2004.
3. *"Limits of Field-Cycling NMR Relaxometry"*, Alpine Group Seminar, March 17th-21st 2003. Hirschegg, Kleines Walsertal, Austria.
4. *"NMR Relaxation and Diffusion in Partially Filled Porous"*, Abteilungsseminar, Universitt Ulm, Sektion Kernresonanzspektroskopie. November 2002.
5. *"The Effect of Flow on NMR Relaxation in Porous Media. An Introduction"*, Alpine Group Seminar, March 18th-22nd 2002. Hirschegg, Kleines Walsertal, Austria.
6. *"Second harmonic generation in Molecular Solids. Structural influences in the optical non-linear response"*, Fa.M.A.F., National University of Córdoba, Argentine, 1999.
7. *"NQR study of Chlorinated Nitrobenzenes"*, Fa.M.A.F., National University of Córdoba, Argentine, 1999.

Teaching experience

- Analysis I, Instituto Universitario Aeronáutico, Córdoba, Argentine. 1st Semester, 2001.
- Physics I, Instituto Universitario Aeronáutico, Córdoba, Argentine. 1st Semester, 2001.
- Advisory course to secondary school teachers. (Activities and discussion on some aspects of the processes of teaching Mechanics and Thermodynamics). Escuela Superior Integral de Lechera (E.S.I.L.), Villa María, Córdoba, Argentina. March, 2001.
- Physics II (Chemistry Department), U.N.C., 2nd Semester, 2000.
- Admission course, Fa.M.A.F., U.N.C., 1st Semester, 2000.
- Physics I (Mechanics), Fa.M.A.F., U.N.C., 2nd Semester, 1999.
- Laboratory I (Chemistry Department), U.N.C., 1st Semester, 1999.
- Physics III (Electricity and Magnetism), Fa.M.A.F., U.N.C., 2nd Semester, 1998.

Other experiences

- Test-measurements in a Fast Field-Cycling relaxometer in the Company "Stelar SRL", Mede, Italy. November 4th-6th 2004 and June 23rd-25th 2003.
- Member of the Local Organizing Committee of the 6th International Conference on Magnetic Resonance in Porous Media, September 8th-12th 2002, Ulm, Germany.

Lic. Carlos Mattea

Ulm, December 2005

5

Original papers

I

C. Mattea, H. Tiraboschi and R. Kimmich.

Effect of hydrodynamic flow on low-field spin-lattice relaxation in liquids in the nanoscopic vicinity of solid surfaces: Theory and Monte Carlo simulations of model pore spaces.

Phys. Rev. E. **72**, 021602 (2005).

Effect of hydrodynamic flow on low-field spin-lattice relaxation in liquids in the nanoscopic vicinity of solid surfaces: Theory and Monte Carlo simulations of model pore spaces

Carlos Mattea, Hernan Tiraboschi, and Rainer Kimmich
Sektion Kernresonanzspektroskopie, Universität Ulm, 89069 Ulm, Germany
(Received 19 April 2005; published 22 August 2005)

It is shown that slow hydrodynamic flow with velocities of a few millimeters per second reduces the spin-lattice relaxation rate of fluids confined to pores of a diamagnetic, polar, solid material. The effect is predicted by an analytical theory and Monte Carlo simulations of model pore spaces. Adsorbate molecules diffusing in the vicinity of pore surfaces can perform adsorption, desorption, and readsorption cycles, effectively leading to displacements along the surface (also termed "bulk mediated surface diffusion" or BMSD). Since the surface determines the orientation of the adsorbed molecule relative to the external magnetic field, desorption at one site and readsorption at another site of a nonplanar surface will cause molecular reorientation. This is the basis of the "reorientation mediated by translational displacements" (RMTD) relaxation mechanism. If hydrodynamic flow is superimposed on diffusion, the RMTD process will be accelerated in a sort of rotational analog to translational hydrodynamic (or Taylor-Aris) dispersion. This reveals itself by a prolongation of spin-lattice relaxation times at low frequencies. The flow-relaxation effect takes place in the vicinity of the pore surfaces on the order of nanometers. The conclusions are (i) the BMSD and RMTD relaxation mechanism of fluids in porous materials is corroborated, (ii) hydrodynamic dispersion affects molecular displacements at surfaces, and (iii) interfacial slip in the sense of a molecular hopping, i.e., a desorption-readsorption process takes place.

DOI: 10.1103/PhysRevE.72.021602 PACS number(s): 47.55.Mh, 76.60.Es, 82.56.Na, 83.50.Lh

I. INTRODUCTION

The objective of this study is to examine the influence of hydrodynamic flow on low-frequency spin-lattice relaxation in fluids confined in microporous media analytically and numerically. The envisaged frequency and time scales are $10^3 < \nu < 10^8$ Hz and $10^{-9} < t < 10^{-4}$ s, respectively, corresponding to field-cycling NMR relaxometry [1]. Following our previous report [2], the motivation to do so has three aspects.

First, this sort of study is suitable to elucidate the low-field spin-lattice relaxation mechanism for strong adsorbate fluids in porous media suggested in Refs. [3,4]. Dipolar and quadrupolar orientation correlation times up to seven orders of magnitude longer than in the bulk fluid were observed in nanoporous materials. The explanation was the so-called reorientation mediated by translational displacements (RMTD) process. Adsorbate molecules are subject to frequent adsorption-desorption-readsorption cycles at the pore walls [5]. Bulk mediated surface diffusion (BMSD) produces Lévy-walk-like displacements along the pore surface [5–8], which explain how the adsorbate molecules probe the surface topology with respect to the orientation relative to the main magnetic field [4,9,10]. Under such conditions hydrodynamic flow superimposed on surface diffusion is expected to accelerate the RMTD process (see Fig. 1).

Second, hydrodynamic (or Taylor-Aris) dispersion [11,12], that is, the superposition of incoherent Brownian particle motions and coherent flow, is of general interest [13–18]. In the vicinity of surfaces the question arises whether interfacial slip exists. Since we are dealing with a surface relaxation process, a detailed examination of the valid flow boundary condition is possible.

Finally, field-cycling NMR relaxometry [1] probes molecular mechanisms on a time scale up to 10^{-4} s. That is, molecular root mean square displacements by Brownian motions are much less than 100 nm in water at room temperature. Flow can therefore influence surface relaxation only in a surface layer thinner than 100 nm. In a sense, nanofluidics can be examined on this basis.

The flow and relaxation scenario considered here is illustrated in Fig. 1. The model refers to a liquid in the pore space of a porous medium. We distinguish the phase of molecules adsorbed at the surface from the bulklike phase. On the time scale of the proton spin-lattice relaxation times, which is for field-cycling relaxometry typically $10\ \text{ms} < T_1 < 1$ s, fast molecular exchange between the two phases occurs. Hydrodynamic flow is assumed to be superimposed on Brownian motion of the molecules. In case the liquid molecules and the pore surfaces are both polar, molecules in the vicinity of the surfaces will be subject to adsorption and desorption kinetics including possible readsorption cycles. The reorientation of molecules that happen to be adsorbed initially as well as finally will thus depend on displacements and readsorption at a more or less distant surface site of a different orientation. These displacements are the combined result of Brownian motions and laminar flow, that is, hydrodynamic dispersion.

The hydrodynamic dispersion properties are usually characterized by the Péclet number defined by

$$\text{Pe} = \frac{f\xi}{wD_m}, \tag{1}$$

where ξ is the correlation length of the pore space, f is the hydrodynamic flux, D_m is the molecular diffusion constant in the bulk, and w is the pore width. In the following the Péclet number will be taken as a measure of the mean flow velocity relative to Brownian diffusion.

 ©2005 The American Physical Society

Following the bulk mediated surface diffusion formalism of Bychuk and O'Shaughnessy [5,6] different adsorption and desorption probabilities per time unit, Q_{ads} and Q_{des}, respectively, can be distinguished. The adsorption on surfaces can be characterized by a number of characteristic parameters. The retention time t_h reflects how long it takes until the initial adsorbate population on a surface is finally replaced by molecules initially in the bulklike phase. The retention time is related to the so-called adsorption depth h according to

$$t_h = \frac{h^2}{D_m}. \tag{2}$$

On the other hand, the adsorption length can be expressed by

$$h = \lambda \frac{Q_{ads}}{Q_{des}}, \tag{3}$$

where λ is the "capture range" within which a molecule can directly be adsorbed on the surface. This equation is based on a dynamic equilibrium of the one-dimensional "reaction-diffusion" process as which adsorption and translational diffusion to and from the surface can be interpreted. The time scale of desorption-diffusion-readsorption cycles is given by $Q_{des}^{-1} < t < t_h$, and was shown to be of the same order of magnitude as the time scale probed by field-cycling NMR relaxometry [1,4].

The weak-adsorption limit is characterized by

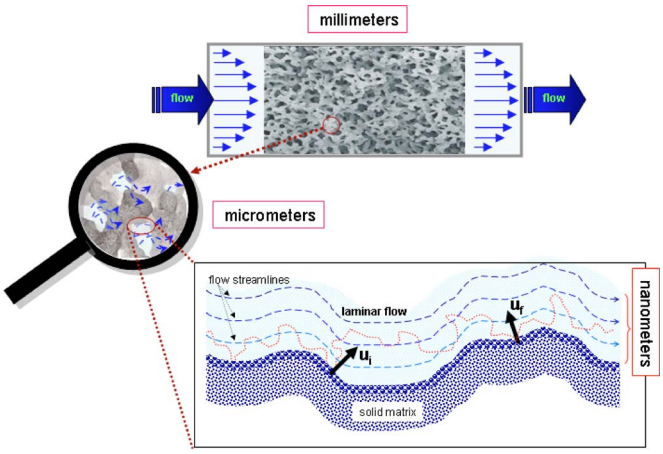

FIG. 1. (Color online) Illustration of the flow-relaxation effect and adsorbate reorientation by hydrodynamic dispersion. A liquid is pressed through a porous sample (top part of the figure). The liquid flows along the pore surfaces (bottom part of the figure). The dotted line represents a trajectory of a molecule by Brownian motion in the presence of laminar flow along the surface. Flow streamlines are drawn as broken lines. The adsorption layer on the solid matrix is indicated. The arrows refer to the local preferential orientations of molecules at the initial and final pore surface sites. The thickness of the fluid layer along the surface in which the flow enhanced RMTD process is expected to take place ranges from molecular diameters up to about 100 nm.

$$t_h Q_{des} \ll 1. \tag{4}$$

That is, the adsorbate molecules are most likely exchanged to the bulklike phase immediately after desorption. This is in contrast to the strong-adsorption limit

$$t_h Q_{des} \gg 1, \tag{5}$$

in which numerous desorption-readsorption cycles occur before an adsorbate molecule finally disappears in the bulklike phase. This strong-adsorption limit must be assumed for a combination of polar adsorbate molecules and polar surfaces [3,4]. In the present study we are dealing with this case.

In Sec. II a general analytical formalism will be outlined for the flow-relaxation effect in terms of the dipolar autocorrelation function and spectral density. Representing the pore space by a number of simplified model structures permits one to examine the principal properties of this effect with the aid of Monte Carlo simulations as described in Sec. III. The results of analytical model treatments specific for those model structures will be compared and fitted to the evaluations of the simulations. Finally we will discuss the intricacies of experimental verifications of the flow-relaxation effect.

II. GENERAL THEORY OF THE FLOW-NMR-RELAXATION EFFECT

The spin-lattice relaxation rate of a two-spin-1/2 system ensemble of like nuclei subject to dipolar coupling is given by [19,20]

$$\frac{1}{T_1} = K[I(\omega) + 4I(2\omega)], \tag{6}$$

where K is a constant determined by the type and strength of the spin interaction. The spectral density (or intensity function) $I(\omega)$ depends on the resonance angular frequency $\omega = \gamma B_0$, where γ is the gyromagnetic ratio and B_0 is the flux density of the main magnetic field. The spectral density is the

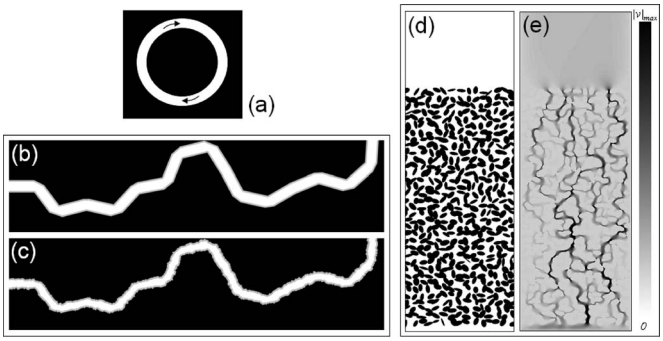

FIG. 2. The diverse geometries of two-dimensional pore spaces used for the Monte Carlo simulations. The pores are represented in white. (a) Circular pore. Random-walk-shaped pipes with (b) smooth and (c) rough surfaces. (d) Ellipsoidal-grain pack. (e) Map of the magnitudes of the flow velocity simulated with the finite volume method for the ellipsoidal-grain pack. The velocity field obtained in this way was used for the Monte Carlo simulations of the flow-relaxation effect described in Sec. IV B 3.

Fourier transform of the autocorrelation function $G(t)$. For intramolecular dipolar interaction (which is relevant here [3,4]), $G(t)$ refers to spherical harmonics of second order characterizing the orientation of the two-spin system relative to the main magnetic field. That is, spin-lattice relaxation probes molecular reorientations.

Spin-lattice relaxation in porous media at frequencies much less than the bulk reorentation rates of the molecules was shown to be governed by the RMTD mechanism at the pore surfaces [4,9,20]. The problem is now to generalize this formalism for superimposed hydrodynamic flow, i.e., hydrodynamic dispersion.

The curvilinear coordinate along a streamline along the surface will be defined as x (see Fig. 1). Descriptions of hydrodynamic dispersion in bulk fluids can be found in Refs. [21–24]. For scalar fields and incompressible fluids, the convective-diffusion equation applies:

$$\frac{\partial \Psi}{\partial t} + \vec{V} \cdot \nabla \Psi = \tilde{D} \cdot \nabla^2 \Psi. \tag{7}$$

The function Ψ is the propagator, $\vec{V}$ is the average over the local velocities $\vec{v}$, and $\tilde{D}$ is the dispersion tensor. In the case of macroscopically homogeneous and isotropic porous media, $\tilde{D}$ can be decomposed into the components $D_\perp$ and $D_\parallel$ orthogonal and parallel to the flow velocity $\vec{V}$, respectively. The convective-diffusion equation then becomes

$$\frac{\partial \Psi}{\partial t} + \vec{V} \cdot \nabla \Psi = D_\perp \nabla_\perp^2 \Psi + D_\parallel \frac{\partial^2 \Psi}{\partial \mathbf{x}^2}, \tag{8}$$

where $\nabla_\perp^2$ is the Laplace operator in the transverse direction. The dispersion coefficients $D_\perp$ and $D_\parallel$ depend on the flow velocity, of course. In the limit of vanishing flow velocities, $D_\parallel$ becomes equal to the molecular diffusion coefficient (D_m) diminished by the tortuosity factor.

In the present context, only the longitudinal version of hydrodynamic dispersion is of interest, that is, the projection of Eq. (8) on the x direction. In this case, $D=D_\parallel$ can be equated. After Fourier transformation the solution is

$$\psi(k,t) = \hat{\psi}(k) e^{-Dtk^2} e^{-ikvt}, \tag{9}$$

where $\hat{\psi}(k)$ is the Fourier transform of $\Psi(x,0)$ and v is the velocity component in longitudinal direction. The "wave number" k is the reciprocal-space variable conjugate to the real-space variable x. With the initial condition $\Psi(x,0) = c_0 \delta(x)$ the conjugate Fourier expression reads

$$\Psi(x,t) = \frac{c_0}{2\pi} \int_{-\infty}^{+\infty} e^{-(Dtk^2+ikvt)} e^{ixk} dk. \tag{10}$$

Note that the Gaussian term in the propagator given in Eq. (9) or Eq. (10) anticipates ordinary diffusion. There is some argument based on the BMSD model by Bychuk and O'Shaughnessy [5,6,8] that features of Lévy walks along the surface are relevant so that a Cauchy propagator would be more appropriate [3,4,25]. For simplicity we will restrict ourselves in the analytical treatment to the ordinary diffusion case. The objective of the present study is to reveal the influence of coherent flow on spin-lattice relaxation whereas the type of diffusion process is considered to be of minor importance in this context. The Monte Carlo simulations should anyway reflect the actual propagators, of course.

The autocorrelation function describing orientational fluctuations of molecules with fixed intramolecular interdipole distances can be expressed by [19,20]

$$G(t) = 4\pi \langle Y_{2,m}(\vec{u}_i) Y_{2,-m}(\vec{u}_f) \rangle_{\vec{u}_i,\vec{u}_f}$$
$$= \int \langle P_c(\vec{u}_i,\vec{u}_f,t) Y_{2,m}(\vec{u}_i) \rangle_{\vec{u}_i} Y_{2,-m}(\vec{u}_f) d\Omega_f, \tag{11}$$

where the angular brackets indicate ensemble averages. $\vec{u}_i$ and $\vec{u}_f$ are unit vectors normal to the surface indicating the initial and the final orientations of the molecule under consideration (see Fig. 1). $d\Omega_f$ is the differential solid angle into which $\vec{u}_f$ points. In the usual spin-lattice relaxation theory of dipolar coupled like spins subscripts $m=1$ and 2 occur [19,20]. However, no distinction will be made in the following since this causes only minor differences in the results. In the Monte Carlo simulations even the value $m=0$ will be used for simplicity without loss of validity of the principle [26].

The conditional probability density can be expressed as

$$P_c(\vec{u}_i,\vec{u}_f,t) = \int_{-\infty}^{\infty} \Theta(\vec{u}_i,\vec{u}_f,x) \Psi(x,t) dx, \tag{12}$$

where $\Psi(x,t)$ is the surface diffusion propagator, i.e., the probability density that the adsorbate molecule is displaced by a curvilinear distance x along the surface in an interval t, and $\Theta(\vec{u}_i,\vec{u}_f,x)$ is the probability that the surface orientation changes from $\vec{u}_i$ to $\vec{u}_f$ in a curvilinear distance x.

Using the expansion in terms of spherical harmonics with the initial condition $\Theta(\vec{u}_i,\vec{u}_f,0) = \delta(\vec{u}_f - \vec{u}_i)$ the surface orientation probability density becomes

$$\Theta(\vec{u}_i,\vec{u}_f,x) = \sum_{l',m'} Y_{l',-m'}(\vec{u}_i) Y_{l',m'}(\vec{u}_f) g(x), \tag{13}$$

where $g(x)$ is the normalized surface orientation correlation function between surface sites separated by a curvilinear distance x. "Normalized" means that $g(x=0)=1$. The combination of Eqs. (11)–(13), and making use of the orthonormal properties of spherical harmonics, leads to

$$G(t) = \int_{-\infty}^{\infty} g(x) \Psi(x,t) dx. \tag{14}$$

Inserting the propagator given in Eq. (10) in Eq. (14) leads to

$$G(t) = \int_{-\infty}^{+\infty} g(x) \left(\frac{c_0}{2\pi} \int_{-\infty}^{+\infty} e^{-(Dtk^2+ikvt)} e^{ikx} dk \right) dx. \tag{15}$$

Regrouping the factors that depend only on the space variable x results in the orientational structure factor

$$S(k) = \frac{c_0}{2\pi}\int_{-\infty}^{+\infty} g(x)e^{ikx}dx. \tag{16}$$

The autocorrelation function given in Eq. (11) can thus be rewritten as

$$G(t) = \int_{-\infty}^{+\infty} S(k)e^{-(Dtk^2+ikvt)}dk. \tag{17}$$

A typical application of this general formula to the case of a simple circular pore is given in Eq. (27). Treatments of other pore-space structures will follow.

The Fourier transform of Eq. (17) is the corresponding spectral density. Its real part reads

$$I(\omega) = \int_{-\infty}^{+\infty} S(k)\frac{2Dk^2}{(Dk^2)^2 + (kv+\omega)^2}dk. \tag{18}$$

Up to now a given flow velocity v was assumed. In reality one expects a distribution of flow velocities, $P(v)$. Averaging the above expression on this basis leads to

$$I(\omega) = \int_{v_{min}}^{v_{max}} P(v)\int_{-\infty}^{+\infty} S(k)\frac{2Dk^2}{(Dk^2)^2 + (kv+\omega)^2}dk\,dv, \tag{19}$$

where v_{min} and v_{max} indicate the velocity range. Combining this expression for the spectral density with Eq. (6) provides a velocity dependent spin-lattice rate. The influence of flow velocity on spin-lattice relaxation will be called the flow-relaxation effect.

III. DETAILED THEORY FOR THE MONTE CARLO SIMULATIONS

A. Definitions

The flow-relaxation effect predicted by Eq. (19) was further examined with the aid of Monte Carlo simulations for a number of simple model structures (see Fig. 2). For the sake of simplicity we restrict ourselves to two-dimensional representations of pores and grain packs. The sole objective of this model treatment is to reveal the relationship between the pore-space structure and the resulting flow-relaxation effect in systems of tractable complexity.

The simulations selectively refer to molecules contributing to the initial surface population. Molecules being initially adsorbed can be subject to three different dynamic evolutions during the time interval to which the autocorrelation function refers. (i) They remain (and possibly diffuse translationally) within the adsorption layer so that they are finally still adsorbed. (ii) They get exchanged with molecules that were initially in the bulklike phase but get readsorbed somewhere on the surface so that they are finally in the adsorbed phase again. (iii) They get exchanged with molecules that were initially in the bulklike phase and reside there finally.

Since the bulklike phase is characterized by rapid rotational diffusion, only the first two cases can retain orientational correlation. We attribute the correlation function $G_{reo}(t)$ to molecules being subject to these two types of dynamic evolution.

On the other hand, initially adsorbed molecules being subject to case (iii) cannot retain any correlated orientations. One may speak of "exchange losses" and attribute a correlation function $G_{ex}(t)$ to this sort of correlation decay.

These two classes of correlation functions are stochastically independent from each other since both can be considered as the result of a large number of random elementary processes and diffusion steps. The total correlation function expected to be relevant for experiments can then be written as a product in the form

$$G_T(t) = G_{ex}(t)G_{reo}(t). \tag{20}$$

The displacement of particles is mimicked by Monte Carlo generated random walks of fixed step length σ and a superimposed velocity field representing laminar flow. The starting position is chosen at random on the surface. In the

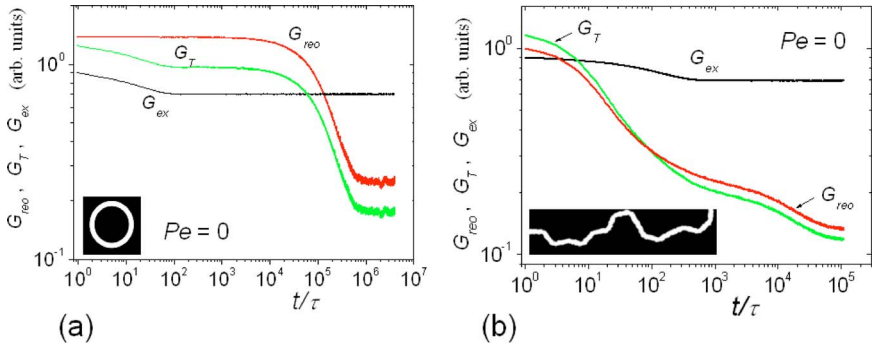

FIG. 3. (Color online) Typical reorientation autocorrelation functions in the absence of flow. (a) Simulation for the two-dimensional circular pore with smooth surfaces schematically shown in the inset. The reorientation and exchange time scales are different enough to identify two corresponding steps in the decay of the total correlation function G_T. The step at short times is obviously due to (velocity independent) exchange losses as demonstrated by the function G_{ex}. The second step at long times must be attributed to the (velocity dependent) reorientational part $G_{reo}=G_T/G_{ex}$. (b) Simulation for the two-dimensional random-walk-shaped pore with rough surfaces schematically shown in the inset. In this case, the two time scales overlap, so that the two sorts of losses do not appear as separate steps in the decay of the total correlation function. The two plots visualize the different behavior for smooth and rough surface topologies. Qualitatively the same tendencies are observed for any of the pore-space geometries shown in Fig. 2.

channel-like pore structures [Figs. 2(a)–2(c)], a parabolic velocity profile about the channel axis was assumed. The velocity field taken for the ellipsoidal-grain pack model [Fig. 2(d)] was simulated with the aid of a computational fluid dynamics technique (software package FLUENT 5.5 based on the finite volume method). The result is represented in Fig. 2(e).

The flux f is given by the integral of the flow velocity over a cross section of the channel. Note that the flux unit in two dimensions is [length]^2/[time] compared to [length]^3/[time] in the three-dimensional case. Instead of assuming cyclic boundary conditions for the noncyclic pore structures shown in Figs. 2(b)–2(d), the simulation runs are stopped and reinitiated whenever the random walker reaches an open end of the structure.

Once a molecule enters an interfacial surface layer of width λ, the so-called capture range, it can get adsorbed. Inside of the interfacial layer the particle is assumed to get adsorbed with the probability Q_{ads} per simulation step (which is taken as time unit). When adsorbed the particle is assumed to get desorbed again with the probability Q_{des} per simulation step.

In the context of the two-dimensional structures shown in Fig. 2, "surface" refers to the lines defining the pore boundaries. Molecular "orientation vector" hence means a vector in the drawing plane defined by the polar angle θ relative to the main magnetic field $\vec{B}_0$, which again is assumed to be an in-plane vector.

B. Evaluation of the correlation function

The Monte Carlo simulations provide the total correlation function which is evaluated according to

$$G_T(t) = \langle C(t) \rangle \tag{21}$$

with

$$C(t) = \begin{cases} Y_{2,m}(\theta_0, \varphi_0) Y_{2,-m}(\theta_s, \varphi_s) & \text{if initially and finally adsorbed,} \\ 0 & \text{otherwise.} \end{cases} \tag{22}$$

The angular brackets indicate an ensemble average. "Otherwise" means that the adsorbate molecule is residing either initially or finally or initially as well as finally in the bulklike phase where rotational diffusion leads to a practically immediate loss of correlation (see Sec. 7.1 in Ref. [1]). That is, the low-frequency relaxation under consideration here is solely due to molecules that are initially and finally in the adsorbed state. The angles θ_0, φ_0 and θ_s, φ_s are the polar coordinates of the surface orientations relative to the main magnetic field at positions $s=0$ at time $t=0$ and s after a time t, respectively. The distance s is measured as a curvilinear length on the surface topology.

All simulations were carried out for $m=0$, i.e., for the spherical harmonics $Y_{2,0}$. The azimuthal angle φ consequently does not matter. In Ref. [26], it was shown that the choice of the subscript m does not influence the results qualitatively. The shortest step time of the molecules is defined by the simulation cycle time τ. For the adsorption and desorption, rates were assumed to be $Q_{ads}=0.99\tau^{-1}$ and $Q_{des}=0.1\tau^{-1}$, respectively (compare the simulations in Ref. [6]).

The exchange loss part of the correlation decay can be simulated by

$$G_{ex}(t) = \langle C_{ex}(t) \rangle \tag{23}$$

and

$$C_{ex}(t) = \begin{cases} 1 & \text{if initially and finally adsorbed,} \\ 0 & \text{otherwise.} \end{cases} \tag{24}$$

The angular brackets indicate an ensemble average again. Starting from $G_{ex}(0)=1$, this function decays with a characteristic time constant τ_{ex}. In the long-time limit, the equilibrium population in the adsorbed phase is approached. Note that this contribution to the total correlation function is independent of the flow velocity.

Dividing G_T by the exchange loss function separately simulated according to Eq. (23) results in the proper RMTD part of the correlation decay,

$$G_{reo} = \frac{G_T}{G_{ex}}. \tag{25}$$

This is the velocity dependent part of the correlation loss and consequently reflects hydrodynamic dispersion. Figure 3 shows typical examples of the contributions to the total correlation function as defined above.

IV. APPLICATION TO MODEL PORE SPACES

The "pore spaces" under consideration were a circular pore [Fig. 2(a)], a chain of randomly oriented, jointed straight pipe sections with smooth [Fig. 2(b)] or rough [Fig. 2(c)] surfaces, and a pack of ellipsoidal grains [Fig. 2(d)]. A fluid is assumed to percolate through such structures. The illustration in Fig. 2(e) shows a typical map of the flow velocity magnitude obtained as a numerical solution of the Navier-Stokes equations applied to the structure shown in Fig. 2(d).

A. Orientational structure factor and simulations for a circular channel

For a two-dimensional circular pore [see Fig. 2(a)] of channel width w which is negligible relative to the mean

circle radius $\bar{R}=(R_{max}+R_{min})/2$, i.e., $w \ll \bar{R}$, an exact solution exists according to the formalism presented above. This type of geometry is characterized by a single wave number $k=k_0=1/\bar{R}$ in a certain analogy to other periodic structures such as the corrugated surface of lipid bilayers in the ripple phase [9,27]. The orientational structure factor is then a δ function,

$$S(k) = c_0 \delta(k - k_0), \tag{26}$$

where c_0 is a constant. Inserting this in Eq. (17) leads to

$$G(t) = c_0 e^{-D_{disp} k_0^2 t} e^{-iv k_0 t} + c_1 = c_0 e^{-\alpha n} e^{-i\beta n} + c_1, \tag{27}$$

where $n=t/\tau$ and D_{disp} is the dispersion coefficient in analogy to the molecular self-diffusion coefficient D_m. Note that $D_{disp}=D_m$ in the static case and $D_{disp}>D_m$, otherwise. The real time is represented by t expressed in units of the simulation cycle time τ. The parameters α and β are given by

$$\alpha = D_{disp} k_0^2 \tau \tag{28}$$

and

$$\beta = k_0 v \tau, \tag{29}$$

respectively. $c_1=\langle Y_{2,m}^2 \rangle$ is a constant accounting for any finite residual correlation in the long-time limit [see Eq. (22)]. The spectral density is given as the Fourier transform of Eq. (27):

$$I(\omega) = \frac{c_0}{2\pi} \frac{\tau\alpha}{\alpha^2 + (\beta + \omega\tau)^2}. \tag{30}$$

This function in turn is the basis for the spin-lattice relaxation rate given in Eq. (6).

For the simulations the outer and inner radii of the circular channel were set as $R_{max}=105\ell$ and $R_{min}=100\ell$, respectively, so that the condition $w \ll \bar{R}$ assumed for the analytical theory is satisfied. ℓ is the length unit on which the Monte Carlo simulations are based. The step length of the random walk was assumed to have the fixed value $\sigma=0.5\ell$.

The correlation length of a circular pore can be estimated in the following way. The orientation correlation function in a circle of radius $\bar{R}$ is

$$\langle \vec{u}(0) \cdot \vec{u}(s) \rangle = \cos(s/\bar{R}), \tag{31}$$

where $\vec{u}(0)$ and $\vec{u}(s)$ are the tangent unit vectors at curvilinear coordinates 0 and s, respectively. The correlation length is then taken as the curvilinear distance on which this correlation function decays to the value $1/e$:

$$\xi = \bar{R} \arccos(1/e) \simeq \bar{R} \times 1.194. \tag{32}$$

For $\bar{R}=(R_{max}+R_{min})/2$ with the above values for R_{max} and R_{min}, the correlation length of the circular pore channel under consideration is $\xi=122.4\ell$. The Péclet number Pe was calculated on this basis according to Eq. (1) as a measure of the relative hydrodynamic flow rate.

Figure 3(a) shows results for the correlation functions G_T, G_{ex}, G_{reo} in the absence of flow. When hydrodynamic flow is turned on, the reorientation correlation function starts to oscillate as a consequence of the periodicity of the cyclic pore

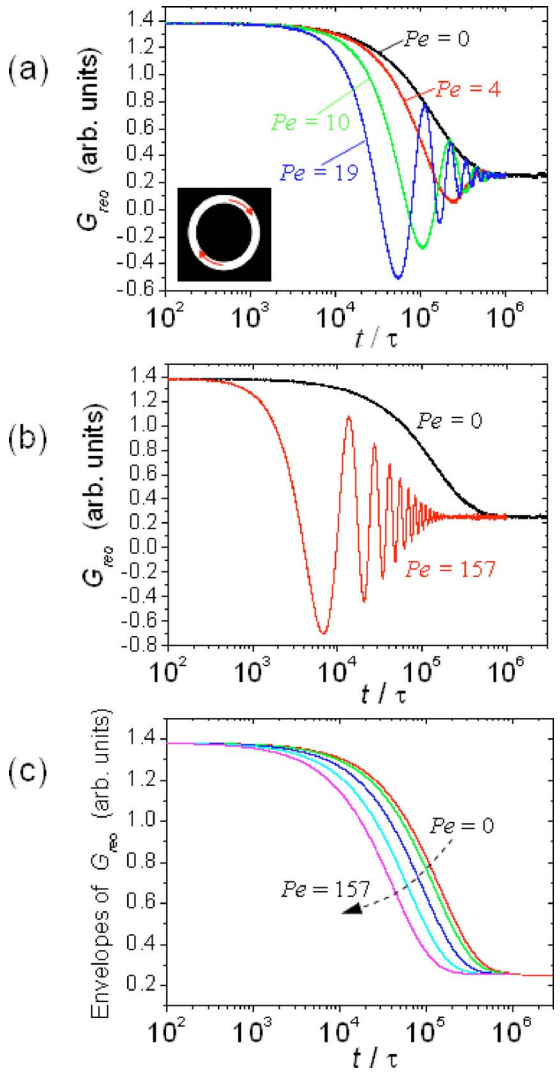

FIG. 4. (Color online) Orientation correlation function G_{reo} for the two-dimensional circular pore model (see inset) resulting from a Monte Carlo simulation. Different flow velocities, that is, different Péclet numbers Pe, were assumed. The oscillations in the presence of flow reflect the periodicity of the structure. Attenuation by hydrodynamic dispersion becomes perceptible only at flow velocities (i.e., Péclet numbers) large enough as expected from the analytical theory [Eq. (27)]. (a) Low flow velocities. The attenuation by hydrodynamic dispersion is negligible. (b) High flow velocity compared to the correlation function in the absence of flow. Attenuation by hydrodynamic dispersion is obvious. (c) Envelopes of the oscillatory functions displayed in (a) and (b). The attenuation with increasing Péclet numbers, i.e., increasing flow velocities, due to hydrodynamic dispersion is obvious. From the top to the bottom the Péclet numbers are 0,39,78,117,157.

(Fig. 4). The oscillatory behavior corresponds to the factor $\exp\{-i\beta n\}$ in Eq. (27). Attenuation by hydrodynamic dispersion [see the factor $\exp\{-\alpha n\}$] becomes more and more effective with increasing flow velocity.

The analytical theory that is the real part of Eq. (27) can be fitted to the results of the Monte Carlo simulations as a function of the hydrodynamic flux. The parameters are listed in Table I. Figure 5 shows the parameter α as a function of

TABLE I. Values of the parameters in Eq. (27) fitted to Monte Carlo simulations of the orientation correlation function for a circular pore (see Fig. 4).

Péclet number	α	β
0.00	6.623×10^{-6}	0.000
1.96	6.623×10^{-6}	5.605×10^{-6}
3.92	6.650×10^{-6}	1.100×10^{-6}
9.79	6.65×10^{-6}	2.740×10^{-5}
19.6	6.90×10^{-6}	5.480×10^{-5}
39.2	7.50×10^{-6}	1.095×10^{-4}
78.3	1.06×10^{-5}	2.190×10^{-4}
117	1.55×10^{-5}	3.28×10^{-4}
157	2.30×10^{-5}	4.36×10^{-4}

the Péclet number (or the mean flow velocity). The fitted data can be represented by a square relationship for the "dispersion parameter" α,

$$\alpha = \alpha_0 + b(\mathrm{Pe})^2, \tag{33}$$

where α_0 and b are constants.

It is worth noting that the local dispersion coefficient in the vicinity of the surface exhibits the universal Aris-Taylor behavior [21]

$$D_{disp} = D_m + \chi\frac{v^2}{D_m}, \tag{34}$$

where χ is a constant related to the geometry of the structure. In a capillary, $\chi=\varrho_s l_s^2/D_m$, where l_s is the length scale of the tube and ϱ_s is a factor that depends on the shape of the cross section [12].

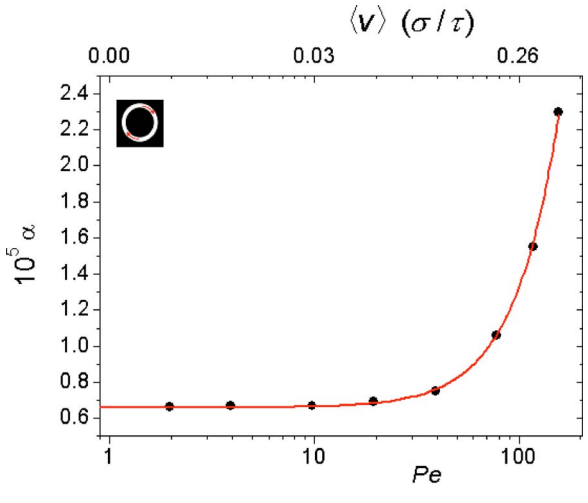

FIG. 5. (Color online) Dispersion parameter α defined in Eq. (27) as a function of the Péclet number (or mean velocity) for a circular channel. The data points were obtained by fitting Eq. (27) to the simulated correlation functions (see Fig. 4). The solid line represents a fit of Eq. (33) to these data points.

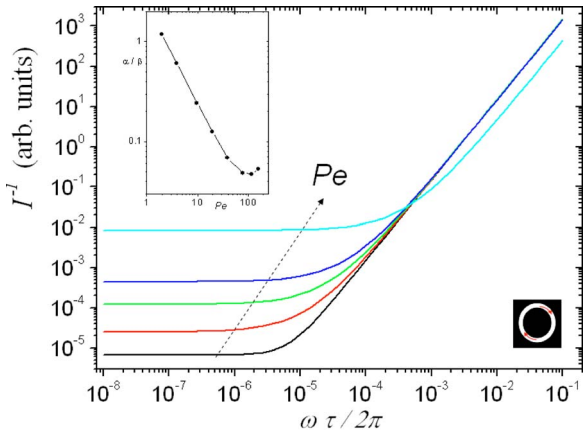

FIG. 6. (Color online) Spectral densities calculated with the aid of Eq. (30) for a circular pore for different fluxes. The pore structure is represented by the symbol in the lower right corner. The parameters α and β were fitted to the simulated correlation functions and are listed in Table I. The Péclet numbers are from the bottom to the top (see arrow) 0,4,10,20,157. The inset plot shows the ratio $\alpha/\beta = k_0 D_{disp}/v$ as a function of the Péclet number. The minimum is related to the shift of the intensity functions for the highest Péclet numbers relative to those for low Péclet numbers (see the curve for Pe ~ 157 in the main plot).

Taking the values of the parameters α and β fitted to the simulated correlation functions [see Eq. (27) and Table I] permits one to calculate the inverse spectral density as a function of the frequency. The relevant formula is given in Eq. (30). The data are plotted in Fig. 6. This essentially represents the shape of the T_1 dispersion curves to be expected in real experiments.

Figure 7 finally shows a comparison between the correlation functions in the strong- and weak-adsorption limits. In the weak-adsorption limit, values $Q_{ads}=0.1\tau^{-1}$ and $Q_{des}=0.9\tau^{-1}$ were assumed for the adsorption and desorption rates, respectively. The exchange correlation function $G_{ex}(t)$ is plotted in the inset. The long-time limit of $G_{ex}(t)$ indicates equilibrium populations deviating by almost two orders of magnitude. The pure orientation correlation functions $G_{reo}(t)$

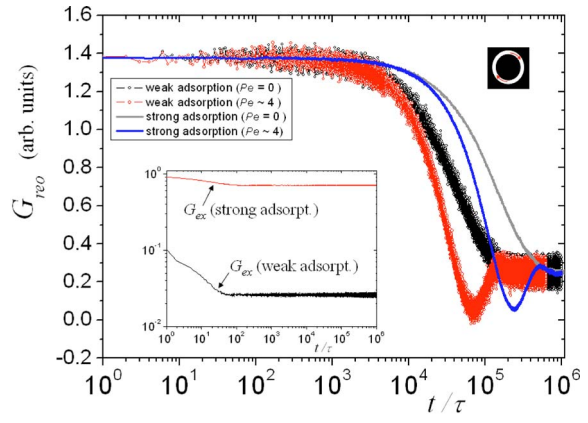

FIG. 7. (Color online) Comparison between the simulated orientation correlation functions in the strong- and weak-adsorption limits in a circular pore. The inset shows the exchange correlation function $G_{ex}(t)$. This function does not vary with flow.

are not that different, but the decay is somewhat faster in the weak-adsorption limit. In the case of weak adsorption the curves are noisy because the relevant particle ensemble is reduced due to the faster exchange with the bulklike phase. That is, there are fewer molecules that are initially and finally in the adsorbed state.

B. Orientational structure factors and simulations for more complex model pore-space structures

The circular channel examined above must be considered as a didactic model revealing the principles of the flow-relaxation effect. Any more realistic pore-space model structure is unavoidably more complex and, as concerns typical porous media, contains random elements. In this sense, two-dimensional random-walk-shaped pipes with smooth [Fig. 2(b)] or rough [Fig. 2(c)] surfaces, and ellipsoidal-grain packs [Fig. 2(d)] will be examined in the subsequent paragraphs as further model pore spaces. In the analytical theory, the topology of the pore space structures can in principle be accounted for by assuming appropriate orientational structure factors [9].

The random character of the pore spaces to be treated may be introduced into the analytical treatment by either a Gaussian distribution about a certain average value k_0 or an equipartition of wave numbers instead of the δ function given in Eq. (26). The orientational structure factor for a Gaussian distribution is given by

$$S(k) = \sqrt{\frac{2}{\pi\epsilon^2}} e^{-(k-k_0)^2/2\epsilon^2}, \tag{35}$$

where ϵ is the standard deviation of $S(k)$. Replacing this function in Eq. (17) leads to the following orientational correlation function:

$$G(t) = \frac{2\pi}{\sqrt{1+2\epsilon^2 D_{disp} t}} e^{-D_{disp} k_0^2 t/(1+2\epsilon^2 D_{disp} t)} \times e^{-(v\epsilon t)^2/2(1+2\epsilon^2 D_{disp} t)} e^{-ik_0 v t/(1+2\epsilon^2 D_{disp} t)}. \tag{36}$$

The velocity v refers to the interface layer where the BMSD process takes place. The dispersion coefficient D_{disp} depends on the flow velocity and the pore geometry. The correlation function Eq. (36) is characterized by three characteristic time constants:

$$\tau_0 = (k_0^2 D_{disp})^{-1}, \tag{37}$$

$$\tau_\epsilon = (2\epsilon^2 D_{disp})^{-1}, \tag{38}$$

$$\tau_v^{Gauss} = (v\epsilon)^{-1}. \tag{39}$$

Another form of the structure factor to be considered here is an equipartition of wave numbers in a certain range [9]:

$$S(k) = \begin{cases} \dfrac{1}{k_u - k_l} & \text{if } k_l \leqslant k \leqslant k_u, \\ 0 & \text{otherwise}, \end{cases} \tag{40}$$

where the upper and lower cutoff values are designated by k_u and k_l, respectively. Inserting this function in Eq. (17) gives

$$G(t) = \frac{\pi^{3/2}}{k_u - k_l} \frac{e^{-v^2 t/4D_{disp}}}{\sqrt{D_{disp} t}} \left(\operatorname{erf}(\sqrt{D_{disp} t} k_u) - \operatorname{erf}(\sqrt{D_{disp} t} k_l) + \frac{e^{-D_{disp} t k_u^2}}{2\pi\sqrt{D_{disp} t} k_u} [1 - \cos(k_u v t)] - \frac{e^{-D_{disp} t k_l^2}}{2\pi\sqrt{D_{disp} t} k_l} [1 - \cos(k_l v t)] \right.$$
$$+ \frac{2}{\pi} e^{-\sqrt{D_{disp} t} k_u} \sum_{n=1}^{\infty} \frac{e^{-(n^2/4)}}{n^2 + 4D_{disp} t k_u^2} f_n^u(x^u, y) - \frac{2}{\pi} e^{-\sqrt{D_{disp} t} k_l} \sum_{n=1}^{\infty} \frac{e^{-(n^2/4)}}{n^2 + 4D_{disp} t k_l^2} f_n^l(x^l, y) + i \frac{e^{-D_{disp} t k_u^2}}{2\pi\sqrt{D_{disp} t} k_u} \sin(k_u v t)$$
$$\left. - i \frac{e^{-D_{disp} t k_l^2}}{2\pi\sqrt{D_{disp} t} k_l} \sin(k_l v t) + i \frac{2}{\pi} e^{-\sqrt{D_{disp} t} k_u} \sum_{n=1}^{\infty} \frac{e^{-(n^2/4)}}{n^2 + 4D_{disp} t k_u^2} g_n^u(x^u, y) - i \frac{2}{\pi} e^{-\sqrt{D_{disp} t} k_l} \sum_{n=1}^{\infty} \frac{e^{-(n^2/4)}}{n^2 + 4D_{disp} t k_l^2} g_n^l(x^l, y) \right), \tag{41}$$

where

$$f_n^{u,l}(x^{u,l}, y) = 2x^{u,l} - 2x^{u,l} \cosh(ny) \cos(2x^{u,l} y) + n \sinh(ny) \cos(2x^{u,l} y), \tag{42}$$

$$g_n^{u,l}(x^{u,l}, y) = 2x^{u,l} \cosh(ny) \sin(2x^{u,l} y) + n \sinh(ny) \cos(2x^{u,l} y). \tag{43}$$

The quantities $x^{u,l}$ and y are defined by $(D_{disp} t)^{1/2} k_{u,l}$ and $\frac{1}{2} v \sqrt{t/D_{disp}}$, respectively. The characteristic time constants are

$$\tau_u = (k_u^2 D_{disp})^{-1}, \tag{44}$$

$$\tau_l = (k_l^2 D_{disp})^{-1}, \tag{45}$$

$$\tau_{\Delta k} = [(\Delta k)^2 D_{disp}]^{-1}, \tag{46}$$

$$\tau_v^{equip} = 4D_{disp}/v^2, \tag{47}$$

where $\Delta k = k_u - k_l$.

1. Random-walk-shaped pipe with smooth surfaces

This pore-space structure consists of two-dimensional straight pipe segments joined in random orientations relative to each other in a nearest-neighbor angle range $-\pi/2 \leqslant \chi$

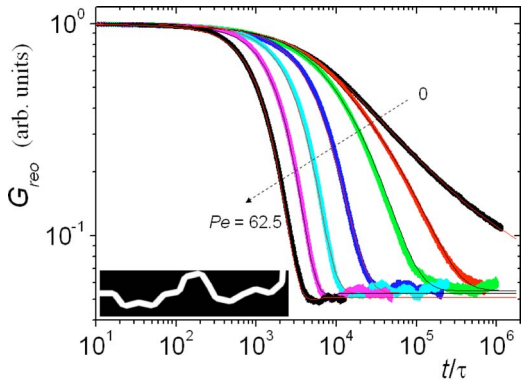

FIG. 8. (Color online) Reorientation autocorrelation function G_{reo} in a random-walk-shaped pipe with smooth surfaces (see lower left corner). The curve parameter is the Péclet number Pe as a measure of the relative flow rate. The values are from the top to the bottom Pe=0.0, 1.25, 2.50, 6.25, 12.5, 25.0, 62.5. The solid lines almost perfectly coinciding with the data points represent fits of Eq. (36) (real part). The resulting parameters are listed in Table II.

$\leqslant \pi/2$ [see Fig. 2(b)]. The segment length $l_{segment}=60\ell$ is short compared to the total system dimensions considered. The pipe width was assumed to be $w=30\ell$. The step width was set as $\sigma=0.2\ell$. The correlation length was evaluated numerically from the segment correlation function $\langle \vec{l}_{segment}(0)\cdot\vec{l}_{segment}(s)\rangle$, where $\vec{l}_{segment}(0)$ and $\vec{l}_{segment}(s)$ are the segment vectors at curvilinear positions 0 and s, respectively. The numerical segment correlation function can be described by an exponential decay plus a constant, that is,

$$\langle \vec{l}_{segment}(0)\cdot\vec{l}_{segment}(s)\rangle \propto \exp\{-s/\xi\} + \text{const.} \qquad (48)$$

The fitted value of the correlation length is $\xi \approx 1.25 l_{segment}$. A random-walk-shaped pipe was also considered by Saffman [28] in a study about hydrodynamic dispersion, and was discussed briefly in Ref. [21].

The time autocorrelation function $G_T(t)$ found with the simulations is characterized by a two-step decay analogous to those shown in Fig. 3. The two steps correspond to the exchange function G_{ex} and the reorientation function G_{reo}. The latter is also plotted in Fig. 8 for different Péclet numbers. These numerically evaluated time correlation functions $G_{reo}(t)$ in Fig. 8 can be well fitted with the real part of Eq. (36), i.e., by assuming a Gaussian structure factor with $\epsilon=0.058\ell^{-1}$ and $k_0=0.053\ell^{-1}$. The fitting parameters are listed in Table II.

The dispersion coefficient increases with the Péclet number as in the case of the circular-pore model. The dependence on the Péclet number can be approximated by (see Fig. 9)

$$D_{disp} \sim \mathrm{Pe}\ln(\mathrm{Pe}). \qquad (49)$$

This result reproduces the behavior reported in Refs. [28,21] where a power law $\sim \mathrm{Pe}^{1.3}$ was stated for a similar range of Péclet numbers in porous media. This sort of behavior is attributed to the so-called boundary-layer dispersion regime [21,29], where diffusion transfers material from the solid walls to faster streamlines.

TABLE II. Values of the parameters in Eq. (36) (real part) fitted to Monte Carlo simulations of the orientation correlation function for the random-walk-shaped pore-space model with smooth surfaces. The wave number and the standard deviation are $k_0=0.053/\ell$ and $\epsilon=0.058/\ell$, respectively.

Péclet number	v (ℓ/τ)	D_{disp} (ℓ^2/τ)
0.00	0.00	1.70×10^{-2}
1.25	6.6×10^{-4}	1.70×10^{-2}
2.50	1.29×10^{-3}	1.70×10^{-2}
6.25	3.19×10^{-3}	1.80×10^{-2}
12.5	5.70×10^{-3}	2.00×10^{-2}
25.0	9.20×10^{-3}	2.50×10^{-2}
62.5	1.49×10^{-2}	4.00×10^{-2}

The characteristic time constants defined in Eqs. (37)–(39) were derived from fits of Eq. (36) to the simulated data and are plotted in Fig. 10(a) as a function of the Péclet number. The parameter τ_v^{Gauss} which accounts for the velocity effect interestingly shows the strongest dependence. The flow velocity, another parameter in Eq. (36), is plotted in Fig. 10(b). As a function of the Péclet number, it grows more slowly than the Péclet number itself and is in all cases smaller than the mean velocity f/w. This finding appears to be plausible since the correlation function always senses the flow behavior in the vicinity of the walls, where the velocity, in the laminar regime, is small. Figure 10(a) also shows the fitted data for τ_v^{equip} defined in Eq. (47) for an equipartition of surface wave numbers. These data were obtained by fitting Eq. (41) to the numerical correlation functions. The velocity effect for an equipartition is obviously much stronger than for a Gaussian distribution of surface wave numbers.

Figure 11 shows the numerical Fourier transforms of the time correlation functions Eq. (35) according to Eq. (18) for the random-walk-shaped pipe model with smooth surfaces. If

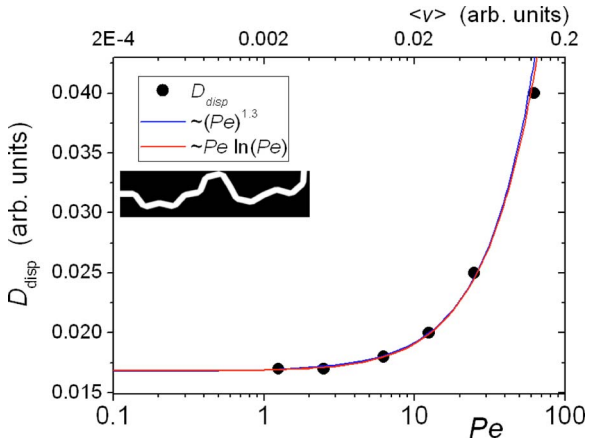

FIG. 9. (Color online) Dispersion coefficient D_{disp} as a function of the Péclet number for the random-walk-shaped pipe model with smooth surface. The data points represent the values obtained by fitting Eq. (36) to the simulated correlation functions. The solid lines represent fits of the laws given in the inset to the data points. Both laws describe the data points very well.

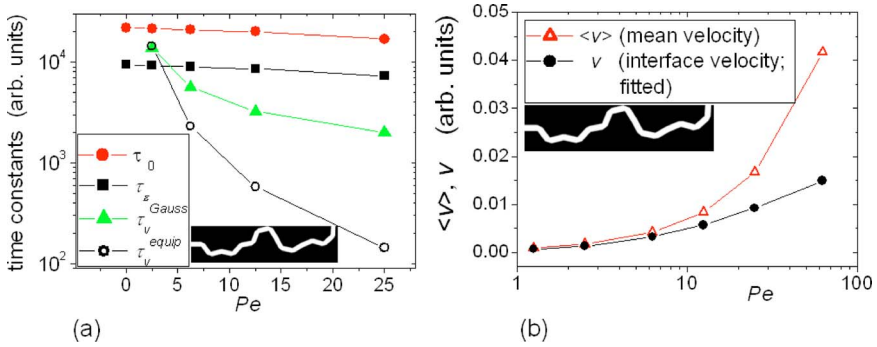

FIG. 10. (Color online) (a) Characteristic time constants defined in Eqs. (37)–(39) as functions of the Péclet number for the random-walk-shaped pipe model with smooth surface (filled data points). The open data points represent data of τ_v^{equip} for an equipartition of wave numbers according to Eq. (47). (b) Flow velocity at the solid liquid interface versus Péclet number for the same pore-space geometry. The data represent fits of Eq. (36) to the simulated correlation functions. All values are smaller than the mean velocity $\langle v\rangle = f/w$. The lines serve to guide the eye.

the pore channel is assumed to have a diameter $w \sim 10^{-6}$ m, and the step time is assumed to be $\tau \sim 10^{-7}$ s, the flow-relaxation effect is expected to become perceptible only below 50 kHz. However, if w is smaller than the above value, the same effect is predicted to occur at higher frequencies.

2. Random-walk-shaped pipe with rough surfaces

This model structure is the same as before but now supplemented with rough surfaces [compare Figs. 2(b) and Fig. 2(c)]. That is, a shorter length scale of the surface topology is introduced whereas the "superstructure" of the random-walk-shaped pipe is maintained. The surface roughness was generated by a sequence of interconnected subsections of length $l_{sub}=0.2\ell \ll l_{segment}$. The angles relative to the superstructure were randomly chosen in the range $-0.9\pi \leqslant \zeta \leqslant 0.9\pi$.

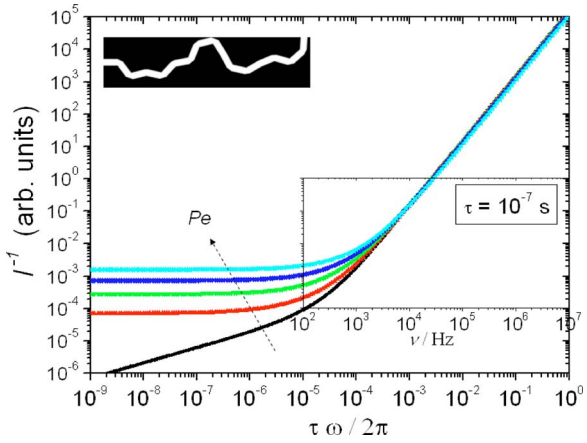

FIG. 11. (Color online) Inverse spectral density versus frequency for different Péclet numbers. The data have been evaluated with Eq. (18) in combination with Eq. (35) for the random-walk-shaped pipe model. The Péclet numbers are from the bottom to the top (see arrow) 0.0,2.5,6.25,12.5,25.0. The coordinate axes of the inset refer to $\tau=10^{-7}$ s so that the frequency axis is now given in hertz. This corresponds to the typical range accessible by the field-cycling NMR relaxometry technique.

The additional effect introduced by the rough border can be identified by simulating the correlation function in a straight channel without random superstructure as shown in Fig. 12. The combined effect of the superstructure and the surface roughness leads to a two-step decay of the orientation correlation function G_{reo} plotted in Fig. 13. The step at short times with little influence of the velocity is due to the surface roughness whereas the superstructure reveals itself as a strongly velocity dependent decay at long times. The surface topology is directly reflected by the bimodal shape of the correlation function decay as visualized in Fig. 13.

The simulated data can be described by a combination of two correlation functions based on Gaussian orientational structure factors for the short- and long-range topologies. Let us term these correlation functions $G_{sr}(t)$ and $G_{lr}(t)$, respectively. Reorientations by the short- and long-range processes occur on very different time scales, so that they can be con-

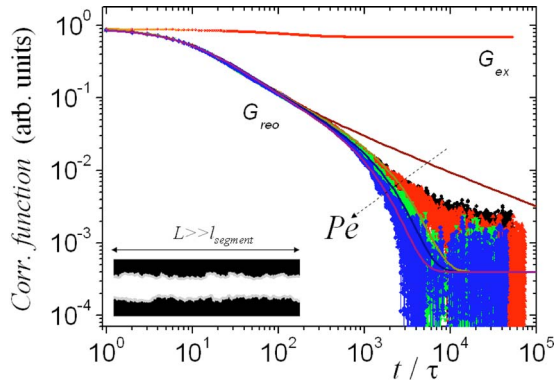

FIG. 12. (Color online) Correlation functions G_{reo} and G_{ex} in a straight pipe with rough borders (see the illustration in the inset). The Monte Carlo simulations were performed for Péclet numbers Pe=0,2.5,12.5,25.0. The exchange correlation function G_{ex} is not perceptibly affected by flow. The relatively weak effect on the orientation correlation function G_{reo} is to be compared with that based on the superstructure with smooth surfaces (see Fig. 8). The combined effect of surface roughness and superstructure will be demonstrated in Fig. 13. The solid lines represent the fits of Eq. (36). With the exception of the static case (Pe=0), the coincidence is almost perfect.

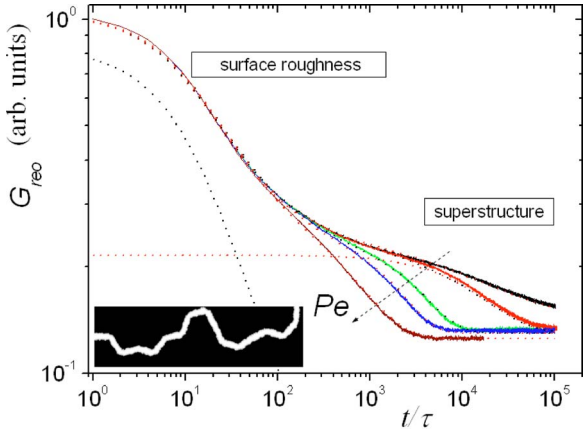

FIG. 13. (Color online) Orientation correlation function G_{reo} in a random-walk-shaped pipe with rough borders (see the illustration in the inset). The Monte Carlo simulations were performed for Péclet numbers Pe=0, 2.5, 12.5, 25.0. The two-step decay reflects the reorientation effects due to the surface roughness at short times and due to the superstructure at long times. The data can be perfectly described by a linear combination of Eqs. (53) and (54). An example is shown by the dotted lines.

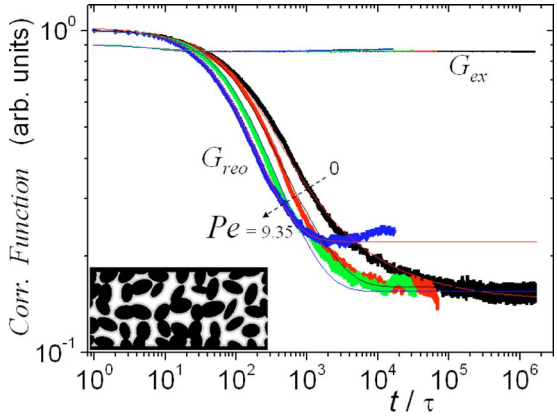

FIG. 14. (Color online) Simulated correlation functions G_{reo} and G_{ex} for the two-dimensional ellipsoidal-grain pack model. The Péclet numbers assumed were Pe=0, 1.92, 4.73, 9.35.

sidered to be stochastically independent. The orientation correlation function can then be expressed by a product according to

$$G_{reo}(t) = \frac{G_T(t)}{G_{ex}(t)} = G_{sr}(t)G_{lr}(t). \tag{50}$$

The short-range term can be analyzed into

$$G_{sr}(t) = g_{sr}(t) + G_{sr}(\infty). \tag{51}$$

The finite quantity $G_{sr}(\infty)$ reflects the anisotropy of the RMTD process on the length scale of surface roughness, whereas $g_{sr}(t)$ represents the proper correlation decay with $g_{sr}(\infty)=0$. On the time scale on which $g_{sr}(t)$ decays to zero, the long-range part remains practically constant under the surface topology conditions considered here, i.e., $G_{lr}(t) \approx G_{lr}(0)$. On this basis, Eq. (50) can be rewritten as

$$\begin{aligned} G_{reo}(t) &= [g_{sr}(t) + G_{sr}(\infty)]G_{lr}(t) \approx g_{sr}(t)G_{lr}(0) + G_{sr}(\infty)G_{lr}(t) \\ &= c_{sr}g_{sr}(t) + c_{lr}G_{lr}(t), \end{aligned} \tag{52}$$

which is approximately a linear combination of the two-time correlation functions with the constant coefficients $c_{sr} \equiv G_{lr}(0)$ and $c_{lr} \equiv G_{sr}(\infty)$.

Let us define a crossover time τ_{co} between the short-range and long-range decay steps of the correlation function so that $g_{sr}(t \gg \tau_{co}) \approx 0$ and $G_{lr}(t \ll \tau_{co}) \approx G_{lr}(0)$. Short-time and long-time limits of the orientation correlation function read then

$$G_{reo}(t) \approx c_{sr}g_{sr}(t) + c_{lr} \quad \text{for } t \ll \tau_{co} \tag{53}$$

and

$$G_{reo}(t) \approx c_{lr}G_{lr}(t) \quad \text{for } t \gg \tau_{co}, \tag{54}$$

respectively. The correlation functions in these two limits may be identified with the correlation functions fitted to the simulation data for a straight pore with rough surfaces (short-time limit) and that fitted to the simulation data for a random-walk-shaped pore (long-time limit). Figure 13 shows a typical example of a superposition of these two functions. The fitting parameters, listed in Table III, show that diffusion at the level of the roughness is not affected by flow.

3. Ellipsoidal-grain packs

As a further model structure a two-dimensional random distribution of ellipsoidal grains in a conducting channel was considered as illustrated in Fig. 2(d). The porosity was evaluated as $p \approx 0.415$ with a mean porous size around 1.1 μm. The correlation length ξ is taken as half the semimajor axis

TABLE III. Values of the parameters in Eq. (36) (real part) fitted to Monte Carlo simulations of the orientation correlation function for the random-walk-shaped pore-space model with rough borders. The wave number and the standard deviation for the superstructure are $k_0=0.053/\ell$ and $\epsilon=0.058/\ell$, respectively. The same parameters corresponding to the short length scale of the structure are $k_0=1.5/\ell$ and $\epsilon=0.84/\ell$, respectively.

Péclet number	v^{long} (ℓ/τ)	D_{disp}^{long} (ℓ^2/τ)	v^{short} (ℓ/τ)	D_{disp}^{short} (ℓ^2/τ)
0.00	0.00	1.00×10^{-2}	0.00	2.60×10^{-2}
2.50	1.10×10^{-3}	1.00×10^{-2}	6.90×10^{-3}	2.60×10^{-2}
12.5	4.50×10^{-3}	1.80×10^{-2}	7.90×10^{-3}	2.40×10^{-2}
25.0	7.70×10^{-3}	2.50×10^{-2}	9.30×10^{-3}	2.40×10^{-2}

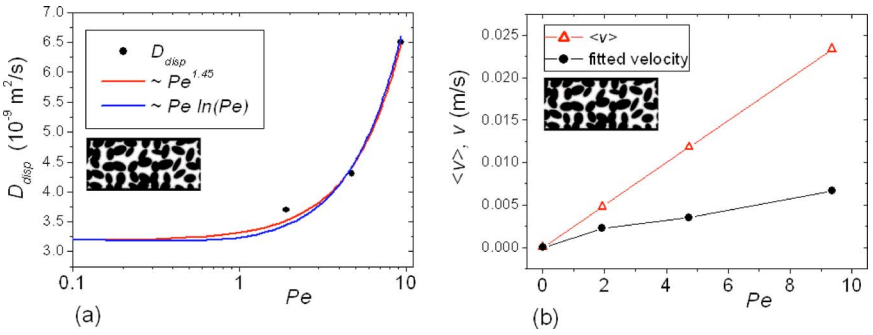

FIG. 15. (Color online) (a) Dispersion coefficients D_{disp} versus Péclet number for the ellipsoidal grain model. The lines have been calculated according to the relationships given in the inset. (b) Flow velocities versus Péclet number in the same model structure. The values fitted to the simulated reorientation autocorrelation functions G_{reo} based on the real part of Eq. (36) tend to be below the mean velocity $\langle v \rangle$.

of the ellipses. The velocity field was imported from the computational fluid dynamics simulation shown in Fig. 2(e). The mean velocity $\langle v \rangle$ is calculated as an average over the magnitudes of this velocity field. The correlation functions can be analyzed into two decay steps by exchange (G_{ex}) and the (flow enhanced) RMTD mechanism (G_{reo}). Figure 14 shows typical examples.

The Gaussian distribution of the orientational structure factor may again be assumed as an analytical representation of the correlation function. The solid lines in Fig. 14 represent fits of the real part of Eq. (36) to the simulated data. The fitting parameters are listed in Table IV.

The dispersion coefficient increases with the Péclet number as shown in Fig. 15(a). In the Péclet number range $0 \leqslant \mathrm{Pe} < 10$ investigated, the effect of molecular Fickian diffusion is comparable to that of convective flow. The data may be described either by a power law $D_{disp} \propto (\mathrm{Pe})^{1.45}$ or by a law $D_{disp} \propto \mathrm{Pe}\ \ln(\mathrm{Pe})$ [see the solid lines in Fig. 15(a)]. The velocity values fitted to the simulated data turned out to be less than the mean velocity as demonstrated in Fig. 15(b).

The inverse spectral density numerically evaluated from Eq. (18) in combination with Eq. (35) is plotted in Fig. 16 as a function of the Péclet number. Assuming the values for the computer unit length and time according to $\ell = 10^{-6}$ m and $\tau = 10^{-7}$ s, respectively, leads to an expected experimental window as shown in the inset box of Fig. 16. According to this, the flow-relaxation effect is expected to show up at frequencies below 100 kHz.

V. DISCUSSION

The effect of hydrodynamic flow on spin-lattice relaxation near solid surfaces was treated analytically and with the aid of Monte Carlo simulations for diverse model situations. Due to the faster surface displacements an enhancement of the spin-lattice relaxation rate is expected in a frequency range where local rotational motions are irrelevant. Experimentally this range can be probed with the aid of the field-cycling NMR relaxometry technique [1]. Judged from the "experimental window" suggested by the inset data shown in Figs. 11 and 16, the effect cannot be expected to be very pronounced. Anyway, a demonstration was possible with water flowing through a Chromolith column as used in high-pressure liquid chromatography [2] although some obvious modifications of the pore surface chemistry encountered in more recent relaxometry experiments with this sort of sample still need to be explained.

The main difficulty one is facing in experimental studies of the flow-relaxation effect is that hydrodynamic flow should be homogeneously distributed in the whole sample in order to achieve the best efficiency. However, hydrodynamic flow tends to occur along certain percolation pathways as demonstrated in the computational fluid dynamics simulation shown in Fig. 2(e). Similar flow patterns were measured in

TABLE IV. Values of the parameters in Eq. (36) (real part) fitted to Monte Carlo simulations of the ellipsoidal-grain pack model. The wave number and the standard deviation are $k_0 = 1.04 \times 10^6$ m^{-1} and $\epsilon = 7.0 \times 10^5$ m^{-1}, respectively.

Péclet number	v (m/s)	D_{disp} (m^2/s)
0.00	0.00	3.1×10^{-9}
1.92	2.228×10^{-3}	3.7×10^{-9}
4.73	3.479×10^{-3}	4.3×10^{-9}
9.35	6.680×10^{-3}	6.5×10^{-9}

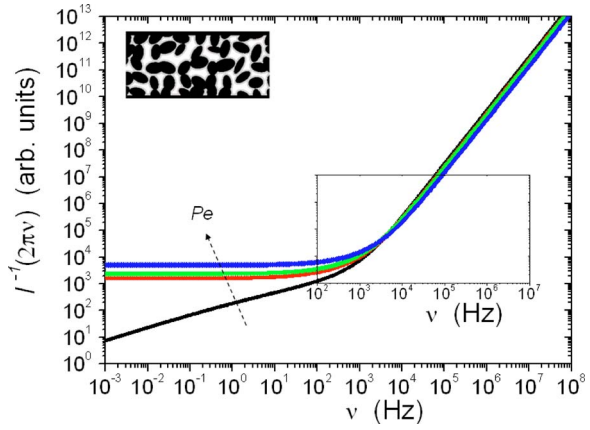

FIG. 16. (Color online) Inverse spectral density versus frequency for different Péclet numbers in the ellipsoidal-grain model. The data represent the numerical Fourier transform of the simulated reorientation autocorrelation function. The frequency scale corresponds to a computer cycle time $\tau \sim 10^{-7}$ s. The Péclet numbers are from the bottom to the top (see arrow) 0,1.92,4.73,9.35. The inset box indicates the typical window accessible in experiments relative to that frequency scale.

percolation model objects with a magnetic resonance microscopy technique [30]. The consequence is that most of the sample volume is not affected by flow of sufficient velocity or is even subject to stagnant zones. What one measures under such conditions is an average relaxation rate between flowing and stagnant material. The flow-relaxation effect is consequently expected little above the experimental error intrinsic to the field-cycling technique.

Mansfield and Issa [31] found in flow mapping experiments in sandstone some stochastic variability of the flow patterns in repeated experiments. This finding may also be relevant for the flow-relaxation effect reported here. It appears that there is some instability of the flow conditions in microscopic pore spaces. Currently we are therefore pursuing a different strategy by employing electroosmotic flow promising more uniform and stable flow velocity distributions.

The flow-relaxation effect can be described theoretically based on the formalism outlined above. For the orientational structure factor an equipartition of wave numbers was assumed [see Eq. (40)]. The distribution of velocities is also approached by an equipartition given by

$$P(v) = \begin{cases} \dfrac{1}{v_{max}} & \text{if } 0 \leqslant v \leqslant v_{max}, \\ 0 & \text{otherwise}, \end{cases} \tag{55}$$

where v_{max} is the upper cutoff value of the velocity distribution. The effective spectral density thus reads

$$I_{equi}(\omega) = \frac{2}{v_{max}(k_u - k_l)} \int_0^{v_{\max}} \int_{k_l}^{k_u} \frac{D_{disp} k^2}{(D_{disp} k^2)^2 + (kv + \omega)^2} dk\, dv. \tag{56}$$

Combining Eqs. (6) and (56) leads to the final expression for the spin-lattice relaxation rate under flow conditions. The lower-cutoff wave number k_l is responsible for the crossover to the low-frequency plateau. The shift of the T_1 data to higher values upon hydrodynamic flow was well reproduced. The upper- and lower-cutoff values of the wave number, k_u and k_l, respectively, indicate the different length scales of the surface orientation. Interestingly these length scales coincide with the bimodal pore size distribution by which Chromolith is specified, that is, "nanometers" corresponding to k_u and "micrometers" corresponding to k_l [2]. The low-frequency spin-lattice relaxation dispersion thus directly reflects features of the surface topology in this way.

VI. CONCLUSIONS

Low-field spin-lattice relaxation of polar liquids filled into a polar, diamagnetic porous medium takes place at the liquid/solid interfaces via the BMSD and RMTD mechanism. This is effectively a surface diffusion process. If hydrodynamic flow is superimposed to molecular diffusion, displacements along surfaces are accelerated in the sense of hydrodynamic dispersion.

There are different aspects that can be associated with this effect. (i) The influence of flow on low-field spin-lattice relaxation can be considered as evidence for the BMSD and RMTD surface relaxation mechanism [3,4]. (ii) Since low-field spin-lattice relaxation in samples of this sort is governed by intramolecular spin interactions [3,4], the relevant fluctuation of the spin interactions is molecular reorientation. That is a sort of rotational analog of Taylor-Aris dispersion [11,12]. (iii) The time scale corresponding to the frequency range on which the flow-relaxation effect occurs implies that the relevant molecular displacements perpendicular to the surface occur on a length scale of a few nanometers only [32]. This may be regarded as an example of "nanofluidics near surfaces" [33]. (iv) There is a discussion in the literature about the relevant interfacial boundary condition [34]. Judged from the present results, one is dealing with a modified interfacial slip boundary condition in the sense that molecules move in a sort of hopping process along the surfaces (see the illustration in Fig. 1).

These findings can be considered to be relevant for high-pressure liquid chromatography and catalysis applications where surface transport and molecular exchange play a crucial role [35,36]. The adsorption-desorption cycles on surfaces underlying the flow-relaxation effect are also of some theoretical interest, since anomalous or superdiffusive Lévy-walk-like behavior was predicted for such scenarios [5,37]. The flow-relaxation effect may open a wide field of potential studies of nanometric surface effects provided that samples and experimental setups permitting stable and uniform flow patterns along curved surface topologies are established.

ACKNOWLEDGMENTS

Bogdan Buhai has contributed the computational fluid dynamics simulation. The authors thank Esteban Anoardo and Hans Wiringer for discussions and assistance. This work was funded by the Deutsche Forschungsgemeinschaft.

[1] R. Kimmich and E. Anoardo, Prog. Nucl. Magn. Reson. Spectrosc. **44**, 257 (2004).
[2] C. Mattea and R. Kimmich, Phys. Rev. Lett. **94**, 024502 (2005).
[3] S. Stapf, R. Kimmich, and R.-O. Seitter, Phys. Rev. Lett. **75**, 2855 (1995).
[4] T. Zavada and R. Kimmich, J. Chem. Phys. **109**, 6929 (1998).
[5] O. V. Bychuk and B. O'Shaughnessy, J. Chem. Phys. **101**, 772 (1994).
[6] R. Valiullin, R. Kimmich, and N. Fatkullin, Phys. Rev. E **56**, 4371 (1997).
[7] P. Levitz, E. Lecolier, A. Mourchid, A. Delville, and S. Lyonnard, Europhys. Lett. **49**, 672 (2000).
[8] J. A. Revelli, C. E. Budde, D. Prato, and H. S. Wio, New J. Phys. **7**, 15 (2005).
[9] R. Kimmich and H. W. Weber, Phys. Rev. B **47**, 11788 (1993).

[10] M. Vilfan and M. Vuk, J. Chem. Phys. **120**, 8638 (2004).
[11] G. I. Taylor, Proc. R. Soc. London, Ser. A **219**, 186 (1953).
[12] R. Aris, Proc. R. Soc. London, Ser. A **235**, 67 (1956).
[13] A. Compte and J. Camacho, Phys. Rev. E **56**, 5445 (1997).
[14] M. G. Gauthier, G. W. Slater, and K. D. Dorfman, Eur. Phys. J. E **15**, 71 (2004).
[15] M. Al-Ghoul and B. C. Eu, Phys. Rev. E **70**, 016301 (2004).
[16] D. Kandhai, D. Hlushkou, A. G. Hoekstra, P. M. A. Sloot, H. Van As, and U. Tallarek, Phys. Rev. Lett. **88**, 234501 (2002).
[17] H. Schwarze, U. Jaekel, and H. Vereecken, Transp. Porous Media **43**, 265 (2001).
[18] C. P. Lowe and D. Frenkel, Phys. Rev. Lett. **77**, 4552 (1996).
[19] A. Abragam, *The Principles of Nuclear Magnetism* (Clarendon Press, Oxford, 1961).
[20] R. Kimmich, *NMR Tomography, Diffusometry, Relaxometry* (Springer, Berlin, 1997).
[21] M. Sahimi, *Flow and Transport in Porous Media and Fractured Rock* (VCH, Weinheim, 1995); Rev. Mod. Phys. **65**, 1393 (1993).
[22] F. A. L. Dullien, *Porous Media: Fluid Transport and Pore Structure* (Academic Press, San Diego, 1992).
[23] L. de Arcangelis, J. Koplik, S. Redner, and D. Wilkinson, Phys. Rev. Lett. **57**, 996 (1986).
[24] J. C. Bacri, N. Rakotomalala, and D. Salin, Phys. Rev. Lett. **58**, 2035 (1987).
[25] J. Klafter, M. F. Shlesinger, and G. Zumofen, Phys. Today **49**(2), 33 (1996).
[26] E. Anoardo, F. Grinberg, M. Vilfan, and R. Kimmich, Chem. Phys. **297**, 99 (2004).
[27] R.-O. Seitter, T. Link (Zavada), R. Kimmich, A. Kobelkov, P. Wolfangel, and K. Müller, J. Chem. Phys. **112**, 8715 (2000).
[28] P. G. Saffman, J. Fluid Mech. **6**, 321 (1959).
[29] D. L. Koch and J. F. Brady, J. Fluid Mech. **154**, 399 (1985).
[30] A. Klemm, R. Kimmich, and M. Weber, Phys. Rev. E **63**, 041514 (2001).
[31] P. Mansfield and B. Issa, J. Magn. Reson., Ser. A **122**, 137 (1996).
[32] Y. Leng, P. T. Cummings, Phys. Rev. Lett. **94**, 026101 (2005).
[33] K. P. Travis and K. E. Gubbins, J. Chem. Phys. **112**, 1984 (2000).
[34] L. Léger, J. Phys.: Condens. Matter **15**, S19 (2003).
[35] M. Krucker, A. Lienau, K. Putzbach, M. D. Grynbaum, P. Schuler, and K. Albert, Anal. Chem. **76**, 2623 (2004).
[36] M. Coppey, O. Bénichou, J. Klafter, M. Moreau, and G. Oshanin, Phys. Rev. E **69**, 036115 (2004).
[37] A. M. Lacasta, J. M. Sancho, A. H. Romero, I. M. Sokolov, and K. Lindenberg, Phys. Rev. E **70**, 051104 (2004).

II

C. Mattea and R. Kimmich.

Flow-Enhanced Molecular Reorientations and Interfacial Slip Probed by Field-Cycling NMR Relaxometry in Microscopic Pores.

Phys. Rev. Lett.. **94**, 024502 (2005).

Flow-Enhanced Molecular Reorientations and Interfacial Slip Probed by Field-Cycling NMR Relaxometry in Microscopic Pores

Carlos Mattea and Rainer Kimmich

Sektion Kernresonanzspektroskopie, Universität Ulm, 89069 Ulm, Germany

(Received 1 September 2004; published 19 January 2005)

It is shown that hydrodynamic flow has an effect on spin-lattice relaxation in water filled into a porous monolithic silica material. This is a rotational analogue of translational hydrodynamic (or Taylor-Aris) dispersion arising from incoherent Brownian motion in combination with coherent flow. The effect is demonstrated with the aid of field-cycling NMR relaxometry and confirmed by theoretical considerations. The results directly verify bulk mediated surface diffusion and reveal interfacial slip at fluid-solid interfaces.

DOI: 10.1103/PhysRevLett.94.024502 PACS numbers: 47.55.Mh, 76.60.Es, 82.56.Na, 83.50.Lh

Hydrodynamic (or Taylor-Aris) dispersion is a well known transport mechanism important for Péclet numbers around 1 when translational displacements of fluid molecules are efficiently subject to the combined action of Brownian motion and laminar hydrodynamic flow [1,2]. In this Letter we demonstrate that rotational diffusion as probed by field-cycling NMR relaxometry [3], that is, the frequency dependence of the proton spin-lattice relaxation time T_1, is also influenced by flow in a certain analogy.

The motivation for this work arose from the question whether and how translational and rotational diffusion are correlated when intermittent adsorption at pore walls occurs. Bychuk *et al.* suggested in 1994 ''bulk mediated surface diffusion'' (BMSD) as a mechanism for displacements of adsorbate molecules along walls confining a fluid [4]. It implies a sequence of desorption-diffusion-readsorption cycles so that the displacement trajectories on the surface can be described as Lévy walks. Since molecules adsorbed on a solid surface tend to be oriented along a preferential direction relative to the local surface, this translational surface diffusion stipulates reorientations of molecules in porous media according to the surface topology (Fig. 1). This ''reorientation mediated by translational displacements'' (RMTD) was demonstrated by field-cycling NMR relaxometry in porous glasses with polar liquids [5,6]. In the present study, we have exerted a pressure gradient to water in a porous material so that Brownian motion was superimposed by a steady hydrodynamic flow as illustrated in Fig. 1.

The experiments were carried out with water in a commercial high-pressure liquid chromatography column (Merck, Chromolith^{TM}, 25 mm long, 4.6 mm wide). Chromolith consists of a silica skeleton with 13 nm and 2 μm pores. The overall porosity of the monolithic matrix is about 85% [7]. 80% of the total porosity can be ascribed to the 2 μm pores [8]. The specific surface area is 300 m^2/g [9]. Tallarek *et al.* [10] showed that this kind of monolithic structure exhibits a macroscopic fluid dynamical behavior, hydraulic permeability, and hydrodynamic dispersion equivalent to a column packed with spherical beads. The ordinary RMTD relaxation mechanism governed by self-diffusion in the absence of hydrodynamic flow [6] is expected to be relevant in all pores irrespective of the size. Perceptible flow effects depend on sufficiently high flow velocities (or local Péclet numbers), and must therefore be allocated to the 2 μm pores.

A field-cycling relaxometer (STELAR S.R.L, Italy) covering proton frequencies from 1 kHz to 10 MHz was used. It is equipped with homemade auxiliary coils for the compensation of the earth field and stray fields from other magnets. The precision of the field cycles was checked with the aid of a fast Hall teslameter (Projekt Elektronik FM 210) probing the flux density at the sample position during test field cycles. The bandwidth of the teslameter is 35 kHz, the resolution 0.01 mT. Within the experimental errors, all relaxation curves could be described by monoexponential functions over about one decade of the signal amplitude. The flow across the sample was controlled by a chromatographic pump Gynkotek 500B. The maximum flow rate was 2.5 ml/min at pressure differences up to 25 bar. The measurements were carried out at 20 °C.

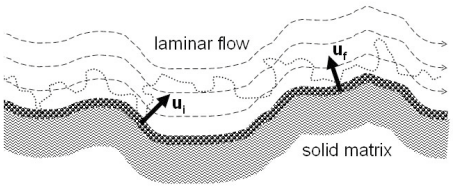

FIG. 1. Illustration of adsorbate reorientation by hydrodynamic dispersion. The dotted line represents a trajectory of a molecule by Brownian motion in the presence of laminar flow along the surface. Flow streamlines are drawn as broken lines. The adsorption layer on the solid matrix is indicated. The arrows refer to the local preferential orientations of molecules at the initial and final pore surface sites. The thickness of the fluid layer along the surface in which the flow-enhanced RMTD process is expected to take place ranges from molecular diameters up to about 100 nm.

 © 2005 The American Physical Society

Figure 2 shows the frequency dependences of the proton spin-lattice relaxation time in static water in Chromolith in comparison to Vycor porous glass (pore size 4 nm) and Vitrapor porous glass (pore size 1 μm) [11]. Because of the bimodal pore space structure of Chromolith, its spin-lattice relaxation data are between those of Vycor and Vitrapor. This indicates the strong sensitivity of spin-lattice relaxation to the pore size and the pore size distribution. The frequency dependence observed with polar adsorbate molecules in pores with polar surfaces was explained before [6] by a combination of local motions and translational displacements along rough surfaces. The plateau at about 10 MHz is attributed to the regime of local motions like restricted rotational diffusion of the adsorbed molecules about their preferential orientations at the local surface sites. The main frequency dispersion at medium frequencies reflects the RMTD process of adsorbate molecules and originates from molecules being adsorbed initially as well as finally during the autocorrelation function decay. That is, molecules starting at a surface site can travel by translational diffusion to another surface site with a different orientation, so that the reorientation rate of molecules being initially and finally adsorbed depends both on the diffusivity and on the surface topology (see Fig. 1). On the other hand, molecules that are not in the adsorbed state at the beginning and at the end of the considered time interval completely lose any orientational correlation already by local rotational diffusion. Therefore, they cannot contribute to the frequency dependence in the main-dispersion regime.

Hydrodynamic flow through the pore space enhances the translational displacement rate by Taylor-Aris dispersion. The consequence is that the RMTD processes get faster whereas local motions remain unaffected. This is demonstrated in Fig. 3. The data measured in the presence of flow are shifted to higher values in the main-dispersion regime while the data around 10 MHz coincide with the measurements in the static state. The shift of the main-dispersion data indicates a faster decay of the dipolar correlation function. That is, the reorientation times are shorter due to faster displacements along the surface topology. The flow effect on spin-lattice relaxation is again demonstrated in Fig. 4 where flow was switched on only in the interval in the middle.

When a fluid is pressed through a porous network, the power dissipated in the material is $\partial W/\partial t = \Delta p \partial V/\partial t$, where Δp is the pressure drop across the sample and $\partial V/\partial t$ is the flow rate. In our case we estimate $\frac{\partial W}{\partial t} \approx$ 63 mW or less. In principle, this heat dissipation could lead to an increase of the sample temperature. However, under our experimental conditions any perceptible change of the temperature can safely be ruled out. Direct measurement of the sample temperature with a thermocouple suggests that any such change is less than 0.2 °C. The coinciding data points around 10 MHz where local motions dominate irrespective of the flow rate (see Fig. 3) corroborate the constancy of the temperature. Finally, a test experiment was carried out by heating the sample to a temperature at which the spin-lattice relaxation times in

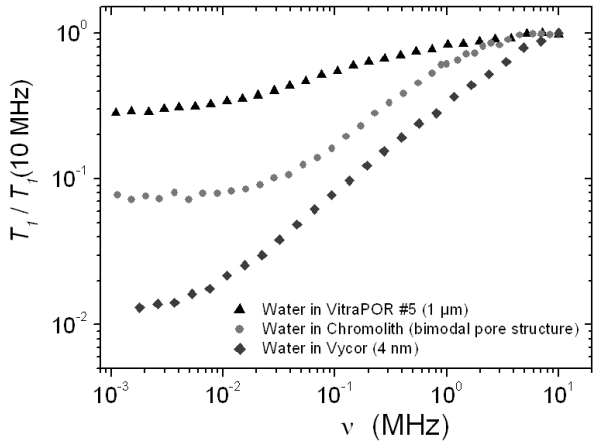

FIG. 2. Proton spin-lattice relaxation dispersion in static water in three different porous silica materials.

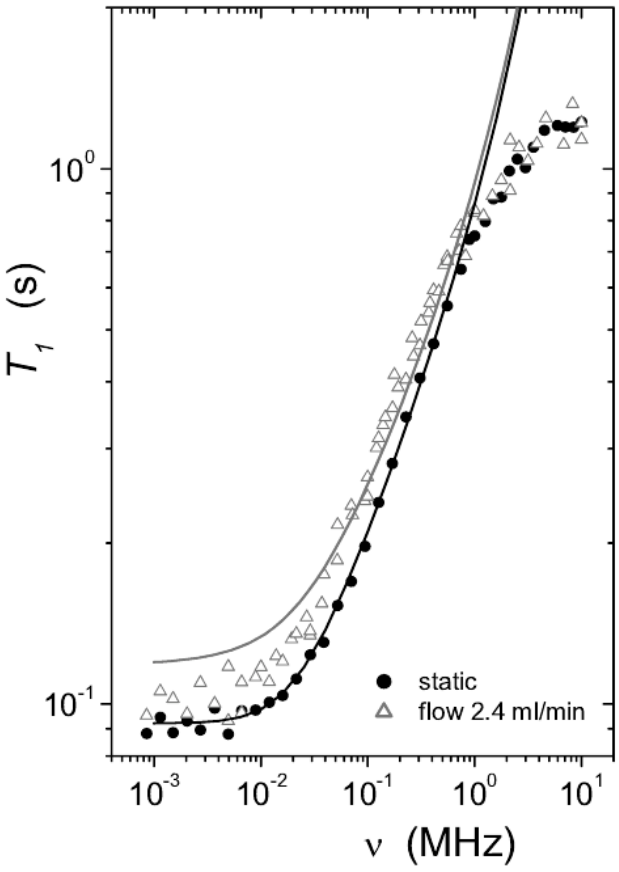

FIG. 3. Comparison of the proton spin-lattice relaxation dispersion in water in Chromolith under static and flow conditions. The solid lines represent Eq. (15) for $v_{\max} \to 0$ (lower line) and $v_{\max} = 0.04$ m/s (upper line). The other parameters are commonly $D = 2 \times 10^{-9}$ m^2/s; $k_l = 1 \times 10^7$ m^{-1}; $k_u = 2 \times 10^8$ m^{-1}.

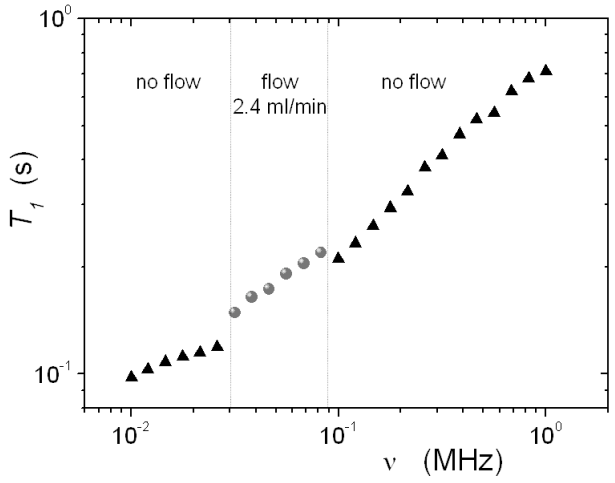

FIG. 4. Proton spin-lattice relaxation dispersion in water in Chromolith when hydrodynamic flow is switched on and off as indicated in the plot.

the main-dispersion regime take equivalent values compared to the observed flow effect. A 10 °C temperature rise was needed to reach a similar increase of the relaxation times. This is far beyond the accuracy of the sample temperature control used. Also, the plateau around 10 MHz is shifted by temperature variation in the same way as the main-dispersion regime in contrast to the flow effect. We therefore emphasize that the flow effect reported in this Letter is not of a thermal origin.

For a theoretical description of the flow effect we refer to the one-dimensional version of the RMTD formalism for simplicity [12,13]. We define x as a curvilinear coordinate along a streamline along the surface. The flow effect on spin-lattice relaxation can be explained by hydrodynamic dispersion of the adsorbate molecules [14–17]. Restricting ourselves to scalar fields and incompressible fluids, the transport process can be described by the *convective-diffusion equation*

$$D_{\parallel}\frac{\partial^2\Psi}{\partial x^2} - v\frac{\partial\Psi}{\partial x} = \frac{\partial\Psi}{\partial t} - D_{\perp}\nabla_{\perp}^2\Psi, \tag{1}$$

where Ψ is the propagator, v is the velocity in x direction, and $\nabla_{\perp}^2$ is the Laplacian in transverse direction. $D_{\parallel}$ and $D_{\perp}$ are coefficients characterizing the dispersion longitudinally and transversely to the flow, respectively. The dispersion coefficients depend on the flow velocity. In the limit of vanishing flow velocities, $D_{\parallel}$ becomes equal to the molecular diffusion coefficient diminished by the tortuosity factor. Focusing on the longitudinal version of hydrodynamic dispersion and equating $D = D_{\parallel}$, we find after Fourier transformation of Eq. (1)

$$\phi(k, t) = \hat{\phi}(k)e^{-Dtk^2}e^{-ikvt}, \tag{2}$$

where $\hat{\phi}(k)$ is the Fourier transform of $\Psi(x, 0)$. Assuming $\Psi(x, 0) = c_0\delta(x)$ results in

$$\Psi(x, t) = \frac{c_0}{2\pi}\int_{-\infty}^{+\infty} e^{-(Dtk^2+ikvt)}e^{ixk}dk. \tag{3}$$

Low-field spin-lattice relaxation in water is dominated by intramolecular dipolar interaction [5], the spatial part of which can be expressed in terms of spherical harmonics of second order [18]. The corresponding autocorrelation functions describing the orientational fluctuations of molecules with fixed intramolecular interdipole distances can then be expressed by [13]

$$\begin{aligned} G(t) &= 4\pi\langle Y_{2,m}(\vec{u}_i)Y_{2,-m}(\vec{u}_f)\rangle_{\vec{u}_i,\vec{u}_f} \\ &= \int\langle P_c(\vec{u}_i, \vec{u}_f, t)Y_{2,m}(\vec{u}_i)\rangle_{\vec{u}_i}Y_{2,-m}(\vec{u}_f)d\Omega_f \end{aligned} \tag{4}$$

where the brackets indicate ensemble averages, $\vec{u}_i$ and $\vec{u}_f$ are the unitary vectors normal to the surface indicating the initial and the final orientation, respectively, and $d\Omega_f$ is the differential solid angle into which $\vec{u}_f$ points. The subscript m can have the values 1 or 2, but no distinction will be made in the following. The conditional probability density can be expressed as

$$P_c(\vec{u}_i, \vec{u}_f, t) = \int\Theta(\vec{u}_i, \vec{u}_f, x)\Psi(x, t)dx, \tag{5}$$

where $\Psi(x, t)$ is the surface diffusion propagator, i.e., the probability density that the adsorbate molecule is displaced by a curvilinear distance x along the surface in an interval t, and $\Theta(\vec{u}_i, \vec{u}_f, x)$ is the probability that the surface orientation changes from $\vec{u}_i$ to $\vec{u}_f$ in a curvilinear distance x. Using the expansion in terms of spherical harmonics, with the initial condition $\Theta(\vec{u}_i, \vec{u}_f, 0) = \delta(\vec{u}_f - \vec{u}_i)$, the surface orientation probability density becomes

$$\Theta(\vec{u}_i, \vec{u}_f, x) = \sum_{l',m'} Y_{l',-m'}(\vec{u}_i)Y_{l',m'}(\vec{u}_f)g(x), \tag{6}$$

where $g(x)$ is the normalized surface orientation correlation function between surfaces sites separated by x. Combining Eqs. (4)–(6) and making use of the orthonormal properties of spherical harmonics leads to

$$G(t) = \int_{-\infty}^{\infty} g(x)\Psi(x, t)dx. \tag{7}$$

The correlation function is based on the probability that a particle is displaced a distance in the range x to $x + dx$ in a time t with velocity v along the direction dx, given by the propagator (3). That is,

$$G(t) = \int_{-\infty}^{+\infty} g(x)\left(\frac{c_0}{2\pi}\int_{-\infty}^{+\infty} e^{-(Dtk^2+ikvt)}e^{ikx}dk\right)dx. \tag{8}$$

Regrouping the factors that depend only on the space variable x leads to the orientational structure factor

$$S(k) = \frac{c_0}{2\pi}\int_{-\infty}^{+\infty} g(x)e^{ikx}dx. \tag{9}$$

Equation (4) can thus be rewritten as

$$G(t) = \int_{-\infty}^{+\infty} S(k) e^{-(Dtk^2 + ikvt)} dk. \quad (10)$$

The corresponding real part of the spectral density is obtained performing the Fourier transform of Eq. (10)

$$I(\omega) = \int_{-\infty}^{+\infty} S(k) \frac{2Dk^2}{(Dk^2)^2 + (kv + \omega)^2} dk. \quad (11)$$

In porous materials, the structure factor may be assumed to have a (normalized) equipartition of wave numbers in a certain range:

$$S(k) = \begin{cases} \frac{1}{k_u - k_l} & \text{if } k_l \le k \le k_u \\ 0 & \text{otherwise} \end{cases} \quad (12)$$

where the upper and lower cutoff values are designated by k_u and k_l, respectively. In this approach hydrodynamic flow is accounted for by the flow velocity v. More realistically, the velocity is also subject to a distribution. We assume an equipartition for simplicity again,

$$P(v) = \begin{cases} \frac{1}{v_{\max}} & \text{if } 0 \le v \le v_{\max} \\ 0 & \text{otherwise} \end{cases} \quad (13)$$

where $v_{\max}$ is the upper cutoff value for the velocity. The velocity distribution is assumed to start at $v = 0$ although interfacial slip is concluded from our experiments. The reason is that the 20% volume fraction of nanometer pores in Chromolith are not expected to contribute perceptibly to transport by flow so that $v = 0$ occurs in any case. Combining the last three equations, the spectral density function takes the form

$$I_{\text{equi}}(\omega) = \frac{2}{v_{\max}(k_u - k_l)} \times \int_0^{v_{\max}} \int_{k_l}^{k_u} \frac{Dk^2}{(Dk^2)^2 + (kv + \omega)^2} dk\, dv. \quad (14)$$

The spin-lattice relaxation rates are calculated by [18]

$$\frac{1}{T_1} = K[I_{\text{equi}}(\omega) + 4I_{\text{equi}}(2\omega)], \quad (15)$$

where K is a constant and $I_{\text{equi}}(\omega)$ is the intensity function given in Eq. (14). The theory can be fitted to the experimental T_1 values numerically (see solid lines in Fig. 3). The lower cutoff wave number k_l is responsible for the crossover to the low-frequency plateau. The shift of the T_1 data to higher values upon laminar flow is well reproduced.

The flow effect on low-field spin-lattice relaxation in a sense corroborates interfacial slip at fluid-solid interfaces. This phenomenon was recently concluded from an optical near-field velocimetry study even for wetting fluids by Léger [19]. According to the present study, "interfacial slip" appears in a molecular picture including intermittent adsorption-desorption surface hopping cycles as illustrated in Fig. 1. Note that the length scale on which the processes detected by NMR relaxometry occur is below 100 nm and approaches molecular dimensions, so that a very sensitive probe of the effective slip boundary condition becomes available this way. This aspect of the present study appears to be important for microfluidics as it is relevant for microsystem technology.

We thank E. Anoardo, H. Tiraboschi, and H. Wiringer for discussions and assistance. S. Grissmer and I. Melzner from this University kindly provided the HPLC pump used in our experiments.

[1] G. I. Taylor, Proc. R. Soc. London A **219**, 186 (1953).
[2] R. Aris, Proc. R. Soc. London A **235**, 67 (1956).
[3] R. Kimmich and E. Anoardo, Prog. Nucl. Magn. Reson. Spectrosc. **44**, 257 (2004).
[4] O. V. Bychuk and B. O'Shaughnessy, J. Chem. Phys. **101**, 772 (1994).
[5] S. Stapf, R. Kimmich, and R.-O. Seitter, Phys. Rev. Lett. **75**, 2855 (1995).
[6] T. Zavada and R. Kimmich, J. Chem. Phys. **109**, 6929 (1998).
[7] K. Cabrera, J. Sep. Sci. **27**, 843 (2004).
[8] M. Al-Bokari, D. Cherrak, and G. Guiochon, J. Chromatogr., A **975**, 275 (2002).
[9] K. Miyabe and G. Guiochon, J. Sep. Sci. **27**, 853 (2004).
[10] F. C. Leinweber and U. Tallarek, J. Chromatogr., A **1006**, 207 (2003).
[11] C. Mattea, R. Kimmich, I. Ardelean, S. Wonorahardjo, and G. Farrher, J. Chem. Phys. **121**, 10648 (2004).
[12] R. Kimmich and H. W. Weber, Phys. Rev. B **47**, 11788 (1993).
[13] R. Kimmich, *NMR Tomography, Diffusometry, Relaxometry* (Springer, Berlin, 1997).
[14] M. Sahimi, *Flow and Transport in Porous Media and Fractured Rock* (VCH, Weinheim, 1995); Rev. Mod. Phys. **65**, 1393 (1993).
[15] F. A. L. Dullien, *Porous Media: Fluid Transport and Pore Structure* (Academic Press, San Diego, 1992).
[16] L. de Arcangelis, J. Koplik, S. Redner, and D. Wilkinson, Phys. Rev. Lett. **57**, 996 (1986).
[17] J. C. Bacri, N. Rakotomalala, and D. Salin, Phys. Rev. Lett. **58**, 2035 (1987).
[18] A. Abragam, *The Principles of Nuclear Magnetism* (Clarendon Press, Oxford, 1961).
[19] L. Léger, J. Phys. Condens. Matter **15**, S19 (2003).

III

C. Mattea, R. Kimmich, I. Ardelean, S.Wonorahardjo, and G. Farrher.

Molecular exchange dynamics in partially filled microscale and nanoscale pores of silica glasses studied by field-cycling nuclear magnetic resonance relaxometry.

J. Chem. Phys. **121**, 10648 (2004).

Molecular exchange dynamics in partially filled microscale and nanoscale pores of silica glasses studied by field-cycling nuclear magnetic resonance relaxometry

C. Mattea and R. Kimmich
Sektion Kernresonanzspektroskopie, Universität Ulm, 89069 Ulm, Germany

I. Ardelean
Physics Department, Technical University, 400020 Cluj-Napoca, Romania

S. Wonorahardjo[a] and G. Farrher
Sektion Kernresonanzspektroskopie, Universität Ulm, 89069 Ulm, Germany

(Received 19 May 2004; accepted 30 August 2004)

Nuclear magnetic spin-lattice relaxation experiments have been performed in partially filled porous glasses with wetting and nonwetting fluids. The frequency dependence of the spin-lattice relaxation rate in Vycor (4 nm pores) and VitraPOR #5 (1 μm pores) silica glasses was studied as a function of the filling degree with the aid of field-cycling NMR relaxometry. The species of primary interest were water (''polar'') and cyclohexane (''nonpolar''). Spin-lattice relaxation was examined in the frequency range from 1 kHz to 400 MHz with the aid of a field-cycling NMR relaxometer and an ordinary 400 MHz NMR spectrometer. Three different mobility states of the fluid molecules are distinguished: The adsorbed state at the pore walls, the bulklike liquid phase, and the vapor phase. The adsorbate spin-lattice relaxation rate is dominated by the ''reorientation mediated by translational displacements'' (RMTD) mechanism taking place at the adsorbate/matrix interface at frequencies low enough to neglect rotational diffusion of the molecules. The experimental data are analyzed in terms of molecular exchange between the different mobility states. Judged from the dependence of the spin-lattice relaxation rates on the filling degree, limits for slow and fast exchange (relative to the RMTD time scale) can be distinguished and identified. It is concluded that water always shows the features of slow exchange irrespective of the investigated pore sizes and filling degrees. This is in contrast to cyclohexane which is subject to slow exchange in micrometer pores, whereas fast exchange occurs in nanoscopic pores. The latter case implies that the vapor phase contributes to molecular dynamics in this case at low filling degrees while it is negligible otherwise. © *2004 American Institute of Physics.* [DOI: 10.1063/1.1808423]

I. INTRODUCTION

Molecular dynamics in liquids filled into nanoscopic or microscopic pores of silica glasses is substantially different from that found in bulk samples of the same fluid species. This was demonstrated in numerous self-diffusion[1–11] and spin-lattice relaxation[9–16] studies revealing effects of geometrical restrictions in the pore space and of adsorption at pore walls. Thermodynamics properties of fluids confined in mesoporous structures were also found to change relative to their bulk state.[17,18] Most investigations published so far refer to saturated samples where one merely needs to distinguish between adsorbed and bulklike mobility states of the adsorbate molecules.

In the present work we focus on pore spaces partially filled with liquids coexisting with their vapor phases. Figure 1 shows a schematic illustration of the situation to be examined. In previous papers[2–5] it was shown that translational diffusion can be strongly enhanced by contributions of the vapor phase to translational displacements. A corresponding formalism was elaborated including fast and slow exchange limits between the liquid and vapor phases.[7] Features predicted on this basis were verified in field-gradient NMR diffusometry experiments.

The time scale of NMR diffusometry[15,16,19–22] ranges from about 10^{-3} to 10^{0} s. The present work refers to the much shorter time scale of field-cycling NMR relaxometry[23] which is typically 10^{-10}–10^{-4} s. Unlike the NMR diffusometry case where adsorption at pore walls plays a minor role and can be neglected, the dominant NMR relaxation mechanism occurs at the pore walls. We are dealing with a two-step exchange scheme of molecules in the adsorbed, liquid, and gaseous state as illustrated in Fig. 1. In any case, the primary low-frequency spin-lattice relaxation mechanism was previously shown to be ''reorientations mediated by translational displacements'' (RMTD) at the pore walls.[12,13,24,25]

There are mainly two questions arising in this context: First, is there any perceptible influence of molecular exchange between the liquid and the vapor phases on spin-lattice relaxation, and second, can we distinguish fast and slow exchange limits between the adsorbed and bulklike liquid phases? In the following, it will be elucidated and dem-

[a]Current address: Department of Chemistry, The State University of Malang, Malang, Indonesia.

 © 2004 American Institute of Physics

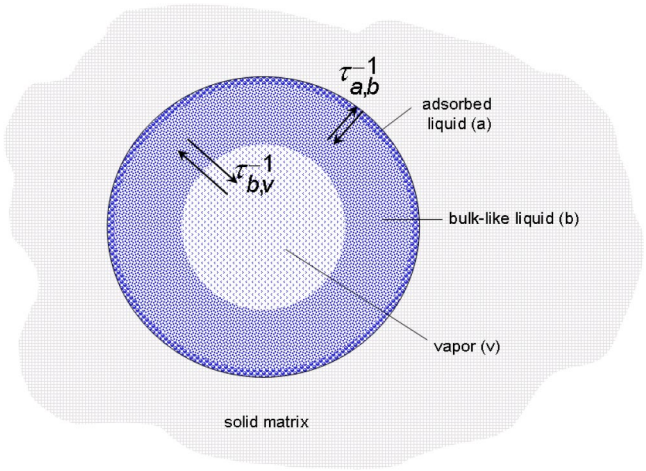

FIG. 1. Schematic representation of a pore partially filled with an adsorbate liquid. Three phases are distinguished: ''adsorbed,'' ''bulklike,'' and ''vapor.'' NMR signals are dominated by the two liquid phases. The exchange rate between the adsorption layer and the bulklike liquid, $\tau^{-1}_{a,b}$, directly affects spin-lattice relaxation to be examined in this study. The exchange rate between the bulklike and the vapor phases, $\tau^{-1}_{b,v}$, is shown to affect spin-lattice relaxation only indirectly via the enhanced diffusivity in the vapor phase. Merely at the lowest filling degrees when the bulklike phase more or less vanishes, a direct impact on the relaxation behavior of the liquid can be stated.

onstrated under which conditions these phenomena occur and show up in experiments.

The silica glasses examined are Vycor (4 nm pores) and VitraPOR #5 (1 μm pores). Both materials have polar pore surfaces. One consequently expects a different dynamic and exchange behavior for polar (wetting) and nonpolar (nonwetting) adsorbate fluids.[12,13] As typical examples of such adsorbate species we have chosen water and cyclohexane, respectively.

II. FORMALISM FOR THE RMTD/EXCHANGE RELAXATION MODEL

A. Theoretical background of spin-lattice relaxation

The comparison of proton and deuteron spin-lattice relaxation data[13] and isotopic dilution experiments[12,26] indicate that intramolecular dipolar interactions largely dominate proton relaxation in the adsorbate species considered here. Relaxation by electron paramagnetic impurities can be excluded on a similar basis.[12,13] That is, spin-lattice relaxation is predominantly caused by molecular reorientations.

Molecules can be reoriented by rotational diffusion and the RMTD process. Of course, rotational diffusion in the adsorbed and bulklike phases or even in the vapor phase (see Fig. 1) tends to be so fast at room temperature that no direct contribution to the spin-lattice relaxation dispersion at kHz and MHz frequencies can be expected. What remains for the low-frequency regime is the RMTD mechanism. Since rotational diffusion is restricted to a certain solid angle range when the molecule is adsorbed at a solid surface, translational diffusion to different surface adsorption sites of different orientation will reorient the adsorbate molecules relative to the initial adsorption site. This is the essence of the RMTD mechanism which is subject to translational diffusion properties and exchange rates between the different phases.

RMTD means that molecules probe the surface topology via translational diffusion and molecular exchange. That is, the mechanism contains elements both of a geometrical and molecular dynamics nature as verified for different pore wall topologies in Refs. 12, 14, and 15 experimentally and with the aid of Monte Carlo simulations in Ref. 27.

In the case of relaxation by intramolecular dipolar coupling, the general expression for the spin-lattice relaxation rate is

$$\frac{1}{T_1} = K[J_1(\omega) + 4J_2(2\omega)], \tag{1}$$

where K is a constant, ω is the Larmor frequency, and the functions $J_m(\omega)$ $(m=1,2)$ are spectral densities given by the cosine Fourier transform of the autocorrelation functions of spherical harmonics of second order:

$$J_m(\omega) = 2\int_0^\infty G_m(t)\cos(\omega t)dt,$$
$$G_m(t) = \langle Y_{2,-m}(0)Y_{2,m}(t)\rangle. \tag{2}$$

The spherical harmonics at times 0 and t define the initial and final orientations of the adsorbate molecule in terms of the polar and azimuthal angles of the internuclear vector relative to the external magnetic field.

B. Exchange limits

Ignoring the vapor phase for the moment and coming back to it in the discussion section, molecules coexist in the bulklike phase (subscript *b*) or in the adsorption layer (subscript *a*) (see Fig. 1) whereas the population of the vapor phase is too small to provide any perceptible NMR signal in this sort of experiment. Exchange between the two liquid phases can be classified in two ways by defining a mean exchange time $\tau_{a,b}$ characterizing the exchange rate between the two phases. Whether exchange must be considered to be fast or slow depends on the reference time scale. Here we refer either to the (spin-lattice) ''relaxation time scale'' or to the ''correlation time scale.''

The *fast relaxation exchange limit*, $T_1 \gg \tau_{a,b}$, manifests itself by monoexponential relaxation curves. This is the basis of the so-called ''two-phase fast-exchange model'' often referred to in the literature.[24] In the present application, monoexponential spin-lattice relaxation curves were observed over at least one decade. We therefore anticipate this limit throughout all evaluations and treatments.

The *fast and slow correlation exchange limit*, $t_c \gg \tau_{a,b}$ and $t_c \ll \tau_{a,b}$, respectively, relate the time scale of the correlation function decay (characterized by a time constant t_c) to the exchange time $\tau_{a,b}$. Note that exchange which is *slow* on the correlation time scale likely is *fast* on the relaxation time scale since T_1 is much longer than the molecular reorientation time constants on which spin-lattice relaxation is based.

C. Correlation functions

According to Eq. (2), only the molecular orientations at times 0 and t matter for the decay of the correlation function irrespective of what happens in between. Four different situations can be distinguished in a two-phase system and characterized by the following exclusive probabilities: $p_{a,a}(t)$, fraction of spins which are initially and finally located in the adsorbed phase; $p_{a,b}(t)$, fraction of spins which happen to be initially in the adsorbed phase and finally in the bulklike phase; $p_{b,a}(t)$, fraction of spins which happen to be initially in the bulklike phase and finally in the adsorbed phase; $p_{b,b}(t)$, fraction of spins which happen to be initially and finally in the bulklike phase. These probabilities are normalized of course,

$$p_{a,a}(t)+p_{a,b}(t)+p_{b,a}(t)+p_{b,b}(t)=1. \tag{3}$$

With field-cycling NMR relaxometry we are preferentially probing the long-time limit $t \gg \tau_{rot}$, where τ_{rot} is the correlation time for rotational diffusion in bulk or, in restricted form, in the adsorbed phase. Contributions by rotational diffusion therefore do not affect the low-frequency relaxation dispersion monitored with this technique. The two processes of interest, namely, ''RMTD along surfaces'' and ''rotational diffusion'' (either restricted or isotropic) will be indicated by subscripts ''RMTD'' and ''rot,'' respectively. The correlation function given in Eq. (2) can formally be analyzed for the two-phase system into four partial correlation functions for four subensembles of spins (assuming the fast relaxation exchange limit):

$$\begin{aligned} G_m(t)=&p_{a,a}(t)\langle Y_{2,-m}(0)Y_{2,m}(t)\rangle_{\mathrm{RMTD},rot}+p_{a,b}(t)\\ &\times\langle Y_{2,-m}(0)Y_{2,m}(t)\rangle_{rot}+p_{b,a}(t)\\ &\times\langle Y_{2,-m}(0)Y_{2,m}(t)\rangle_{rot}+p_{b,b}(t)\\ &\times\langle Y_{2,-m}(0)Y_{2,m}(t)\rangle_{rot}. \end{aligned} \tag{4}$$

In the limit $t \gg \tau_{rot}$ the partial correlation function for isotropic rotational diffusion (i.e., in the bulklike phase) vanishes, and we may write

$$G_m(t \gg \tau_{rot}) \approx p_{a,a}(t)\langle Y_{2,-m}(0)Y_{2,m}(t)\rangle_{\mathrm{RMTD},rot}. \tag{5}$$

Rotational diffusion on surfaces is restricted and leaves a finite residual correlation that can only decay to zero in the adsorbed state by RMTD along more or less randomly curved surfaces. RMTD and rotational diffusion can, moreover, be considered to be independent of each other on their very different time scales. Equation (5) can therefore be analyzed according to

$$\begin{aligned} &\langle Y_{2,-m}(0)Y_{2,m}(t\gg\tau_{rot})\rangle_{\mathrm{RMTD},rot}\\ &\quad=\langle Y_{2,-m}(0)Y_{2,m}(t\gg\tau_{rot})\rangle_{\mathrm{RMTD}}\\ &\qquad\times\langle Y_{2,-m}(0)Y_{2,m}(t\gg\tau_{rot})\rangle_{rot}\\ &\quad=\langle Y_{2,-m}(0)Y_{2,m}(t\gg\tau_{rot})\rangle_{\mathrm{RMTD}}\\ &\qquad\times[(\langle Y_{2,-m}(0)Y_{2,m}(t)\rangle_{rot}-g_{rot}(\infty))\\ &\qquad+g_{rot}(\infty)]\approx\langle Y_{2,-m}(0)\\ &\qquad\times Y_{2,m}(t\gg\tau_{rot})\rangle_{\mathrm{RMTD}}g_{rot}(\infty) \end{aligned} \tag{6}$$

so that

$$G_m(t\gg\tau_{rot})\approx p_{a,a}(t)g_{rot}(\infty)\langle Y_{2,-m}(0)Y_{2,m}(t)\rangle_{\mathrm{RMTD}}, \tag{7}$$

where $g_{rot}(\infty)\equiv\langle Y_{2,-m}(0)Y_{2,m}(\infty)\rangle_{rot}=\text{const}$ is the finite residual correlation left over in the long-time limit of restricted rotational diffusion before RMTD becomes effective.

Equation (7) tells us, that the correlation function relevant for the field-cycling frequency range is composed of two time dependent factors, namely, the probability $p_{a,a}(t)$ the decay of which represents exchange losses of the initial surface population, and the RMTD correlation function in the proper sense, $\langle Y_{2,-m}(0)Y_{2,m}(t)\rangle_{\mathrm{RMTD}}$. This function refers to the fraction of molecules that are initially and finally in the adsorbed state.

Relative to the time scales of exchange ($\tau_{a,b}$) and rotational diffusion (τ_{rot}), two further time limits can be distinguished.[25]

(i) In periods t obeying the ''fast correlation exchange limit,'' $t \gg \tau_{a,b} \gg \tau_{rot}$, the initial and final probabilities to be in either phase become independent of each other, so that

$$\begin{aligned} &p_{a,a}(t)\approx p_a^2,\\ &p_{a,b}(t)\approx p_{b,a}(t)\approx p_a(1-p_a),\\ &p_{b,b}(t)\approx(1-p_a)^2, \end{aligned} \tag{8}$$

where p_a and $1-p_a$ are the (constant) populations of the adsorbed phase and of the bulklike phase, respectively. Assuming the same rotational correlation time τ_{rot} in both phases for simplicity, we obtain the following expression for the total correlation function, Eq. (4), in the fast correlation exchange limit:

$$\begin{aligned} G_m(t)\approx&p_a^2 g_{rot}(\infty)\langle Y_{2,-m}(0)Y_{2,m}(t)\rangle_{\mathrm{RMTD}}+(1-p_a^2)\\ &\times\langle Y_{2,-m}(0)Y_{2,m}(t)\rangle_{rot}. \end{aligned} \tag{9}$$

In the long-time limit $t \gg \tau_{rot}$, it reduces to

$$G_m(t\gg\tau_{rot})\approx p_a^2 g_{rot}(\infty)\langle Y_{2,-m}(0)Y_{2,m}(t)\rangle_{\mathrm{RMTD}}. \tag{10}$$

The correlation function given at Eq. (10) is characterized by a *square* dependence on p_a. Such a dependence was also concluded in Ref. 28.

(ii) In the ''slow correlation exchange limit,'' $\tau_{rot} \ll t \ll \tau_{a,b}$, exchange is unlikely to occur during the period t, and we may approximate as

$$\begin{aligned} &p_{a,a}(t)\approx p_a,\\ &p_{a,b}(t)\approx p_{b,a}(t)\approx 0,\\ &p_{b,b}(t)\approx(1-p_a). \end{aligned} \tag{11}$$

Under such conditions, the total correlation function given at Eq. (4) becomes a *linear* function of p_a according to

$$\begin{aligned} G_m(t)\approx&p_a g_{rot}(\infty)\langle Y_{2,-m}(0)Y_{2,m}(t)\rangle_{\mathrm{RMTD}}+(1-p_a)\\ &\times\langle Y_{2,-m}(0)Y_{2,m}(t)\rangle_{rot} \end{aligned} \tag{12}$$

or

$$G_m(t\gg\tau_{rot})\approx p_a g_{rot}(\infty)\langle Y_{2,-m}(0)Y_{2,m}(t)\rangle_{\mathrm{RMTD}} \tag{13}$$

in the long-time limit.

In both cases, the RMTD process obviously dominates the long-time correlation decay, where we are referring to molecules initially and finally in the adsorbed phase. The low-frequency relaxation dispersion, $T_1 = T_1(\omega)$, for two-phase fast relaxation exchange systems is thus obtained by combining Eqs. (10) or (13) with Eqs. (2) and (1).

D. Population in the adsorbed phase as a function of the filling degree

In partially filled pores, the population in the adsorbed phase p_a, varies with the filling degree. Expressing it as the mass fraction of the adsorbed phase, we find

$$p_a = \frac{m_a}{m_a + m_b} = \frac{1}{1 + \frac{V_b}{V_a}} = \frac{1}{1 + \frac{V_b}{\lambda A}}, \tag{14}$$

where we have assumed that the densities in both phases are equal. V_b is the volume of the bulklike phase, A is the total area of the liquid-solid interface, and λ is the average width of the adsorbed layer.

The pore filling factor (or filling degree) with respect to liquid phases is defined by

$$f = \frac{V_b + \lambda A}{V_0}, \tag{15}$$

where V_0 represents the total pore volume. The population in the adsorbed phase can thus be written as

$$p_a = \frac{\lambda A}{V_0}\frac{1}{f}. \tag{16}$$

E. Total relaxation rates

Combining Eqs. (1), (2), (9), and (16) we obtain for the slow correlation exchange limit (ii),

$$\frac{1}{T_1(\omega, f)} = \frac{1}{T_{1,b}(\omega)} + \frac{\lambda A}{V_0}\left(\frac{1}{T_{1,a}(\omega)} - \frac{1}{T_{1,b}(\omega)}\right)\frac{1}{f}, \tag{17}$$

where $T_{1,a}(\omega)$ and $T_{1,b}(\omega)$ are the spin-lattice relaxation times selectively expected for the RMTD mechanism in the adsorbed layer and the rotational diffusion process in the bulklike phase, respectively. This equation looks similar to the one considered in Ref. 8.

The spin-lattice relaxation rate in the fast correlation exchange limit (i) is derived analogously as

$$\frac{1}{T_1(\omega, f)} = \frac{1}{T_{1,b}(\omega)} + \left(\frac{\lambda A}{V_0}\right)^2\left(\frac{1}{T_{1,a}(\omega)} - \frac{1}{T_{1,b}(\omega)}\right)\frac{1}{f^2}. \tag{18}$$

The relaxation rate expressions given in Eqs. (17) and (18) have a very similar structure apart from the linear and quadratic dependence on the filling factor. That is, the two limits can be distinguished experimentally by varying the pore filling degree.

III. SAMPLES AND EXPERIMENTAL METHODS

Vycor porous glass VPQ # 7930 was purchased from Corning Ltd. It consists of 96% SiO_2. The nominal mean pore size is 4 nm (± 0.6 nm) and the porosity is 28% according to specifications by the manufacturer. The specific surface area is 250 m^2/g, and the apparent density (dry) is 1500 kg/m^3. VitraPOR #5 was purchased from ROBU Glasfilter-Geräte GmbH. The silica content is 80.6% by weight. The pore size is between 1.0 and 1.6 μm. The porosity is 45%, the specific surface area is 1.75 m^2/g, and the density is 2230 kg/m^3. Electron micrographs of the two samples recorded with a Hitachi S-5200 microscope are shown in Fig. 2.

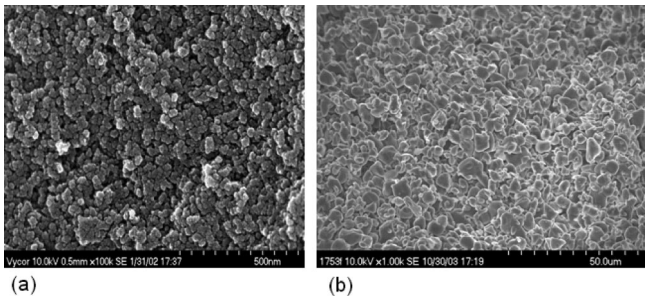

FIG. 2. Electron micrographs of (a) Vycor porous glass with a nominal mean pore size of 4 nm$\pm$0.6 nm, and (b) VitraPOR #5 with a pore size specified between 1.0 and 1.6 μm.

The samples were pretreated by boiling them for 60 min in 30% H_2O_2. After that, washed with distilled water and evacuated at 95 °C for 24 h. After this treatment, the samples were considered to be dry with a nominal filling factor 0. The solvents were then filled into the porous glass with the aid of the bulk-to-bulk method resulting in a filling factor 1. Samples partially filled with water were prepared by evaporation of a fraction of the pore water in open air until the desired filling degree was reached. In the case of cyclohexane, evaporation was performed in a glove bag in a dry nitrogen atmosphere in order to avoid any replacement of cyclohexane by water from the air humidity. The final solvent content was determined by weighing. The samples were placed in a sealed container with practically no empty space that would allow for further evaporation. All experiments were performed after about 1 h permitting the fluid to equilibrate with respect to phase distributions. After this annealing period no further changes were perceptible, and the samples were stable over periods much longer than needed for the experiments.

As adsorbate fluids, water and cyclohexane were chosen as typical representatives of polar (wetting) and nonpolar (nonwetting) species, respectively. The water was demineralized: *N*-cyclohexane was purchased from Fluka Chemika, Germany. The equilibrium vapor pressure of cyclohexane at room temperature is about four times larger than that of water, the surface tension is three times smaller. The consequence is that cyclohexane evaporates much faster than water. The vapor phase of cyclohexane in partially filled pores is thus expected to contain about four times as many molecules as in the case of water. As a polar species, water tends to cover all pore surfaces with a liquid film the mean thickness of which corresponds to the filling factor. This is in contrast to the nonpolar cyclohexane which fills first smaller pores and then the larger ones until all the pore surface is covered at the highest filling degrees.[29] All experimental data

TABLE I. Parameters fitted to the experimental data according to Eqs. (17) and (18).

ν (MHz)	a	$T_{1,b}$ (s)	ρ (m s^{-1})	$f_{\mathrm{exp}}/f_{\mathrm{min}}$
Cyclohexane in VitraPOR #5 (1–1.6 μm pore size)				
400	0.0037	7.22	7.72×10^{-10}	14
400 (open air)	0.0283	3.28	7.40×10^{-10}	14
10	0.0980	1.78	5.30×10^{-9}	82
0.011	0.0036	1.60	1.98×10^{-8}	67
Water in VitraPOR #5 (1–1.6 μm pore size)				
400	0.154	2.07	3.73×10^{-8}	32
10	0.645	1.51	1.47×10^{-7}	27
0.011	0.251	⋯	8.23×10^{-7}	51
0.0012	0.228	⋯	9.03×10^{-7}	53
Water in Vycor (4.0±0.6 nm pore size)				
400	0.2507	1.60	2.60×10^{-10}	0.27
10	1.4983	0.460	1.55×10^{-9}	0.90
0.011	112.71	0.012	1.17×10^{-7}	0.90
Cyclohexane in Vycor (4.0±0.6 nm pore size)				
400	0.016	4.10	⋯	0.05
10	0.191	1.65	⋯	0.02
0.011	2.10	0.15	⋯	0.02

refer to room temperature and proton resonance.

In the case of cyclohexane, a strong relaxation enhancement by (paramagnetic) oxygen dissolved in the fluid was observed at 400 MHz when the samples were exposed to open air for a while [see Fig. 6(a) below and Table I]. The analysis according to the formalism given above shows that this refers especially to the bulklike phase at the highest available frequency. The liquids were therefore degassed before preparing the samples in an atmosphere of dry nitrogen. After this treatment, no influence of oxygen could be detected anymore. Note that relaxation enhancement by dissolved oxygen is a high-frequency phenomenon anyway because of the extremely short correlation times governing the proton-oxygen spin interactions. These are known to be of the order 10^{-12}–10^{-11} s in water[30] or hydrocarbon phases.[31] No such enhancement effect is known for frequencies typical for field-cycling NMR relaxometry.

Another problem that may arise in relaxation studies of cyclohexane in porous silica glasses at low filling factors is the influence of traces of water taken up from the air humidity if the samples are not carefully prevented from any such contact (see the proton spectrum in Fig. 3). Such traces may even dominate the total relaxation rate below the MHz regime as demonstrated in Fig. 4 for a filling factor $f=0.39$. The abrupt increase of the spin-lattice relaxation rate at about 100 kHz is due to water traces that start to dominate the spin-lattice relaxation rate below this frequency while the cyclohexane contribution becomes negligible. This crossover is accompanied by nonexponential relaxation curves composed of contributions of the two adsorbate species. It has nothing much to do with cyclohexane dynamics and must therefore be identified and eliminated carefully. All cyclohexane data reported in the following were recorded with samples prepared under conditions where no perceptible influence of water traces could be detected.

Judged from the relaxation behavior, there was no indication of any influence of paramagnetic impurities in the silica glasses investigated. In the context of the present molecular exchange study, paramagnetic relaxation contributions would anyway be irrelevant, since we take the spin-lattice relaxation time in the adsorption layer, $T_{1,a}$, as a fitting parameter.

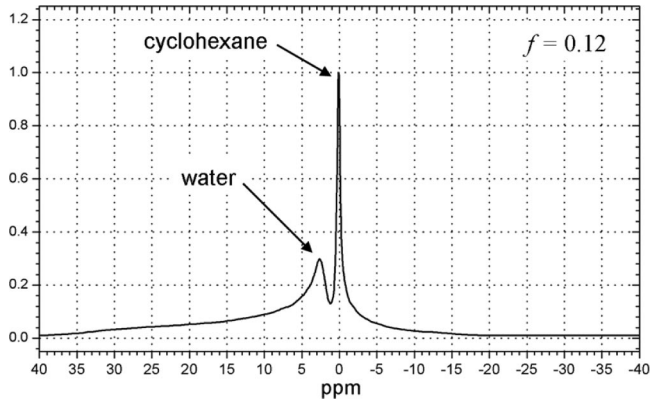

FIG. 3. 400 MHz proton spectrum of nanoporous glass Vycor exposed to open air for some time. The pores were filled with cyclohexane at a filling factor of 0.12. Apart from the cyclohexane line, a relatively strong water resonance is visible. This water originates mainly from the air humidity. Preparing the samples under absolutely dry conditions and sealing the samples carefully during the experiments reduces the water content to a level where no perceptible influence on spin-lattice relaxation can be detected even at the lowest filling degrees and frequencies.

The field-cycling NMR relaxometry measurements were performed with a Stelar relaxometer covering proton frequencies from 1 kHz to 10 MHz. The field-cycling relaxometer was equipped with home made auxiliary compensation coils ensuring that the earth field and stray fields from other magnets in the lab did not interfere. The precision of the field cycles especially at the lowest frequencies and for short relaxation times was checked with the aid of a fast Hall teslameter (Projekt Elektronik FM 210) probing the flux density at the sample position during test field cycles. The bandwidth of the teslameter is 35 kHz, the resolution 0.01 mT. All relaxation curves could be described by monoexponential

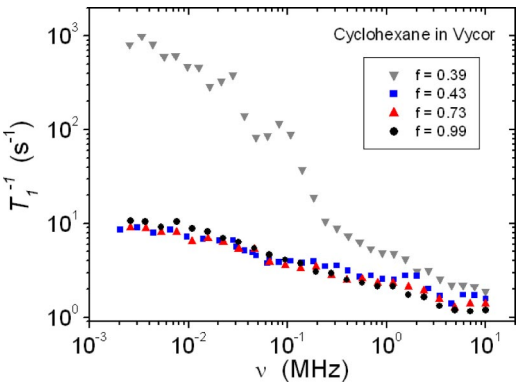

FIG. 4. Spin-lattice relaxation rates in Vycor partially filled with cyclohexane vs the frequency. The sample was kept at open air for some time, so that water was taken up from the air humidity. Such water traces cause the apparent dispersion step visible at about 100 kHz for cyclohexane filling degrees of $f\approx0.4$ or less. This experimental artifact can safely be avoided by preparing the samples in a dry atmosphere and keeping them carefully sealed during the experiments.

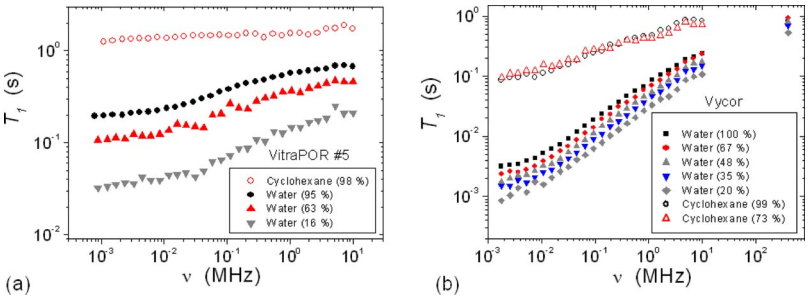

FIG. 5. Dispersion curves of the spin-lattice relaxation time in (a) water and cyclohexane in VitraPOR #5 (pore size 1–1.6 μm) and (b) water and cyclohexane in Vycor (nominal pore size 4 nm) for different filling factors.

functions over about one decade of the signal amplitude. No separate relaxation component could be identified as long as the pores were filled with a single adsorbate species.

The low-frequency range was supplemented by the 400 MHz channel of a conventional Bruker DSX 400 NMR spectrometer. In this case, the spin-lattice relaxation measurements were performed with the standard saturation recovery method providing again monoexponential relaxation curves over at least one decade of the signal amplitude.

IV. RESULTS AND DISCUSSION

The spin-lattice relaxation dispersion of water and cyclohexane in completely filled porous glasses deviate strongly from each other, which was interpreted in our previous papers as a manifestation of the ''strong'' (water) and ''weak'' (cyclohexane) adsorption limits.[12,13] Figure 5 shows the data obtained with the samples of the present study at different filling degrees. A more or less strong dependence on the filling factor is obvious.

The dependences of the adsorbate proton spin-lattice relaxation time on the filling factor at various frequencies are plotted in Figs. 6(a)–6(d). Since we are particularly interested on the distinction of the two limits represented by Eqs. (17) and (18), it may be more elucidating to plot the quantity f/T_1 versus f in order to reveal any dominance of the linear or square relationship with f, respectively. The corresponding data are plotted in Figs. 7(a)–7(d).

The data can be well described by the formalism described above. The solid lines in Figs. 6(a)–6(c) and 7(a)–7(c), that is, for water and cyclohexane in VitraPOR and water in Vycor represent the slow correlation exchange limit given in Eq. (17), whereas the data for cyclohexane in Vycor [Figs. 6(d) and 7(d)] can be described by the fast correlation exchange limit represented by Eq. (18). The different behavior for different pore sizes is particular obvious for the cyclohexane data in Figs. 7(a) and 7(d) which suggest the applicabilities of the slow [Eq. (17)] and fast [Eq. (18)] correlation exchange limits, respectively. However, even the water data show dramatic variations with respect to the f/T_1 values which deviate from each other by more than a decade at low frequencies [see Figs. 7(b) and 7(c)].

The fitting parameters used for the description of the model are $T_{1,b}$ and $a=(\lambda A/V_0)(1/T_{1,a}-1/T_{1,b})$ in the case of Eq. (17) or $a=(\lambda A/V_0)^2(1/T_{1,a}-1/T_{1,b})$ for Eq. (18) as listed in Table I. The parameter

$$\rho=\lambda(1/T_{1,a}-1/T_{1,b}) \tag{19}$$

is a phenomenological constant considered to be characteristic for the surface interaction.[8] The ratio $f_{\mathrm{exp}}/f_{\mathrm{min}}$ is the quotient between the lowest filling factor f_{exp} that can be handled experimentally, and the theoretical filling factor f_{min} corresponding to an adsorption layer of an average thickness λ on the pore walls. f_{min} is calculated with Eq. (15) for $V_b=0$.

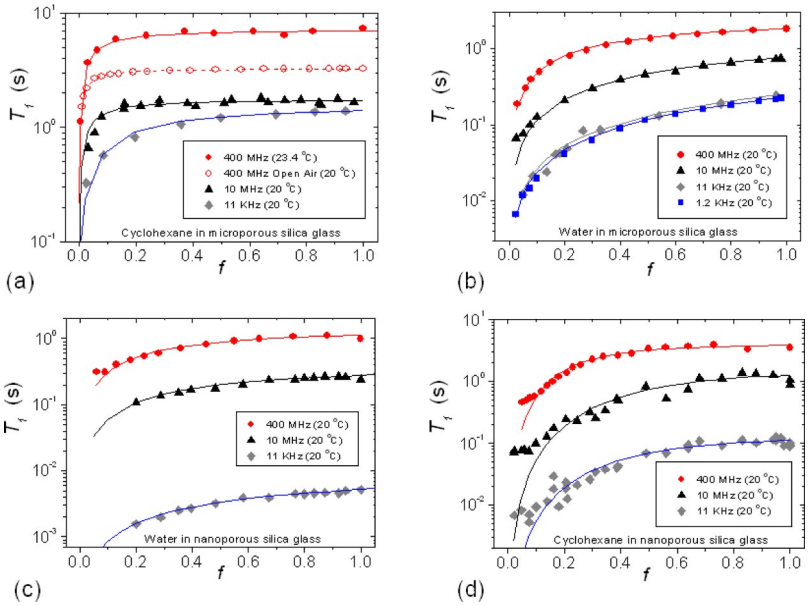

FIG. 6. Spin-lattice relaxation time T_1 as a function of the filling factor. (a) Cyclohexane and (b) water in microporous sample glass (VitraPOR #5). (c) Water and (d) cyclohexane in nanoporous sample glass (Vycor). The solid lines represent fits of the slow correlation exchange limit Eq. (17) [to the data in (a), (b), and (c)] and of the fast correlation exchange limit Eq. (18) [to the data in (d)].

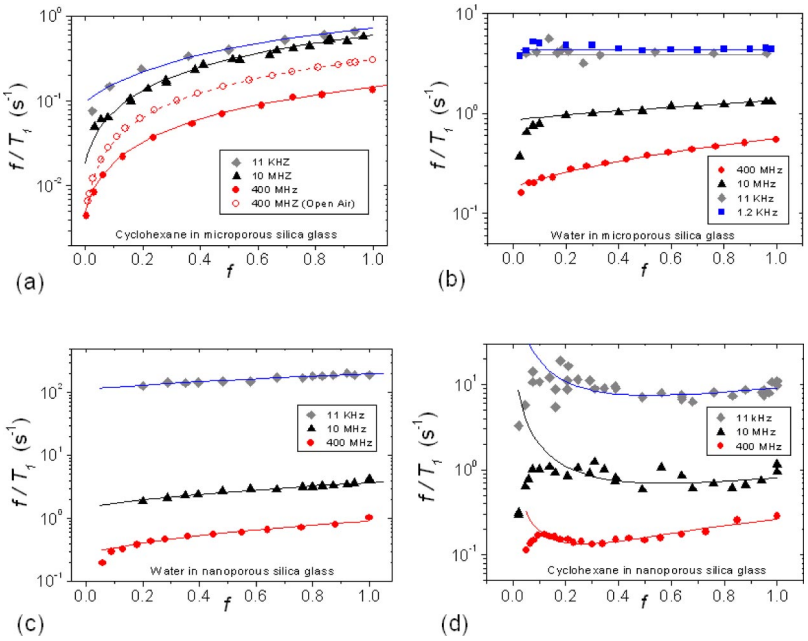

FIG. 7. Spin-lattice relaxation rates weighted with the filling factor f as a function of the filling factor f. (a) Cyclohexane and (b) water in microporous sample glass (VitraPOR #5). (c) Water and (d) cyclohexane in nanoporous sample glass (Vycor). The solid lines represent fits of the slow correlation exchange limit according to Eq. (17) [(a), (b), and (c)] and of the fast correlation exchange limit according to Eq. (18) [(d)].

For VitraPOR #5 (1 μm pores) the ratio $f_{\mathrm{exp}}/f_{\mathrm{min}}$ is found to be quite large for both adsorbate species. This is in contrast to Vycor (4 nm pores) where very low values were evaluated. The values of the mean adsorption layer thickness λ correspond to about one molecular diameter in the case of water, but are much less than the diameter of an adsorbate molecule in the case of cyclohexane. The latter finding indicates that cyclohexane does not uniformly wet the silica glass surfaces.

The mean water adsorption layer thickness λ is in between two and three molecular diameters.[2] For cyclohexane the thickness λ is less than one or two molecular diameters[6,29] where the molecular diameter is about 5.5 Å.[32]

A different situation appears to apply to the data for cyclohexane in Vycor (4 nm pores) shown in Figs. 6(d) and 7(d). These curves can be better described assuming the fast correlation exchange limit, i.e., Eq. (18). Only at the lowest filling factors, $f<0.2$, the theoretical curve significantly deviates from the experimental data. This finding is considered to be an indication of a *direct* influence of the vapor phase on spin-lattice relaxation in the adsorption layer. In all other cases, the effect is an *indirect* one due to the different populations of the adsorbed and bulklike phases upon variation of the filling degree.

When molecular exchange with the vapor phase becomes effective on the time scale of the NMR correlation function, the effective diffusivity will be much larger.[5] The RMTD correlation function therefore decays faster and the spin-lattice relaxation times become longer than expected in the absence of the vapor phase. This vapor phase effect clearly shows up in Fig. 6(d) at the lowest filling degrees below about 0.2 for cyclohexane in Vycor.

Nevertheless, the two-phase assumption for our formalism is still maintained at all filling degrees. The vapor phase need not be considered explicitly as such. The reasons are the low density of this phase and the relatively low spin-lattice relaxation rates. At the finite filling degrees of our experiments, both the signal and relaxation contributions are negligible.

Figure 8 shows the variation of the ratio f/f_{min} as a function of the filling factor. The data for VitraPOR #5 (1 μm pores) are more than two decades larger than those for Vycor (4 nm pores). This is considered to be a consequence of the different surface-to-volume ratios in the two materials and, with respect to the differences between the two adsorbate species, of the different wetting properties.

The frequency scale of our experimental window corresponds to a time scale in the inverse sense: $2\pi\nu \triangleq t^{-1}$. That is, a crossover between the slow and fast correlation exchange limits could be passed when scanning the spin-lattice relaxation dispersion from high to low frequencies. Judged from the data in Figs. 6(a)–6(c) and 7(a)–7(c) for cyclohexane and water confined in microporous glasses and water confined in nanoporous glasses, such a crossover cannot be concluded compellingly. Rather the slow correlation exchange limit ($\tau_{rot} \ll t \ll \tau_{ex}$) appears to apply in the whole frequency range for these samples apart from some minor deviations. The lowest frequencies accessible thus permit

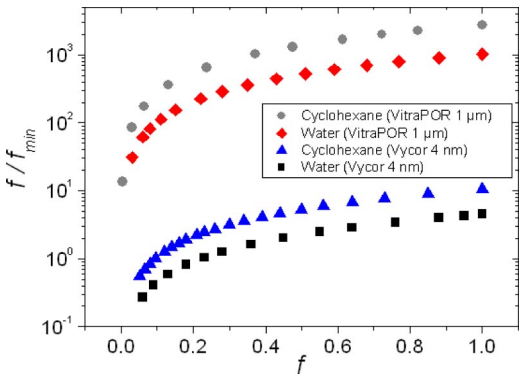

FIG. 8. Plots of f/f_{min} vs the filling factor f. The quantity f_{min} is the filling factor resulting from a surface layer of thickness λ (adsorption layer).

one to estimate the longest times probed in the experiments. In this way, one can estimate lower limits of the exchange time $\tau_{a,b}$.

Vice versa, the fast correlation exchange limit ($t \gg \tau_{a,b} \gg \tau_{rot}$) which appears to apply to cyclohexane in 4 nm pores suggests upper limits of the exchange time $\tau_{a,b}$. The lowest frequency at which the dependence on the filling factor was examined in detail was 11 kHz for cyclohexane. Water in micrometer pores was also investigated at 1.2 kHz, but there was little variation of the data [see Figs. 6(b) and 7(b)]. Taking 11 kHz as the relevant frequency limit, we estimate a respective minimum or maximum value of 10^{-5} s for the exchange time.

The evaluation of the experimental data with the aid of Eqs. (17) and (18) provides values of the spin-lattice relaxation time $T_{1,b}$ (see Table 1). In the adsorption layer, the spin-lattice relaxation time $T_{1,a}$ may be estimated based on literature values of λ. These two relaxation times are considered to reflect molecular dynamics in the two phases in the absence of exchange. As a feature intrinsic to the evaluation formalism, there is no dependence on the filling factor. However, there is a significant frequency dependence down to the lowest frequencies [compare Figs. 5(a) and 5(b)]. The explanation for this dependence is due to the dispersion of $T_{1,a}$ in the adsorption layer following from the RMTD mechanism as discussed in previous papers for polar and nonpolar adsorbate species.[12,13]

On the other hand, the frequency dependence and the low values of $T_{1,b}$ indicate that molecular dynamics in the bulklike phase deviates from that in bulk unconfined liquids, where no low-frequency dispersion is observed and where the spin-lattice relaxation times are much longer. The conclusion is that rotational diffusion is affected by the confinement even if the molecules are not directly adsorbed. This effect is consequently stronger in the nanoscopic than in the microscopic pores.

Porous silica glasses saturated with polar and nonpolar organic solvents such as pyridine-d_5 and cyclohexane-d_{12}, respectively, were studied by Jonas *et al.*[33] as a function of the pore size in the range from 1.8 to 15.2 nm. Also assuming a two-phase fast-exchange model they conclude a linear dependence of the spin-lattice relaxation rate of polar liquids on the reciprocal pore radius. Actually this is another way to express Eq. (16) in the saturation limit (filling factor $f = 1.0$) assuming that the layer thickness λ is constant. That is a linear dependence of T_1^{-1} on the probability p_a. On the other hand, in the case of cyclohexane-d_{12}, the spin-lattice relaxation rate obeys a square dependence on the reciprocal pore radius, that is, $T_1^{-1} \sim p_a^2$. These results consequently are in full accordance with the model proposed in the present paper.

V. CONCLUSIONS

We have studied the molecular exchange dynamics in two porous silica glasses partially filled with water (polar) or cyclohexane (nonpolar) with the aid of field-cycling NMR relaxometry. The nominal pore sizes were of the order 4 nm and 1 μm.

A formalism for the effective spin-lattice relaxation time as a function of the filling degree was developed describing the experimental data very well. Two limits with respect to the molecular exchange rates between the adsorption layer and the bulklike phase are distinguished. In the fast and slow correlation exchange limits, the exchange time is considered to be short and long relative to the time at which the dipolar correlation function is considered, respectively. The relevant time scale of the dipolar correlation function is defined by the experimental frequency window (10^3–10^8 Hz). These cases on the other hand imply that exchange on the time scale of spin-lattice relaxation is fast, of course. The exchange time is estimated to be of the order 10^{-5} s.

That is, our formalism anticipates a ''two-phase fast relaxation exchange situation'' with respect to the liquid phases. The vapor phase contributes indirectly via the different populations of the liquid phases upon variation of the filling degree. There is also a vapor phase contribution by the enhanced diffusivity becoming effective in the fast correlation exchange limit at low filling factors ($f < 0.2$) for cyclohexane in nanoscopic pores. The effect is that the spin-lattice relaxation times are longer than expected from the two-phase fast relaxation exchange model.

In the frame of our formalism, the spin-lattice relaxation time in the bulklike phase, $T_{1,b}$, is taken as a fitting parameter for the description of the dependences on the filling factor. Based on this sort of evaluation, we find that the spin-lattice relaxation times in the liquid phase depend on the pore size and on the frequency down to the lowest fields in contrast to the behavior of unconfined bulk samples. This in particular refers to confinements by nanoscopic pores. The conclusion is that the thermodynamic state of the bulklike phase and consequently molecular dynamics varies with the length scale of the confinement.

The slow correlation exchange limit characterized by a linear dependence of the spin-lattice relaxation rate on the filling degree was verified for all samples except for cyclohexane in nanoscopic pores. In the latter case, the quadratic dependence characteristic for the fast correlation exchange limit fits much better to the experimental data. This finding correlates well with the direct influence of the vapor phase for $f < 0.2$ observed for cyclohexane in Vycor.

The slow correlation exchange behavior found in three of the four sample configurations has some impact on the type of molecular dynamics in the adsorption layer. The conclusion is that the relaxation mechanism dominant at low frequencies, that is RMTD, takes place in the adsorption layer in the sense of a surface diffusion process. The adsorption layer implies some degree of lateral translational mobility on the pore surfaces. ''Excursions to the bulklike phase'' anticipated in the ''bulk mediated surface diffusion'' model proposed by Bychuk and O'Shaughnessy[34] are therefore not really needed for an efficient RMTD relaxation mechanism.

Monte Carlo computer simulations are currently employed for further elucidation of the complex situation one is facing in partially filled nanoscopic or microscopic pores. The results will be published elsewhere.

ACKNOWLEDGMENTS

The authors thank Esteban Anoardo for helpful discussions. This work was supported by the Deutsche Forschungsgemeinschaft and the Alexander von Humboldt Foundation.

[1] J. Kärger, H. Pfeifer, E. Riedel, and H. Winkler, J. Colloid Interface Sci. **44**, 187 (1973).
[2] F. D'Orazio, S. Bhattacharja, W. P. Halperin, and R. Gerhardt, Phys. Rev. Lett. **63**, 43 (1989).
[3] R. Kimmich, S. Stapf, P. Callaghan, and A. Coy, Magn. Reson. Imaging **12**, 339 (1994).
[4] R. Kimmich, S. Stapf, R. O. Seitter, P. Callaghan, and E. Khozina, Mater. Res. Soc. Symp. Proc. **366**, 189 (1995).
[5] I. Ardelean, C. Mattea, G. Farrher, S. Wonorahardjo, and R. Kimmich, J. Chem. Phys. **119**, 10358 (2003).
[6] R. Kimmich, S. Stapf, A. I. Maklakov, V. D. Skirda, and E. V. Khozina, Magn. Reson. Imaging **14**, 793 (1996).
[7] I. Ardelean, G. Farrher, C. Mattea, and R. Kimmich, J. Chem. Phys. **120**, 9809 (2004).
[8] F. D'Orazio, S. Bhattacharja, W. P. Halperin, K. Eguchi, and T. Mizusaki, Phys. Rev. B **42**, 9810 (1990).
[9] J. P. Korb, M. Whaley-Hodges, and R. G. Bryant, Phys. Rev. E **56**, 1934 (1997).
[10] D. W. Aksnes and L. Gjerdaker, J. Mol. Struct. **475**, 27 (1999).
[11] J. R. Banavar and L. M. Schwartz, Phys. Rev. Lett. **58**, 1411 (1987).
[12] T. Zavada and R. Kimmich, J. Chem. Phys. **109**, 6929 (1998).
[13] S. Stapf, R. Kimmich, and R.-O. Seitter, Phys. Rev. Lett. **75**, 2855 (1995).
[14] T. Zavada, R. Kimmich, J. Grandjean, and A. Kobelkov, J. Chem. Phys. **110**, 6977 (1999).
[15] R.-O. Seitter, T. Link (Zavada), R. Kimmich, A. Kobelkov, P. Wolfangel, and K. Müller, J. Chem. Phys. **112**, 8715 (2000).
[16] P. Levitz, J. P. Korb, and D. Petit, Eur. Phys. J. E **12**, 29 (2003).
[17] C. L. Jackson and G. B. McKenna, J. Chem. Phys. **93**, 9002 (1990).
[18] J. H. Strange, M. Rahman, and E. G. Smith, Phys. Rev. Lett. **71**, 3589 (1993).
[19] I. Ardelean and R. Kimmich, Annu. Rep. NMR Spectrosc. **49**, 43 (2003).
[20] J. Kärger, H. Pfeifer, and W. Heink, Adv. Magn. Reson. **12**, 1 (1988).
[21] W. S. Price, Concepts Magn. Reson. **9**, 299 (1997).
[22] P. Stilbs, Prog. Nucl. Magn. Reson. Spectrosc. **19**, 1 (1987).
[23] R. Kimmich and E. Anoardo, Progr. NMR Spectrosc. **44**, 257 (2004).
[24] R. Kimmich, Chem. Phys. **284**, 253 (2002).
[25] E. Anoardo, F. Grinberg, M. Vilfan, and R. Kimmich, Chem. Phys. **297**, 99 (2004).
[26] S. Stapf and R. Kimmich, Mol. Phys. **92**, 1051 (1997).
[27] R. Valiullin, R. Kimmich, and N. Fatkullin, Phys. Rev. E **56**, 4371 (1997).
[28] E. E. Burnell, M. E. Clark, J. A. M. Hinke, and N. R. Chapman, Biophys. J. **33**, 1 (1981).
[29] S. G. Allen, P. C. L. Stephenson, and J. H. Strange, J. Chem. Phys. **106**, 7802 (1997).
[30] R. Hausser and F. Noack, Z. Naturforsch. **20a**, 1668 (1965).
[31] R. Kimmich and A. Peters, Chem. Phys. Lipids **14**, 350 (1975).
[32] J. Jonas, D. Hasha, and S. G. Huang, J. Phys. Chem. **84**, 109 (1980).
[33] G. Liu, Y. Li, and J. Jonas, J. Chem. Phys. **95**, 6892 (1991).
[34] O. V. Bychuk and B. O'Shaughnessy, J. Chem. Phys. **101**, 772 (1994).

IV

C. Mattea, N. Fatkullin, E. Fischer, U. Beginn, E. Anoardo, M. Kroutieva and R. Kimmich.

The "corset effect" of spin-lattice relaxation in polymer melts confined in nanoporous media.

Appl. Magn. Reson. **27**, 371 (2004).

Appl. Magn. Reson. 27, 371–381 (2004)

Applied Magnetic Resonance

© Springer-Verlag 2004
Printed in Austria

The "Corset Effect" of Spin-Lattice Relaxation in Polymer Melts Confined in Nanoporous Media

C. Mattea[1], N. Fatkullin[2], E. Fischer[1], U. Beginn[3], E. Anoardo[4], M. Kroutieva[2], and R. Kimmich[1]

[1] Universität Ulm, Ulm, Germany
[2] Kazan State University, Kazan, Russian Federation
[3] Rheinisch-Westfälische Technische Hochschule Aachen, Aachen, Germany
[4] Universidad Nacional de Córdoba, Ciudad Universitaria, Córdoba, Argentina

Received October 30, 2003

Abstract. Linear polyethylene oxides with molecular weights M_w of 1665 and 10170 confined in pores with variable diameters in a solid methacrylate matrix were studied by proton field-cycling nuclear magnetic resonance relaxometry. The pore diameter was varied in the range of 9–57 nm. In all cases, the spin-lattice relaxation time shows a frequency dependence close to $T_1 \propto \nu^{3/4}$ in the range of $\nu = 3 \cdot 10^{-1}$–$2 \cdot 10^{1}$ MHz as predicted by the tube-reptation model. This proton T_1 dispersion essentially reproduces that found in a previous deuteron study (R. Kimmich, R.-O. Seitter, U. Beginn, M. Möller, N. Fatkullin: Chem. Phys. Lett. 307, 147, 1999). As a feature particularly characteristic for reptation, this finding suggests that reptation is the dominating chain dynamics mechanism under pore confinement in the corresponding time range. The absolute values of the spin-lattice relaxation times indicate that the diameter of the effective tubes in which reptation occurs is much smaller than the pore diameters on the time scale of spin-lattice relaxation experiments. An estimation leads to a value $d^* \sim 0.5$ nm. The impenetrability of the solid pore walls, the uncrossability of polymer chains ("excluded volume") and the low value of the compressibility in polymer melts create the "corset effect" which reduces the lateral motions of polymer chains to a microscopic scale of only a few tenths of a nanometer.

1 Introduction

In previous papers [1–3] it was shown that polymer melts confined in porous media are subject to chain dynamics considerably deviating from the behavior in bulk. These studies were performed by field-cycling nuclear magnetic resonance (NMR) relaxometry and field-gradient NMR diffusometry in the fringe-field variant [4, 5]. It turned out that the dynamical limits predicted for the tube-reptation model [6, 7] can be well reproduced with experiments in polymer melts confined in nanoporous solid matrices. The motivation of the present work is the attempt to detect experimentally the crossover from confined to bulk behavior by varying the pore diameter, or more precisely, to probe the length scale

on which pores give rise to confined chain dynamics. A theoretical treatment and a Monte Carlo simulation of this sort of phenomenon was recently published in ref. 8. A further objective of this article is to estimate theoretically the diameter of the "tube" (in contrast to that of the pores) effective under confinement conditions on the time scale of spin-lattice relaxation experiments.

2 Samples and Techniques

The nanoporous methacrylate samples were prepared as semi-interpenetrating networks from a variable mixture of hydroxyethyl-methacrylate, dodecyl-methacrylate and 1,2-ethyleneglycol-dimethacrylate in which linear polyethylene oxide (PEO) was incorporated in pores. The experiments refer to mainly two almost monodisperse PEO fractions purchased from Aldrich and characterized by gel permeation chromatography in our laboratory. The molecular weights were M_w = 1665 and 10170, the polydispersity was $M_w/M_n \approx 1.08$ and $M_w/M_n \approx 1.07$, respectively. The bulk value of the critical molecular weight of PEO is reported to be in the range M_c = 3600–5900 [9, 10]. That is, polymer dynamics was examined below as well above M_c.

The preparation method is similar to that published in refs. 11 and 12. A more detailed description and additional sample characterization experiments were reported in ref. 13. Figure 1 shows typical electron micrographs visualizing the pore channels in which the PEO chains are free to move. The pore diameters can be estimated crudely from the electron micrographs and more precisely by fitting the theoretical spin echo attenuation curves to field-gradient NMR diffusometry data [13]. Values between 9 and 57 nm were found, depending on the composition of the matrix. The samples were evacuated over night in order to remove any volatile constituents.

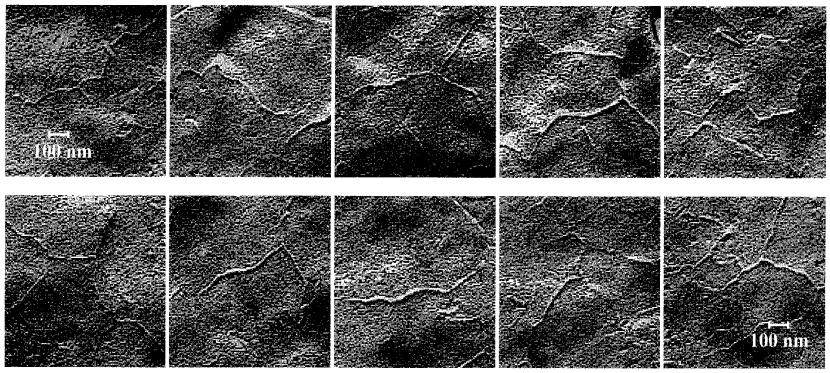

Fig. 1. Typical freeze-fracture electron micrographs of semi-interpenetrating networks formed of cross-linked methacrylate and linear PEO (M_w = 6000). The "worm-like" structures represent PEO that was contained in pores with a diameter of about 10 nm.

An important feature of these methacrylate samples is that polymers are studied in a polymer matrix. That is, the environment of the molecules of interest is of a similar chemical and therefore almost inert composition. This is in contrast to our previous attempt to study the confinement effect on polymer dynamics in pores by filling polydimethylsiloxane in porous silica glasses. In that case, the differences in chain dynamics between the bulk and confined states are partly concealed by strong wall adsorption effects [14].

The NMR measurements were carried out with the aid of a STELAR relaxometer supplemented by two conventional high-field instruments operating at 4.7 (200 MHz) and 9.4 T (400 MHz). The influence of the earth field and other spurious fields in the laboratory to the field-cycling magnet were compensated by auxiliary compensation coils [15, 16], so that measurements down to less than 1 kHz became reliably possible. The timing and level precision of the field cycle was checked at the sample position with the aid of a sensitive digital teslameter (Projekt Elektronik FM210) having a bandwidth of 35 kHz and a resolution of 0.01 mT. The measuring principle is based on the Hall effect.

In contrast to our previous investigation [1], all data refer to proton resonance. It appears that the same information is obtained from this nucleus, although the solid matrix contains protons as well. The fact is that the free-induction signal of matrix protons dies away to a negligible contribution within a very short time (less than 50 μs). This was tested with the matrix material alone studied under the same conditions as the PEO filled samples. All signals evaluated for measuring the PEO spin-lattice relaxation dispersion were recorded after a corresponding delay so that no matrix signal above noise level contributed. All longitudinal relaxation curves recorded in this way could be fitted by monoexponential functions in a time range of at least $4T_1$. The comparison with the deuteron relaxation dispersion reported in ref. 1 also indicates that cross-relaxation between PEO and the matrix has no perceptible influence.

Proton transverse relaxation times of the PEO component were measured at 200 MHz by the Hahn echo method. The relaxation curves could be fitted by a monoexponential decay function over at least half a decade. Note that any matrix signal is totally negligible at the times when the Hahn echoes were recorded.

3 Experimental Results

Figure 2 shows the proton spin-lattice relaxation dispersion measured in PEO melts both in bulk and confined in pores. The frequency dependence for PEO 1665 in bulk, i.e., for a molecular mass well below the critical value, is characteristic for Rouse dynamics [17, 18]. Above M_c, the T_1 dispersion of bulk PEO is somewhat stronger and corresponds to the behavior reported in previous papers on bulk polymer melts [17, 19]. The low-frequency plateau showing up with the PEO 10170 bulk data indicates the crossover to "component C" of polymer chain dynamics, that is the loss of any orientation correlation beyond the longest correlation time of chain dynamics [17, 20]. The cutoff frequency below which this

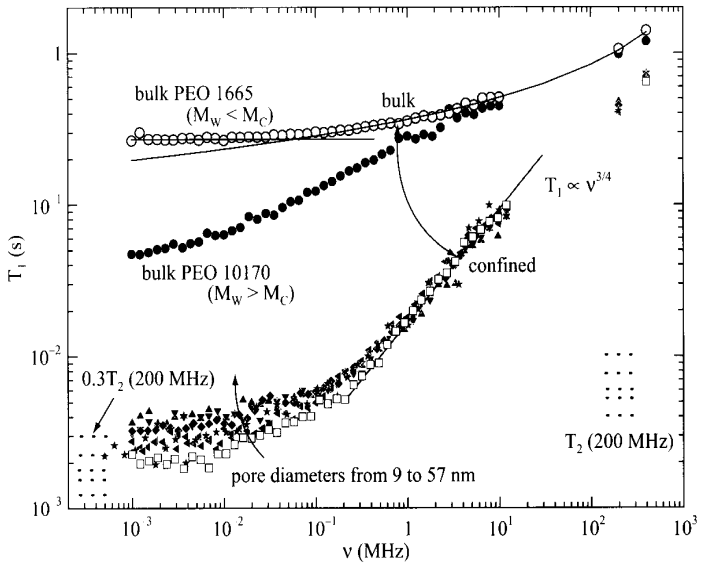

Fig. 2. Frequency dependence of the proton spin-lattice relaxation times of linear PEO in bulk and confined in porous methacrylate samples at 85°C. The data for PEO 1665 and PEO 10170 are represented by open and filled symbols, respectively. The pore diameters of the different methacrylate samples were evaluated from NMR diffusometry data [13] to be 9, 13, 21, 33, and 57 nm. The PEO 1665 data refer to a pore diameter of 9 nm. The proton signal of the matrix was negligible under the experimental conditions. The straight solid line represents the power law $T_1 \propto \nu^{3/4}$ predicted by de Gennes as a law characteristic for reptation [6, 8]. The data at 200 and 400 MHz have been recorded with conventional high-field NMR spectrometers. Transverse relaxation times measured at 200 MHz and 85°C for PEO 10170 in the diverse porous methacrylate samples are indicated as horizontal dotted bars. These values can be extrapolated to the low-frequency limit according to the Bloch-Wangsness-Redfield theory by division by 10/3 [4] as marked in the diagram. The 200 MHz transverse relaxation times of PEO 10170 for the diverse pore diameters are as follows: $T_2(9) = 4$; $T_2(13) = 5.1$; $T_2(21) = 5.9$; $T_2(31) = 7.5$; $T_2(57\text{ nm}) = 10.1$ ms. The upper solid curves were fitted to the experimental data of bulk PEO 1665 using Eqs. (1) and (2) predicted for the Rouse model with some influence of local segment dynamics ("component A"). The fitted parameters are $\tau_s = 4.7 \cdot 10^{-11}$ s, $C_1 = 7.1 \cdot 10^9$ s^{-2}, $C_2 = 3.5 \cdot 10^8$ s^{-2}, $C_1^* = 5.2 \cdot 10^9$ s^{-2}, $C_2^* = 1.5 \cdot 10^9$ s^{-2}. Both the T_2 and the low-frequency T_1 values slightly increase with increasing pore diameter.

sort of plateau arises strongly depends on the molecular weight and is normally only visible in the frequency window of field-cycling NMR relaxometry for molecular weights $M_w \ll 100000$ [17].

The situation changes dramatically when the PEO chains are confined in pores irrespective of whether their molecular weight is below or above M_c. Above 300 kHz, the data can be described by a power law close to $T_1 \propto \nu^{3/4}$ as it was predicted by de Gennes for the time scale below the longest Rouse relaxation time [6, 8]. Note that this power law was verified by deuteron relaxation dispersion in an even wider range [1]. At the highest frequencies of this study, 200 and 400 MHz, some influence of local motions on the length scale of Kuhn segments may already exist causing values somewhat lower than expected from

de Gennes' prediction. It should also be noted that the slopes of the spin-lattice relaxation dispersion observed with protons tend to be slightly flatter than those found with deuterons [1, 17, 19].

The low-frequency plateaus of the confined polymer melts are of a nature different from the component C cutoff mentioned above in context with melts in bulk. The absolute values of the spin-lattice relaxation times of confined polymers are considerably reduced relative to the bulk values. As a consequence there is some tendency that the low-frequency spin-lattice relaxation times are not longer than all correlation times of chain dynamics anymore. All predictions of the standard perturbation theory of spin-lattice relaxation are therefore no longer valid, and the plateau value more or less coincides with the transverse relaxation times extrapolated from 200 MHz to the low-frequency limit [1].

The plateau values are practically independent of the chain length but show a slight increase with the pore diameter. The latter finding indicates that the polymer chains are subject to some immobilization with decreasing pore size. Note that the transverse PEO relaxation times measured at 200 MHz vary in the same way as the low-field T_1 plateaus (Fig. 2).

4 Analysis of the Experimental Data

The time scale of chain modes of interest here, $\tau_s < t < \tau_R$, is limited by the local Kuhn segment fluctuation time τ_s on the one hand and by the (longest) Rouse relaxation time $\tau_R = \tau_s N^2$ on the other [7, 17]. N is the number of Kuhn segments per chain. At frequencies within the limit $\omega\tau_s \ll 1$, that is, at very low frequencies, the spin-lattice relaxation of polymer chains is mainly determined by reorientations of the segment tangent vector due to chain modes [8, 17]. The experimental results suggest that reorientation dynamics of the segment tangent vector is substantially different in polymer melts in bulk and confined in porous media.

Polymer chain dynamics is particularly simple in bulk melts in the "unentangled" state, i.e., for molecular weights $M_s \ll M \ll M_c$, where M_s is the molecular weight of a Kuhn segment, and M_c is the so-called critical molecular weight, an empirical constant indicating the crossover to entangled chain dynamics [8, 17]. The spin-lattice relaxation dispersion within this limit can be derived from the Rouse model for polymers dispersed in an infinite viscous medium as [8, 17, 21, 22]

$$\frac{1}{T_1^R} = 0.63\tilde{M}_2\tau_s \ln\left(\frac{0.95}{\omega\tau_s}\right) + 0.63\tilde{M}_2^*\tau_s = C_1\tau_s \ln\left(\frac{1}{\omega\tau_s}\right) + C_2\tau_s. \qquad (1)$$

The second term on the right-hand side is the low-frequency contribution of all local fluctuations within the Kuhn segments which are usually called component A (see ref. 17 for comparison). The quantity $\tilde{M}_2$ is the residual second moment of spin interactions after averaging over all fast fluctuations occurring on a time scale $t \ll \tau_s$. The quantity $\tilde{M}_2^*$ represents the second moment characterizing the

initial value of the correlation function for component A. The parameters fitted to the experimental data are C_1, C_2 and τ_s.

Equation (1) is valid for polymer melts in bulk at frequencies $1/\tau_R \ll \omega \ll 1/\tau_s$ and for molecular weights $M_s \ll M_w \ll M_c$. At lower frequencies, $\omega \ll 1/\tau_R$, the spin-lattice relaxation time becomes equal to the transverse relaxation time and can be described by

$$\frac{1}{T_1^R} = \frac{1}{T_2^R} = 0.7\tilde{M}_2\tau_s \ln(0.35N^2) + 0.7\tilde{M}_2^*\tau_s = C_1^*\tau_s \ln(M^2) + C_2^*\tau_s, \qquad (2)$$

where M is the molecular weight.

If chain modes are restricted by randomly coiled cylindrical pores in a rigid matrix, polymer dynamics changes considerably and the reptation model becomes relevant as discussed in detail in a previous paper [8]. The "harmonic radial tube potential" theory suggests then

$$\frac{1}{T_1^{rep}} = \frac{2\pi^{1/4}3^{1/2}}{1215}\Gamma(5/4)\cos(\pi/8)(1+2\cdot 2^{1/4})\frac{b^3\tilde{l}}{d^4}\frac{\tilde{M}_2\tau_s}{(\omega\tau_s)^{3/4}}, \qquad (3)$$

where b is the length of a Kuhn segment, d is the effective diameter of the tube in which the polymer chain is confined, $\tilde{l}$ is the persistence length of the randomly coiled tube. Equation (3) is valid in the frequency range $1/\tau_R \ll \omega \ll 1/\tau_e$, where τ_e is the time after which polymer segments start to "sense" the walls of the effective tube. This equation can be obtained from eq. (77) in ref. 8 after correction of a misprint in the numerical coefficient by using eqs. (47) and (48) in ref. 8.

Dividing Eq. (3) by Eq. (1) gives

$$\frac{T_1^R}{T_1^{rep}} = \frac{2\pi^{1/4}3^{1/2}}{765}\Gamma(5/4)\cos(\pi/8)(1+2\cdot 2^{1/4})\frac{b^3\tilde{l}}{d^4(\omega\tau_s)^{3/4}\ln(0.95/\omega\tau_s)}.$$

From this equation we get an expression for the effective diameter of a randomly coiled, cylindric tube confining polymer chains with a harmonic radial potential:

$$d = \left(\frac{T_1^{rep}}{T_1^R}\frac{2\pi^{1/4}3^{1/2}}{765}\Gamma(5/4)\cos(\pi/8)(1+2\cdot 2^{1/4})\frac{\tilde{p}}{(\omega\tau_s)^{3/4}\ln(0.95/\omega\tau_s)}\right)^{1/3} b, \qquad (4)$$

where $\tilde{p} = \tilde{l}/d$. Inserting experimental data for the spin-lattice relaxation time of polymer melts with $M_w < M_c$ measured at the same Larmor frequency ω in the bulk (Rouse; $T_1 \approx T_1^R$) and in the confined state (reptation; $T_1 \approx T_1^{rep}$) permits one to evaluate the effective tube diameter relative to the Kuhn segment length. The accuracy is rather good since $\tilde{p} = \tilde{l}/d$ is of the order 1 and enters Eq. (4) only in cube-root form.

The Kuhn segment relaxation time τ_s can be determined in the following way. The diffusion coefficient measured in unentangled polymer melts according to the Rouse model [7] obeys

$$D^R = \frac{1}{3\pi^2}\frac{R_F^2}{\tau_s N^2},$$

where $R_F^2 = b^2 N$ is the squared Flory radius (or root mean squared chain end-to-end vector) of the polymer chain. For the squared Flory radius we have

$$\frac{R_F^2}{M} = C_\infty l_0^2 / m_0. \tag{5}$$

C_∞ is the so-called characteristic ratio, which is known for most polymer species, l_0 is the average backbone bond length of the polymer, m_0 is the monomer molecular mass per backbone bond. The Flory radius furthermore obeys

$$R_F^2 = Lb,$$

where $L = l_0 M/m_0$ is the length of the stretched chain. The number of Kuhn segments per chain thus is

$$N = \frac{M}{C_\infty m_0}.$$

On this basis the segmental relaxation time can be expressed by

$$\tau_s = \frac{C_\infty^3 l_0^2 m_0}{3\pi^2 D M_w}, \tag{6}$$

where we have equated theoretical and experimental quantities according to $M \approx M_w$ and $D^R \approx D$.

For PEO we have $C_\infty = 5.59$, $l_0 = 0.145$ nm, $m_0 = 14.7$ (see ref. 23, for example). For $M_w = 1665$ at $\vartheta = 85°C$ the self-diffusion coefficient is found to be $D = 1.3 \cdot 10^{-11}$ m^2/s. Inserting these numbers in Eq. (6) gives $\tau_s \approx 7 \cdot 10^{-11}$ s. The Rouse relaxation time of PEO 1665 is then expected to be

$$\tau_R = \tau_s N^2 = \tau_s \frac{M_w^2}{C_\infty^2 m_0^2} \approx 3 \cdot 10^{-8} \text{ s}.$$

For $\nu = \omega/2\pi = 4$ MHz the experimental spin-lattice relaxation times of PEO 1665 at 85°C are $T_1 \approx T_1^R \approx 4 \cdot 10^{-1}$ s in bulk and $T_1 \approx T_1^{rep} \approx 4 \cdot 10^{-2}$ s for the polymer confined in pores. For a crude estimation the different temperatures of

the diffusion and relaxation measurements (and the difference of the fitted segmental relaxation time and the value suggested by Eq. (6)) can be ignored. On this basis, Eq. (4) suggests the following approximate relation between the effective tube diameter and the Kuhn segment length

$$d \approx 0.36b. \tag{7}$$

The Kuhn segment length of PEO is $b = C_\infty l_0 \approx 0.81$ nm, so that the effective tube diameter is predicted to be $d \approx 0.26$ nm. A result numerically very close to that given at Eq. (7) was obtained in a similar way after analyzing experimental data for deuteron spin-lattice relaxation in a deuterated PEO melt with $M_w = 7400$ in nanopores [1, 24].

Note that with an accuracy of a few percent a relation similar to Eq. (7) can be obtained if the low-frequency limit given at Eq. (2) is used instead of Eq. (1) for estimating the effective diameter of the tube:

$$d = \left(\frac{T_1^{rep}}{T_1^R} \frac{2\pi^{1/4} 3^{1/2}}{850} \Gamma(5/4)\cos(\pi/8)(1 + 2 \cdot 2^{1/4}) \frac{\tilde{p}}{(\omega\tau_s)^{3/4} \ln(0.35N^2)} \right)^{1/3} b\,. \tag{8}$$

This is not surprising, because the logarithmic term is an extremely slowly varying function for arguments sufficiently large. Moreover, Eqs. (4) and (8) contain cube root terms further diminishing the difference. For the same reason, the minor difference in the numerical coefficient of Eq. (1) and the expressions given in refs. 21 and 22 is unimportant.

It is a good place here to point out that the quantity d^2 termed the "square of the effective diameter of the harmonic radial potential" in our previous paper [8] actually has the meaning of the long-time mean-squared displacement of polymer segments in directions lateral to the axis of a cylindrical harmonic radial potential (compare eq. (38) of ref. 8). By taking this into account, the diameter of a cylindrical tube with impenetrable walls is given by $d^* = 2d$.

5 Discussion and Conclusions

In this study we compare the spin-lattice relaxation dispersion in polymer melts in bulk and confined in nanoporous materials with varying pore diameters. The spin-lattice relaxation dispersion in bulk PEO melts below the critical molecular mass can be described by the Rouse model characterized by a logarithmic frequency dependence. Bulk melts above the critical molecular mass, that is, so-called entangled polymers, show a steeper dispersion which however is still far away from the $T_1 \propto \nu^{3/4}$ law predicted by the tube-reptation model for the range $1/\tau_R < 2\pi\nu < 1/\tau_e$. These findings are documented and discussed in our previous publications [17, 19].

The findings for bulk melts are in strong contrast to those for confined polymers. We have studied mobile linear PEO in a quasi-solid, cross-linked polymetha-

crylate matrix. That is, instead of the fictitious tubes assumed by Doi and Edwards [7] to represent entanglements by neighboring chains, we now consider real tubes formed by the nanoporous matrix. The most exciting result is that neither the Doi-Edwards fictitious tube diameter nor the real pore diameter limit fluctuations by chain modes. It is rather an effective tube diameter essentially coinciding with the nearest neighbor distance characteristic for the tight chain packing in polymer melts.

PEO both below and above the critical molecular weight are shown to have a dynamic behavior in common when confined in pores with diameters ranging from 9 to 57 nm. Under these conditions, the frequency dependence of the PEO spin-lattice relaxation time corresponds closely to the tube-reptation prediction, $T_1 \propto \nu^{3/4}$ (see Eq. (3)). Varying the molecular mass has no perceptible effect. Also, increasing the pore diameter merely leads to slightly higher low-frequency plateau values but does not change the high-frequency dispersion indicative for reptation.

The $\nu^{3/4}$ law was observed with deuteron relaxation in an even wider range than with protons [1]. The deviations of the proton data shown in Fig. 2 at very high and very low frequencies can be explained by the influence of local motions ("component A" [17]) and the crossover to another dynamic limit, respectively. Equation (3) is expected to apply to the range $1/\tau_R < 2\pi\nu < 1/\tau_e$ (limit II of the tube-reptation model; for a review see ref. 17). For PEO 1665 and PEO 10170 we have $\nu_{II,III} \approx 1/2\pi\tau_R \approx 5$ MHz and $\nu_{II,III} \approx 1/2\pi\tau_R \approx 145$ kHz, respectively, as crossover frequencies from limit II to limit III of the tube-reptation model [1, 17]. The spin-lattice relaxation dispersion in limit III is expected to be flatter according to $T_1 \propto \nu^{1/2}$ as shown in refs. 6 and 8. Unfortunately the low-frequency plateau, which is of a nature entirely different from those dynamic limits, arises in the same frequency range as expected for limit III, so that the two superimposed phenomena cannot be distinguished unambiguously in the analysis of the experimental data.

The Flory radii of bulk PEO 1665 and PEO 10170 are $R_F \approx 4$ and $R_F \approx 9$ nm, respectively, in accordance with Eq. (5). The largest pore is 15 times wider than the Flory radius of PEO 1665. The confinement effect relative to the behavior in bulk melts is nevertheless clearly visible. The absolute values of the spin-lattice relaxation times indicate that the tube diameter effective for confined polymer chain dynamics is only $d^* = 0.5$ nm on the time scale corresponding to frequencies $\nu \gg 100$ kHz.

This striking behavior will be called the corset effect resulting in a combined way from the impenetrability of the pore walls, from the uncrossability of polymer chains ("excluded volume"), and from the low compressibility of polymer melts. The argument is that polymers confined in cylindrical pores with diameters $d_{pore} \ll R_F$ reptate in tubes with the effective diameter

$$d^* \approx \sqrt{k_B T \kappa_T / p}, \tag{9}$$

where $p = (b^2\rho_m)^{-1}$ is the so-called packing length of the polymer melt and ρ_m is the number density of Kuhn segments. k_BT is the Boltzmann factor multiplied by the absolute temperature, κ_T is the isothermal compressibility.

The question is at what pore diameter the transition from confined to bulk dynamics occurs. The answer is that the bulk behavior is expected for

$$d_{\text{pore}} \gg \frac{b}{(k_B T \kappa_T)^{1/3}} R_F. \tag{10}$$

The corset effect is expected to work when $R_F \gg d_{\text{pore}}$ and disappears in the case of $d_{\text{pore}} \gg b/(k_B T \kappa_T)^{1/3} R_F$. The packing length of PEO is $p = 0.193$ nm [10], the isothermal compressibility is $\kappa_T = 5.5 \cdot 10^{-10}$ m^2/N [25]. For room temperature, Eq. (9) gives $d^* = 0.1$ nm. This is in accordance with the estimation of the effective tube diameter $d^* = 2d \approx 0.5$ nm derived in Sect. 4 from absolute values of spin-lattice relaxation times measured experimentally.

The pore diameter at which the crossover from confined to bulk behavior occurs can be estimated from Eq. (10). Most importantly it depends on the isothermal compressibility as reflected by the prefactor $b/(k_B T \kappa_T)^{1/3}$. Due to the low value of the isothermal compressibility, this quantity is rather large. For PEO at $\vartheta = 85$°C, Eq. (10) suggests

$$d_{\text{pore}} \gg 10 R_F \tag{11}$$

as a condition for bulk behavior. Clearly, in our experiments this condition was not fulfilled by the porous media available. In other words, merely the bulk samples complied to Eq. (11).

Acknowledgements

We thank Magdalene Zimmermann and Hans Wiringer (both University of Ulm, Ulm, Germany) for assistance in the course of the experiments. Grants by the Volkswagen-Stiftung, the Deutsche Forschungsgemeinschaft, CRDF and RFBR are gratefully acknowledged.

References

1. Kimmich R., Seitter R.-O., Beginn U., Möller M., Fatkullin N.: Chem. Phys. Lett. **307**, 147 (1999)
2. Fischer E., Kimmich R., Beginn U., Möller M., Fatkullin N.: Phys. Rev. E **59**, 4079 (1999)
3. Kimmich R., Fatkullin N., Seitter R.-O., Fischer E., Beginn U., Möller M.: Macromol. Symp. **146**, 109 (1999)
4. Kimmich R.: NMR Tomography, Diffusometry, Relaxometry. Berlin: Springer 1997.
5. Ardelean I., Kimmich R.: Annu. Rep. NMR Spectrosc. **49**, 43 (2003)
6. de Gennes P.G.: J. Chem. Phys. **55**, 572 (1971)
7. Doi M., Edwards S.F.: The Theory of Polymer Dynamics. Oxford: Clarendon 1986.
8. Denissov A., Kroutieva M., Fatkullin N., Kimmich R.: J. Chem. Phys. **116**, 5217 (2002)
9. Ferry J.D.: Viscoelastic Properties of Polymers. New York: Wiley 1980.
10. Fetters L.J., Lohse D.J., Milner T.S., Graessley W.W.: Macromolecules **32**, 6847 (1999)
11. Beginn U., Fischer E., Pieper T., Mellinger F., Kimmich R., Möller M.: J. Polym. Sci. A Polym. Chem. **38**, 2041 (2000)

12. Fischer E., Beginn U., Denissov A., Kroutieva M., Fatkullin N., Kimmich R.: Polym. Prepr. **44**, 295 (2003)
13. Fischer E., Beginn U., Fatkullin N., Kimmich R.: Macromolecules **37**, 3277 (2004)
14. Stapf S., Kimmich R.: Macromolecules **29**, 1638 (1996)
15. Seitter R.-O., Kimmich R. in: Encyclopedia of Spectroscopy and Spectrometry (Lindon J.C., Tranter G.E., Holmes J.L., eds.), pp. 2000–2008. London: Academic Press 1999.
16. Anoardo E., Ferrante G.M.: Appl. Magn. Reson. **24**, 85 (2003)
17. Kimmich R., Fatkullin N.: Adv. Polym. Sci. **170**, 1 (2004)
18. Fatkullin N., Kimmich R.: J. Chem. Phys. **101**, 822 (1994)
19. Kimmich R., Fatkullin N., Seitter R.-O., Gille K.: J. Chem. Phys. **108**, 2173 (1998)
20. Kimmich R., Koch H.: Colloid Polym. Sci. **258**, 261 (1980)
21. Khazanovich T.N.: Polym. Sci. USSR **4**, 727 (1963)
22. Ullman R.: J. Chem. Phys. **43**, 3161 (1965)
23. Heimans N.: Macromolecules **33**, 4226 (2002)
24. Denissov A.: Master Thesis, Kazan State University, 2003.
25. Mark J.E. (ed.): Physical Properties of Polymers, Handbook. New York: American Institute of Physics 1996.

Authors' address: Rainer Kimmich, Universität Ulm, Albert-Einstein-Allee 11, 89069, Germany

V

I. Ardelean, C. Mattea, G. Farrher, S. Wonorahardjo and R. Kimmich

Nuclear magnetic resonance study of the vapor phase contribution to diffusion in nanoporous glasses partially filled with water and cyclohexane.

J. Chem. Phys. **119**, 10358 (2003).

Nuclear magnetic resonance study of the vapor phase contribution to diffusion in nanoporous glasses partially filled with water and cyclohexane

Ioan Ardelean
Universität Ulm, Sektion Kernresonanzspektroskopie, 89069 Ulm, Germany and Technical University of Cluj-Napoca, Department of Physics, 3400 Cluj-Napoca, Romania

Carlos Mattea and German Farrher
Universität Ulm, Sektion Kernresonanzspektroskopie, 89069 Ulm, Germany

Surjani Wonorahardjo
Universität Ulm, Sektion Kernresonanzspektroskopie, 89069 Ulm, Germany and The State University of Malang, Department of Chemistry, Malang, Indonesia

Rainer Kimmich
Universität Ulm, Sektion Kernresonanzspektroskopie, 89069 Ulm, Germany

(Received 18 July 2003; accepted 20 August 2003)

The contribution of the vapor phase to the effective diffusion coefficient of solvents in a partially filled nanoporous silica glass (Vycor) was investigated with the aid of nuclear magnetic resonance diffusometry. Water and cyclohexane as polar and nonpolar adsorbate species show opposite dependencies on the filling factor. The effective diffusion coefficient of water increases with the filling factor, whereas that of cyclohexane decreases. A ''two-phase fast-exchange model theory'' is presented accounting for these phenomena. In the vapor phase, both Knudsen and ordinary Einstein diffusion were considered. The different dependencies on the filling factor for polar and nonpolar adsorbate species are attributed to different effective tortuosities represented by different exponents in Archie's law anticipated in the model theory. The fast exchange feature stipulates that the pore size is small enough. © *2003 American Institute of Physics.* [DOI: 10.1063/1.1618214]

I. INTRODUCTION

It is known that water diffusion in materials partially filled with water tends to be enhanced by displacements in the vapor phase, whereas the nuclear magnetic resonance (NMR) signal is totally dominated by the liquid phase.[1–4] The diffusivity in the gas phase is four orders of magnitude larger than in the liquid phase whereas the spin density is three orders of magnitude smaller. Exchange between the two phases on the time scale of the experiment thus leads to an effective water diffusivity enhanced by the vapor while the liquid phase is responsible for most of the signal. Enhancements up to a factor of 10 above the bulk value were observed[4] in spite of the confinement in the pore space (normally giving rise to the opposite tendency[5]). Vapor phase enhancement was directly proven in silica fineparticle powders by varying the accessible volume by compression of the initially loosely packed powder by a factor up to 7. The effective diffusivity was correspondingly diminished until the bulk water diffusion coefficient was reached with the strongest densification.[3]

D'Orazio *et al.*[2] have investigated the contribution of the vapor phase to the effective diffusion coefficient of water in partially saturated porous glasses with pore dimensions ranging from 47 to 240 nm. A progressive increase of the self-diffusion coefficient was observed with reduced filling factor. A simple model that explains the dependence of the measured effective diffusion coefficient on the filling degree was also introduced. The theoretical model takes into account the fast (relative to the NMR time scale) exchange between liquid and vapor phase in the partially filled sample.

The contribution of the vapor phase to the effective diffusion coefficient was also studied for a nonpolar solvent, namely, hexane partially filling a porous glass.[6] The measurements indicate a dependence of the diffusion coefficient on diffusion times. This observation was again interpreted by molecular exchange between the liquid and vapor phases.

In the present study we focus in more detail on the different behavior of polar and nonpolar solvents in partially filled nanoporous silica glasses. As typical examples we have chosen water and cyclohexane in Vycor with a nominal pore diameter of 4 nm. The most conspicuous observation is that the dependence of the effective water and cyclohexane diffusivities on the degree of filling show just opposite tendencies. It will be shown that this finding can be explained on the basis of a two-phase fast-exchange model. The role of Knudsen diffusion will also be considered.

II. THE TWO-PHASE FAST-EXCHANGE MODEL

In an unsaturated porous sample with polar inner surfaces, the liquid and the vapor phase form two interpenetrating systems of different geometry and porosity. A polar adsorbate such as liquid water tends to be distributed in adsorption layers on polar pore walls. The layer thickness depends on the degree of imbibing.[2,7,8] On the other hand, cyclohexane as a nonpolar species is expected to fill the

 © 2003 American Institute of Physics

smaller pores at first and then the bigger ones.[8] In both cases, the remainder of the pore volume is filled by air saturated with the respective vapor phase.

In the fast-exchange limit the stimulated echo (STE) is attenuated by diffusive displacements according to

$$A_{\mathrm{STE}} \propto e^{-D_{\mathrm{eff}}(\gamma G)^2 \delta^2 \Delta}. \tag{1}$$

The effective diffusivity, D_{eff}, is the average between the two subregions, i.e.,

$$D_{\mathrm{eff}} = p_l D_l + p_v D_v . \tag{2}$$

The quantities p_l and p_v are the mass fractions of molecules in the liquid and vapor phases, respectively. The diffusion coefficients in the two phases, D_l and D_v, are reduced relative to the bulk values $D_{l,0}$ and $D_{v,0}$, respectively. This reduction of the diffusion coefficient can be due to both the tortuosities of the liquid and vapor subpore spaces, and the surface roughness. The latter can be important especially in the Knudsen diffusion regime.[9]

The mass fractions in the liquid and vapor phase can be expressed as a function of the respective densities as follows:

$$p_l = \frac{1}{1+\left(\frac{V_0}{V_l}-1\right)\frac{\rho_v}{\rho_l}} = \frac{f}{f+(1-f)(\rho_v/\rho_l)}; \quad p_v = 1 - p_l , \tag{3}$$

where ρ_l and ρ_v are the mass densities in the liquid and vapor phase, respectively. V_0 represents the total pore volume, V_l is the volume of the liquid phase, and $f = V_l/V_0$ is the filling factor.

In completely filled pore spaces, the transport properties are predominantly affected by the geometrical restriction (the tortuosity).[5] The effective diffusion coefficient in the pore space, D, is then reduced by a factor Φ_t^m relative to its bulk value, D_0 (Archie's law).[7,10] Here $\Phi_t = V_0/V_t$ represents the porosity of the sample. V_t is the total volume including the matrix and the pore space, and m is an empirical exponent.

In the case of partially filled porous samples the situation is more complicated since we then have two interpenetrating pore systems of different effective porosities $\Phi_l = V_l/V_t$ and $\Phi_v = (V_0 - V_l)/V_t$ for the liquid and vapor phases, respectively. Assuming Archie's law again[7,10] for the reduced diffusion coefficient one can write for the liquid region the expression,

$$D_l = (\Phi_l)^{m_l} D_{l,0} = \Phi_t^{m_l}\left(\frac{V_l}{V_0}\right)^{m_l} D_{l,0} = \Phi_t^{m_l} f^{m_l} D_{l,0} . \tag{4}$$

The porosity that is effective for the liquid phase, Φ_l, has been expressed as a function of the sample porosity $\Phi_t = \Phi_l + \Phi_v$. The exponent m_l depends both on the sample geometry and the wetting properties of the liquid. It can be determined from diffusion data for completely filled samples, that is a filling factor $f = 1$. The diffusion coefficient in bulk liquid is designated by $D_{l,0}$.

Diffusion in the vapor phase is governed by molecular collisions and by collisions with the pore walls. The term "wall" may refer to the liquid–vapor interface or to inner surfaces of the solid matrix. Taking into account Knudsen diffusion, the effective vapor diffusion coefficient inside a porous system can be derived by adding the diffusion resistances associated with these two types of collisions (molecule–wall and molecule–molecule)[11]

$$\frac{1}{D_v} = \frac{1}{D_K} + \frac{1}{D_E}, \tag{5}$$

where D_K and D_E are the Knudsen and Einstein diffusivities, respectively. Note that D_v approaches D_K in the Knudsen limit $D_K \ll D_E$, so that molecule–wall collisions dominate. It becomes equal to D_E in the Einstein diffusion regime $D_K \gg D_E$, where molecule–molecule collisions prevail.

Using Archie's law, the quantities D_K and D_E can be represented in terms of tortuosity factors as above. This accounts for the differences between the diffusivities in pore spaces relative to the bulk behavior. The results are

$$D_K = (\Phi_v)^{m_{v,K}} D_{K,0} = \Phi_t^{m_{v,K}}\left(1-\frac{V_l}{V_0}\right)^{m_{v,K}} D_{K,0} = \Phi_t^{m_{v,K}}(1-f)^{m_{v,K}} D_{K,0} \tag{6}$$

and

$$D_E = (\Phi_v)^{m_{v,E}} D_{v,0} = \Phi_t^{m_{v,E}}\left(1-\frac{V_l}{V_0}\right)^{m_{v,E}} D_{v,0} = \Phi_t^{m_{v,E}}(1-f)^{m_{v,E}} D_{v,0} . \tag{7}$$

The diffusivities in the bulk vapor phase are given by $D_{v,0}$ and $D_{K,0}$ in the Einstein and Knudsen diffusion limits, respectively. The exponents $m_{v,K}$ and $m_{v,E}$ account for tortuosity effects in the Knudsen and Einstein regimes, respectively, and can be determined with the aid of bulk diffusion data. Recent investigations of ethane in beds of NaX zeolites revealed different tortuosity factors in the Knudsen and Einstein regimes.[11] The exponents $m_{v,K}$ and $m_{v,E}$ may consequently also deviate from each other.

In Eq. (6), $D_{K,0} = (2a/3)\sqrt{8k_BT/\pi M_0}$ represents the reference Knudsen diffusion coefficient,[2] where k_B is the Boltzmann constant, T is the absolute temperature, M_0 is the molecular mass, and a is the size of the vapor-phase domains. The last quantity is related to the pore dimension but also to the pore shape and the thermodynamic and chemical properties of the molecular species.

As a crude approximation, a cylindrical pore geometry can be assumed.[2,11] For wetting liquids, the size of the vapor phase domains can then be expressed as a function of the filling factor as $2a = d(1-f)^{1/2}$, where d represents the mean pore diameter. The reference Knudsen diffusion coefficient can thus be expressed as

$$D_{K,0}(f) = \frac{1}{3} d (1-f)^{1/2} \sqrt{\frac{8k_BT}{\pi M_0}}. \tag{8}$$

Note that this dependence may be different for different chemical species such as water and cyclohexane due to their different wetting properties. The effective diffusion coefficient, Eq. (2), for the fast-exchange limit between two phases in a porous medium can thus be expressed as

$$D_{\mathrm{eff}}(f)=\frac{1}{f+(1-f)\dfrac{\rho_v}{\rho_l}}\left\{\Phi_t^{m_l} f^{m_l+1} D_{l,0} + (1-f)\frac{\rho_v}{\rho_l}\left[\frac{1}{\Phi_t^{m_{v,E}}(1-f)^{m_{v,E}} D_{v,0}} + \frac{1}{\Phi_t^{m_{v,K}}(1-f)^{m_{v,K}} D_{K,0}(f)}\right]^{-1}\right\}, \tag{9}$$

where the reference Knudsen diffusion coefficient, $D_{K,0}(f)$, is given by Eq. (8). The first term in Eq. (9) represents the contribution of the liquid phase to the effective diffusion coefficient, whereas the second term is accounting for the vapor phase contribution.

III. EXPERIMENT

A. Samples

Vycor porous glass VPQ #7930 was purchased from Corning Ltd. It consists of 96% SiO_2. The nominal mean pore size is $d=4$ nm (± 0.6 nm). The porosity is specified as $\Phi_t=0.28$. The specific surface area is 250 m^2/g. Electron micrographs recorded in our lab with a Hitachi S-5200 microscope suggest somewhat larger pores [see Fig. 1(a)].

The samples were pretreated as suggested by the manufacturer. This includes 60 min of boiling in 30% H_2O_2. The samples were then washed with distilled water and left in vacuum for 24 h at 95 °C. After that, the samples are considered to be dry with a nominal filling factor of 0. The solvents were then filled into the porous glass with the aid of the bulk-to-bulk method resulting in a filling factor 1. Samples partially filled with water were obtained by evaporation in open air over varying periods. In the case of cyclohexane, evaporation was performed in a glove bag in a dry nitrogen atmosphere in order to avoid any replacement of cyclohexane by water from the air humidity. The solvent content reached by this procedure is determined by weighing. The samples were placed in a sealed container with practically no empty space that would allow for further evaporation. All experiments were done only after about 1 h permitting the fluid to equilibrate with respect to phase distributions. After this annealing period no changes were perceptible any longer.

The adsorbate fluids, water and cyclohexane, were chosen as typical representatives of polar (wetting) and nonpolar (nonwetting) species. The water was demineralized. *N*-cyclohexane was purchased from Fluka Chemika, Germany. The equilibrium vapor pressure of cyclohexane at room temperature is about four times larger than that of water; the surface tension is three times smaller. The consequence is that cyclohexane evaporates much faster than water [Fig. 1(b)]. The vapor phase of cyclohexane in partially filled pores is thus expected to contain about four times as many molecules as in the case of water.

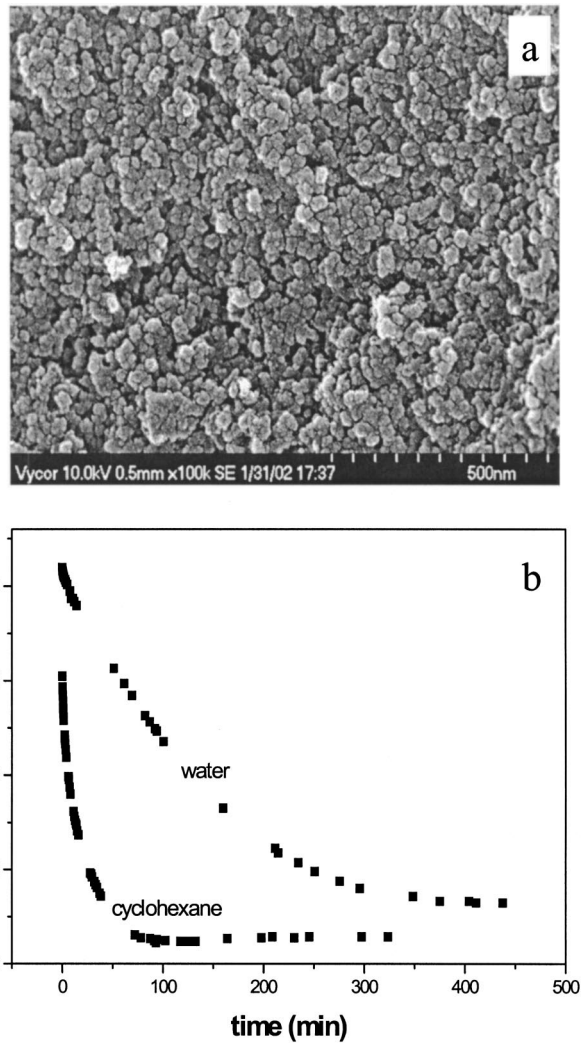

FIG. 1. (a) Electron micrograph of Vycor. (b) Time dependence of solvent content in Vycor for water and cyclohexane as a function of time, when the sample is left in open air at room temperature. The liquid content was measured by weighing the samples with a tare balance. Due to the four times larger vapor pressure, cyclohexane evaporates much faster than water.

B. Instruments and techniques

All diffusion experiments were performed with a Bruker DPX400 NMR spectrometer equipped with a microscopy gradient unit. The data were recorded at room temperature and at a proton resonance frequency of 400 MHz using the standard pulsed field gradient stimulated echo technique described in Ref. 12, for instance. The radio frequency (RF) pulse sequence and pulsed gradient intervals are shown in Fig. 2. The measurements were carried out with a diffusion interval $\Delta=300$ ms, and gradient pulse widths $\delta=2$ ms for water, and $\delta=1$ ms for cyclohexane.

Any influence of internal, susceptibility induced field gradients on the measurements could be excluded with the

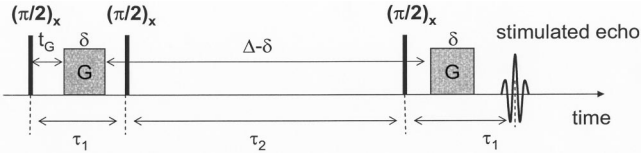

FIG. 2. Schematic RF and field gradient pulse sequence for the stimulated-echo variant of NMR diffusometry. *G* represents the field gradient applied in pulses of width δ and spacing Δ.

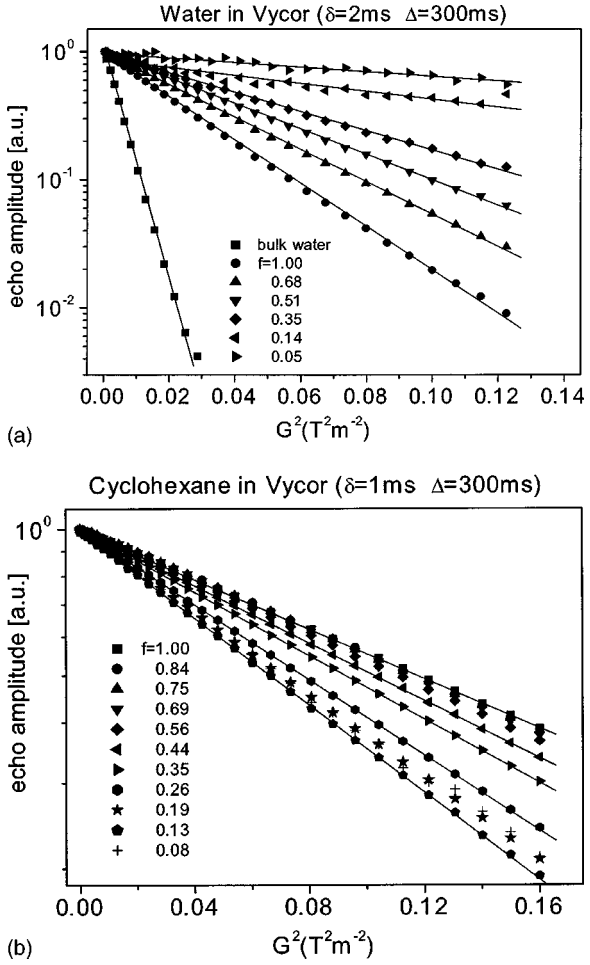

FIG. 3. Echo attenuation curves for water (a) and cyclohexane (b) in Vycor for different degrees of filling *f*. The decay for bulk water for the same experimental parameters is also shown (squares) for comparison. All data can well be represented by monoexponential decays (solid lines) indicating the fast-exchange limit anticipated in the two-phase fast-exchange model theory.

aid of test experiments with a bipolar gradient technique[13] as well as with a rotary echo method.[14] In the latter case a conic RF coil was employed for the production of gradients of the RF amplitude.[15]

IV. RESULTS AND DISCUSSION

Figures 3(a) and 3(b) show typical echo attenuation curves recorded for different filling factors. The decays both for water [Fig. 3(a)] and cyclohexane [Fig. 3(b)] can be described by single exponential functions indicating fast exchange between the liquid and vapor phases. The effective diffusion coefficients were evaluated by fitting Eq. (1) to the attenuation data. The gradient was calibrated with the aid of data for bulk water [squares in Fig. 3(a)] corresponding to a room temperature diffusion coefficient $D_{l,0}^{\text{water}}=2.3\times10^{-9}$ m^2/s.[5,16]

The plot in Fig. 4 shows effective diffusion coefficients measured in water and cyclohexane in Vycor as a function of the filling factor. The data remarkably indicate an opposite tendency for the two solvent species. The water diffusion coefficients *increase* with increasing filling factor as is described by the theoretical curve (solid line). This is in contrast to the cyclohexane diffusion coefficient which *decreases* with increasing filling factor. It appears that the different dependence for the two adsorbate species is due to different contributions by Knudsen diffusion in the vapor phase.

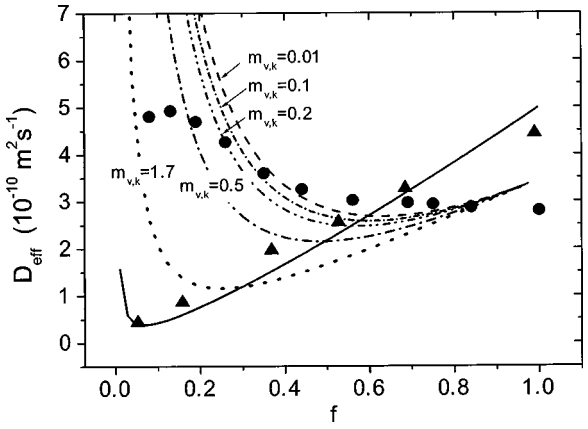

FIG. 4. Effective water (▲) and cyclohexane (●) diffusion coefficients in Vycor as a function of the filling factor. The lines have been calculated with the two-phase fast-exchange formula given at Eq. (9) for the parameters given in the text. The solid line refers to parameters relevant for water, the other curves were calculated for cyclohexane and the values of the exponent $m_{v,K}$ indicated in the plot.

In the calculations, the following parameters have been used for water: $[\rho_v/\rho_l]^{\text{water}}=2.5\times10^{-5}$ for the ratio between the vapor and liquid densities,[2] $D_{v,0}^{\text{water}}=2.4\times10^{-5}$ m^2/s for the water vapor diffusion coefficient in air at 26.6 °C;[2] $\Phi_t=0.28$ for the porosity of Vycor porous glass as specified by the manufacturer; $d=4$ nm the mean pore dimension.

The exponents in Archie's law for the different phases and diffusional mechanisms deserve particular attention in this context. We assume that the ordinary Einstein diffusion behaves in the same way both in the liquid as well as in the vapor phase, $m_l^{\text{water}}=m_{v,E}^{\text{water}}=1.2$, provided that distances longer than the correlation length of the pore space are probed by the molecules during the diffusion time. That is, these parameters are assumed to be commonly determined by the tortuosity of the total pore space.

On the other hand, the Knudsen diffusion in the vapor phase turns out to be determined by an exponent $m_{v,K}^{\text{water}}=2$ which indicates a modified tortuosity effect. Note that differences in the tortuosity in the vapor phase for the Knudsen and Einstein regimes were reported also in literature for ethane in beds of NaX zeolite.[11]

The effective diffusion coefficients of cyclohexane decreasing with the filling factor can best be approached by Eq. (9) using the following parameters: $[\rho_v/\rho_l]^{\text{cyclohexane}}=5.9\times10^{-4}$, the density ratio;[16] $D_{v,0}^{\text{cyclohexane}}=8.5\times10^{-6}$ m^2/s, the diffusion coefficient of cyclohexane vapor in air;[17] $D_{l,0}^{\text{cyclohexane}}=1.4\times10^{-9}$ m^2/s, the diffusion coefficient of bulk liquid cyclohexane at 298 K.[5] As optimal exponents in Archie's law we found $m_l^{\text{cyclohexane}}=m_{v,E}^{\text{cyclohexane}}=1.1$ and $m_{v,K}^{\text{cyclohexane}}=0.01$. Especially the latter value is remarkably different from that for the corresponding water ex-

ponent, and explains the totally different dependence on the filling factor. A family of theoretical curves was also calculated with Eq. (9) for different values of the exponent $m_{v,K}$ in Archie's law for Knudsen diffusion.

Equation (9) describes the cyclohexane data well down to a filling factor of about 0.3. The deviation of the experimental data from the theoretical curve below this value is attributed to traces of residual water that could not be removed with the procedure described above. That is, water traces contributes to the NMR signal relatively more and more at such low degrees of filling and gradually grow in influence. Proton NMR spectroscopy of Vycor samples with low cyclohexane filling factor shows a water line apart from that of cyclohexane indeed.[18]

D'Orazio *et al.*[2] have reported water diffusion coefficients decreasing with increasing filling factor in samples with larger pore sizes. This apparently contradicts the finding of the present study for water. The reason is, that the conditions having led to the parameter set given above are very different for larger pores. That is, the interpretation of the present diffusion data is relevant for polar nanoporous materials whereas microporous media are expected to display a totally different behavior. A corresponding study and analysis will be published elsewhere.[19]

V. CONCLUSIONS

Translational diffusion of water and cyclohexane as polar and nonpolar solvent species was studied with NMR diffusometry in a nanoporous silica glass (Vycor) as a function of the filling factor. The solvent molecules are distributed in the liquid and vapor phases according to a dynamic equilibrium, where fast exchange (relative to the NMR time scale) applies. A ''two-phase fast-exchange model'' for the effective diffusion coefficient was established and compared to experimental data. For diffusion in the vapor phase, we distinguish contributions by ordinary (''Einstein'') and Knudsen diffusion.

The NMR signal is largely dominated by the liquid phase due to the fact that the spin density in the liquid is 10^3 times larger than in the vapor phase. On the other hand, the average translational diffusivity tends to be governed by the vapor phase, where diffusion is four orders of magnitude faster than in the liquid phase. Whether this vapor phase enhancement of diffusion shows up in NMR diffusometry experiments or not, depends on various factors. These are: the pore size, the polar or nonpolar character of the liquid relative to the pore walls, and the filling factor of the pores.

The remarkable result of the experiments is that the effective diffusivity of water in Vycor increases with the filling degree, whereas that of cyclohexane decreases. In both cases, the effective diffusion coefficients are smaller than their bulk values as a consequence of the tortuosity of the pore space.[5]

The two-phase fast-exchange formula for the effective diffusion coefficient given at Eq. (9) appears to be of quite general validity. It represents the complex adsorbate diffusion and phase exchange behavior. The only fitting parameters are the exponents in Archie's law anticipated in the derivation of this model. The values of these parameters for ordinary Einstein diffusion in the liquid and vapor phase and for Knudsen diffusion in the vapor phase are specific for the chemical species both of the adsorbate and of the adsorbent. The fast-exchange character underlying the fact that an effective diffusion coefficient shows up in the experiments is tightly related to the pore size. With pore sizes in the micrometer range or above this feature appears to be no longer valid.[19]

ACKNOWLEDGMENTS

This work was supported by the Alexander von Humboldt Foundation and the Deutsche Forschungsgemeinschaft (SFB 569).

[1] J. Kärger, H. Pfeifer, E. Riedel, and H. Winkler, J. Colloid Interface Sci. **44**, 187 (1973).
[2] F. D'Orazio, S. Bhattacharja, W. P. Halperin, and R. Gerhardt, Phys. Rev. Lett. **63**, 43 (1989).
[3] R. Kimmich, S. Stapf, P. Callaghan, and A. Coy, Magn. Reson. Imaging **12**, 339 (1994).
[4] R. Kimmich, S. Stapf, R. O. Seitter, P. Callaghan, and E. Khozina, Mater. Res. Soc. Symp. Proc. **366**, 189 (1995).
[5] R. Kimmich, S. Stapf, A. I. Maklakov, V. D. Skirda, and E. V. Khozina, Magn. Reson. Imaging **14**, 793 (1996).
[6] R. R. Valiullin, V. D. Skirda, S. Stapf, and R. Kimmich, Phys. Rev. E **55**, 2664 (1997).
[7] F. D'Orazio, S. Bhattacharja, W. P. Halperin, and R. Gerhardt, Phys. Rev. B **42**, 6503 (1990).
[8] S. G. Allen, P. C. L. Stephenson, and J. H. Strange, J. Chem. Phys. **106**, 7802 (1997).
[9] K. Malek and M. O. Coppens, Phys. Rev. Lett. **87**, 125505 (2001).
[10] M. Sahimi, Rev. Mod. Phys. **65**, 1393 (1993).
[11] O. Geier, S. Vasenkov, and J. Kärger, J. Chem. Phys. **117**, 1935 (2002).
[12] R. Kimmich, *NMR Tomography, Diffusometry, Relaxometry* (Springer-Verlag, Berlin, 1997).
[13] R. M. Cotts, M. J. R. Hoch, T. Sun, and J. T. Markert, J. Magn. Reson. (1969-1992) **83**, 252 (1989).
[14] R. Dupeyre, P. H. Devoulon, D. Bourgeois, and M. Decorps, J. Magn. Reson. (1969-1992) **95**, 589 (1991).
[15] I. Ardelean, A. Scharfenecker, and R. Kimmich, J. Magn. Reson. **144**, 45 (2000).
[16] M. Holz and H. Weingärtner, J. Magn. Reson. (1969-1992) **100**, 1 (1992).
[17] Landolt-Börnstein, *Zahlenwerte und Funktionen aus Physik, Chemie, Astronomie, Geophysik und Technik* (Springer-Verlag, Berlin, 1969), Vol. II, Part 5, p. 552.
[18] V. Tsygankov and C. Mattea (unpublished).
[19] I. Ardelean, C. Mattea, G. Farrher, and R. Kimmich (unpublished).